

②

DTIC FILE COPY

AD-A231 957

# NONLINEAR PROPERTIES OF NOVEL MATERIALS

Juan F. Lam  
Hughes Research Laboratories  
3011 Malibu Canyon Road  
Malibu, California 90265

DTIC  
ELECTE  
FEB 25 1991  
S D D

January 1991

DAAL03-87-C-0001

Final Report

1 March 1987 through 28 October 1990

Prepared for  
U.S. ARMY RESEARCH OFFICE  
Physics Division  
P. O. Box 12211  
Research Triangle Park, NC 27709-2211

EXCLUDED FROM AUTOMATIC  
DECLASSIFICATION  
DATE 12-15-2000  
BY 1045

# REPORT DOCUMENTATION PAGE

Form Approved  
OMB No. 0704-0188

Public reporting burden for this collection of information is estimated to average 1 hour per response, including the time for reviewing instructions, searching existing data sources, gathering and maintaining the data needed, and completing and reviewing the collection of information. Send comments regarding this burden estimate or any other aspect of this collection of information, including suggestions for reducing this burden, to Washington Headquarters Services, Directorate for Information Operations and Reports, 1215 Jefferson Davis Highway, Suite 1204, Arlington, VA 22202-4302, and to the Office of Management and Budget, Paperwork Reduction Project (0704-0188) Washington, DC 20503

1. AGENCY USE ONLY (Leave blank)		2. REPORT DATE January 1991		3. REPORT TYPE AND DATES COVERED FINAL, 1 March 1987 - 28 October 1990	
4. TITLE AND SUBTITLE  Nonlinear Properties of Novel Materials				5. FUNDING NUMBERS  DAAL03-87-C-0001	
6. AUTHOR(S)  Juan F. Lam					
7. PERFORMING ORGANIZATION NAME(S) AND ADDRESS(ES)  Hughes Research Laboratories 3011 Malibu Canyon Road Malibu, CA 90265				8. PERFORMING ORGANIZATION REPORT NUMBER	
9. SPONSORING / MONITORING AGENCY NAME(S) AND ADDRESS(ES)  U. S. Army Research Office P. O. Box 12211 Research Triangle Park, NC 27709-2211				10. SPONSORING / MONITORING AGENCY REPORT NUMBER  ARO 23969.6-PH	
11. SUPPLEMENTARY NOTES  The view, opinions and/or findings contained in this report are those of the author(s) and should not be construed as an official Department of the Army position, policy, or decision, unless so designated by other documentation.					
12a. DISTRIBUTION / AVAILABILITY STATEMENT  Approved for public release; distribution unlimited.				12b. DISTRIBUTION CODE	
13. ABSTRACT (Maximum 200 words)  Millimeter wave nonlinearities in semiconductor superlattices are analyzed. Self-induced transparency, giant third order susceptibilities and third harmonic generation are predicted at 250 GHz. Enhanced nonlinear optical properties of quantum dots are quantified, in agreement with experiments. Application to lasers indicates threshold current density of the order of tens of amperes per centimeter squared, temperature independent threshold condition, and visible light emission for 50 Å dots. The origin of sublinear intensity dependence of the erasure rate in barium titanate is attributed to the presence of shallow impurities. The exponent has resonances as a function of the grating wave vector, and is linear function of temperature. Self-oscillatory behavior of phase conjugate wave in self-pumped photorefractive is shown to arise from the photovoltaic effect. We demonstrated the first resonantly enhanced self-pumped phase conjugate mirror at 0.852 nm. Self-starting temporal oscillation in resonant two-wave mixing is attributed to the phenomenon of light induced drift. Third order optical susceptibilities at 10.6 μm in semiconductor superlattices are calculated to be of the order of 10 <sup>-4</sup> esu. Application to laser hardening of FLIR systems, using the technique of light induced prism, shows dynamic range of 10 <sup>4</sup> , subnanosecond response time, and tens of milliwatts per centimeter squared differential intensity threshold at the aperture plane.					
14. SUBJECT TERMS  Millimeter wave nonlinearities, superlattices, quantum dots, lasers, photorefractive materials, phase conjugation, sensor protection				15. NUMBER OF PAGES 186	
				16. PRICE CODE	
17. SECURITY CLASSIFICATION OF REPORT  UNCLASSIFIED	18. SECURITY CLASSIFICATION OF THIS PAGE  UNCLASSIFIED	19. SECURITY CLASSIFICATION OF ABSTRACT  UNCLASSIFIED	20. LIMITATION OF ABSTRACT  UL		

## TABLE OF CONTENTS

SECTION	PAGE
1 INTRODUCTION .....	1
2 BRIEF SUMMARY OF RESEARCH FINDINGS.....	4
2.1 Significant "Firsts" .....	4
2.2 Millimeter Wave Nonlinearities in Superlattices .....	5
2.3 Nonlinear Optics and Lasing Properties of Semiconductor Quantum Dots .....	6
2.4 Optical Physics of Photorefractive Materials .....	7
2.5 Resonantly Enhanced Self-Pumped Phase Conjugation .....	9
2.6 Optical Nonlinearities in HgTe/CdTe Superlattices and Their Applications to 10.6 $\mu$ m Sensor Protection .....	10
2.7 Four-Wave Mixing Spectroscopy of GaAs/AlGaAs Quantum Wells.....	11
3 U.S. ARMY LABORATORY, CONFERENCE, AND UNIVERSITY PRESENTATIONS .....	13
4 INVENTION DISCLOSURE: QUANTUM DOT LASERS.....	16
5 TECHNOLOGY TRANSFER RESULTING FROM WORK PERFORMED UNDER U.S. ARMY RESEARCH OFFICE CONTRACT DAAG29-81-C-0008.....	34
REFERENCES .....	R-1
APPENDICES	
A Theory of Millimeter Wave Nonlinearities in Semiconductor Superlattices.....	A-1
B Theory of Enhanced Optical Nonlinearities in Quantum Dots.....	B-1
C Four-Wave Mixing Spectroscopy of State Selective Collisions in Gases and Solids .....	C-1
D Laser Spectroscopy of Quantum Dots.....	D-1
E Theory of Transient Self-Pumped Phase Conjugation in Photorefractive Materials .....	E-1

# TABLE OF CONTENTS

SECTION		PAGE
F	Origin of Anomalous Relaxation Time in Photorefractive Materials .....	F-1
G	Theory of Stimulated Scattering Phase Conjugation in Resonant Systems .....	G-1
H	Resonant Self-Pumped Phase Conjugation in Cesium Vapor at 0.85 $\mu\text{m}$ .....	H-1
I	Pressure Induced Coherent Energy Transfer and Temporal Oscillation of Two-Wave Mixing in Sodium Vapor.....	I-1
J	Two-Wave Mixing Processes in Resonant Systems .....	J-1



Accession For	
NTIS CRA&I	<input checked="" type="checkbox"/>
DTIC TAB	<input type="checkbox"/>
Unannounced	<input type="checkbox"/>
Justification .....	
By .....	
Distribution/ .....	
Availability Codes	
Dist	Avail and/or Special
A-1	

## SECTION 1

### INTRODUCTION

Advances in the understanding and applications of novel nonlinear optical phenomena depend on the detailed characterization of the appropriate materials. The majority of the discoveries in nonlinear optics has been synonymous with chance observations. Although few theoretical predictions have borne fruits with careful experimental demonstrations. Examples of the former are the discovery of stimulated Raman scattering<sup>1</sup> and stimulated Brillouin phase conjugation.<sup>2</sup> Self-focusing of laser beam<sup>3</sup> and soliton propagation in optical fibers<sup>4</sup> are excellent examples of the latter case. In spite of the success in the interpretation of nonlinear optical phenomena, the understanding of optical materials has followed a path replete with puzzles and contradictions. Photorefractive barium titanate is an example of an optical material whose properties are still being determined, with little success, for the last decade. The main puzzle is that the nonlinear optical processes in barium titanate can be explained at a rather primitive level, regardless of the large amount of contradictory data on the microscopic transport parameters that have been measured.<sup>5</sup> The objective of this contract was to approach nonlinear optics by attempting to understand, using basic physical principles, some critical properties of the materials and predict new phenomena that could be measured in a laboratory setting.

Recent advances in the fabrication of nanometer semiconductor structures have made possible the study of optical properties of quantum confined systems.<sup>6</sup> Semiconductor quantum wells and superlattices have been grown using the technique of molecular beam epitaxy (MBE).<sup>7</sup> The implementation of resonant tunneling devices, based upon the original idea of Tsu and Esaki,<sup>8</sup> has been a subject of intense research. The demonstration of quantum confined Stark effect<sup>9</sup> has led to the invention of the SEED device,<sup>10</sup> a crucial component in the operation of the AT&T Bell Laboratories' optical computer. Nonlinear optical effects in quantum wells have been investigated in both the CW and pulsed regimes.<sup>11</sup> Dynamic Stark effect<sup>12</sup> has been observed in GaAs/AlGaAs quantum wells and was explained using the dressed-atom concept pioneered in the field of atomic physics. In spite of such successes, very little is known concerning the effects of millimeter wave radiation on these quantum confined structures. As part of the general charter of this contract, we carried out a detailed study of nonlinear millimeter wave phenomena in semiconductor superlattices.

Recent developments in focused ion beam technology and MBE have led to the realization of quantum well wires and quantum dots.<sup>13</sup> Quantum wire lasers<sup>14</sup> have been fabricated and their output characteristics appeared to be consistent with the energy dependence of the one-dimensional

density-of-states. Quantum dots have also been demonstrated in GaAs-based materials<sup>15</sup> and II-VI compound semiconductor.<sup>16</sup> The latter are grown by chemical processes and are incorporated in a matrix for optical studies. However, there exists no definitive nonlinear optical measurements that elucidate their unique optical properties. In the case of GaAs materials, surface recombination has been a crucial mechanism that prevented the observation of any significant optical emission. Nonlinear pump-probe techniques have been applied to CdSe quantum dots,<sup>17</sup> revealing that the measured blue shift in the binding energy as a function of particle size is consistent with theoretical predictions.<sup>18</sup> Furthermore, the atomic-like behavior of quantum dots makes them ideal for future optoelectronic device applications. A significant amount of time was devoted in this contract toward the understanding of the nonlinear optical and lasing properties of quantum dots.

Photorefractive nonlinear optics was first discovered by Ashkin et. al<sup>19</sup> during their study of laser beam propagation in lithium niobate. Fundamental understanding of the effect was advanced by Chen.<sup>20</sup> The field was revived in the late 1970s in the Soviet Union by Vinetskii and Kukhtarev<sup>21,22</sup>, who proposed and quantified the idea of energy transfer between two optical beams. Since then, many experiments have demonstrated the intrinsic nonlinear optical properties of photorefractive materials. However, simple linear optical properties, such as the intensity dependence of the grating erasure rate, have been the subject of controversy for the last decade.<sup>23</sup> Only recently, an understanding have been achieved through a more detailed model of the photorefractive material.<sup>24</sup> The present phenomenological model indicates that predictions based on the Kukhtarev model might be at fault. The orientation of this contract was devoted, in part, to the fundamental understanding of the optical response of photorefractive materials.

Useful applications of phase conjugation in tactical lasers has been limited by the availability of optical materials which are fast responding, have a low intensity threshold, have a reasonable phase conjugate reflectivity, and can be operated in the passive mode of operation. The latest development that has the potential of solving all these issues is the demonstration of a resonantly enhanced self-pumped phase conjugate mirror.<sup>25</sup> The experiments indicated that this unique phase conjugate mirror has a response time of tens of nanoseconds, a threshold as low as  $10 \text{ W/cm}^2$ , a reflectivity of 2%, and operates only when an input aberrated laser beam is incident upon it. As part of our effort to understand the area of phase conjugate optics, a significant amount of research was devoted to the understanding of the physical mechanism that gives rise to self-pumped phase conjugate fields.

During the course of this contract, an effort was made to tie our understanding of optical nonlinearities in semiconductors to specific system applications. One of the most important problems is the laser hardening of a Forward Looking Infrared Radar (FLIR), a device that has been fielded in the Army. We exploited the intrinsic properties of II-VI compound semiconductor

superlattices and the behavior of an optical material in the presence of a skewed high intensity laser beam to arrive at an unique solution to the sensor protection issue.

This theoretical effort has benefited from the constant inspiration and information exchange that arose from the active participation in several experimental programs that have being funded by the Army Research Office. Specifically, the substance of this final report is made more relevant to the mission of the Army through the generous critique and technical collaboration by Profs. Bob D. Guenther and David D. Skatrud of Duke University on millimeter wave nonlinearities in superlattices; Prof. Duncan G. Steel of the University of Michigan on laser spectroscopy of quantum wells; and Prof. Harold Fetterman of UCLA on microwave phase conjugation.

The concept of resonant enhanced self-pumped phase conjugation was originally put forward by the principal investigator in a previous ARO funded contract. The understanding of the subject would not have been complete without the experimental help of Dr. Celestino J. Gaeta, who implemented the idea in sodium and cesium vapors. His contribution is gratefully acknowledged.

The enthusiasm of the author on quantum dots was amplified by the constant support and world class focused ion beam fabrication expertise of Dr. Randy Kubena, who produced the first quantum dot in GaAs. The idea of using the third order optical susceptibilities of HgTe/CdTe superlattices in a sensor protection scenario was quantified in a difficult experiment by Dr. Steve Turley, who measured them using phase conjugation techniques. Our quest for the understanding of the physics in these two subjects in a period plagued with turbulence at Hughes could not have been possible without the help of Dr. Ross McFarlane, who was the cheerleader along the way. The fabrication of the large stack of GaAs/AlGa As superlattices would not have been possible without the expertise and perseverance of Dr. Tom Hasenberg, Ms. Leslie Warren, and Mr. Jim Brown.

During the course of the contract, the objectives became more focused to the needs of the Army through technical exchanges with Dr. G. Iafrate (now at ARO) and Mr. C Cook of CECOM Electronic and Device Laboratory at Fort Monmouth on semiconductor nanostructures; Drs. P. Brody and M. Tobin of U.S. Army Harry Diamond Laboratories on photorefractive and superlattice optical devices; and Drs. Ed Sharp and Gary Wood of CECOM Center for Night Vision and Electro-Optics on 10.6- $\mu$ m sensor protection using II-VI compound semiconductor superlattices.

## **SECTION 2**

### **BRIEF SUMMARY OF RESEARCH FINDINGS**

#### **2.1 SIGNIFICANT "FIRSTS"**

- Proposed the use of semiconductor superlattices as nonlinear millimeter wave materials. Predicted self-induced transparency and third harmonic generation at 250 GHz.
- Calculated the nonlinear optical responses of semiconductor quantum dots, and analyzed the output characteristics of a quantum dot laser.
- Developed a theory of transient response of photorefractive materials. Identified, for the first time, shallow impurity as the origin of the sublinear intensity dependence of the grating erasure rate in barium titanate.
- Achieved an understanding of resonantly enhanced self-pumped phase conjugation; and demonstrated, for the first time, a CW self-pumped phase conjugate mirror in cesium vapor that operates at diode laser wavelengths. Identified the phenomenon of light induced drift as the mechanism responsible for pressure induced temporal oscillations of optical beams.
- Proposed the use of HgTe/CdTe superlattices as the nonlinear broadband material for use in the laser hardening of FLIR. Calculated the optimum conditions for the beam bending concept to be effective at 10.6  $\mu\text{m}$ .
- Calculated the effect of exciton-phonon coupling on the spectral lineshape of nearly degenerate four-wave mixing in GaAs/AlGaAs quantum wells, in qualitative agreement with experiments. The Fano or asymmetric profile arises from the configurational mixing due to the existence of a spectrum of longitudinal optical phonons.

The details of these theoretical accomplishments are discussed in later sections.



## 2.2 MILLIMETER WAVE NONLINEARITIES IN SUPERLATTICES

The future needs in applications of secure short range communication systems have led us to explore novel millimeter wave interactions with customized materials. We carried out detailed analytical calculations of nonlinear processes in semiconductor superlattices acted upon by external millimeter wave radiation fields. In spite of the amount of experimental data on III-V semiconductor compounds that have been accumulated in the infrared regime, little is known concerning their behavior in 250 GHz regime.

The starting point in the analysis is the coupled charge transport and crystal momentum equations for the motion of the Bloch carriers directed along the direction of the superlattice growth. The polarization state of the radiation field is oriented along the plane of the superlattice structure. Using the Kronig-Penney model for the band structure of the superlattice, we found that the equation of motion for the carrier velocity obeys a Newton's second law of motion. The nonlinearities arise from the radiation field dependence of the superlattice effective mass. That is, the radiation field induces an additional band nonparabolicity.

The results of our study can be summarized as follows. First, the third order susceptibilities were obtained from a Taylor series expansion of the superlattice effective mass. The expansion is valid provided that the superlattice Rabi flopping frequency ( $\Omega = q d E/h$ ) is less than the radiation frequency  $\omega$ . Here  $q$  is the charge of the carrier,  $d$  is the period of the superlattice,  $E$  is the amplitude of the radiation field and  $h$  is the Planck constant. For radiation fields oscillating at 250 GHz and a superlattice period of 150 Å, the maximum field strength is 690 V/cm in order for the Taylor series expansion to be valid. A direct calculation showed that the third order millimeter wave susceptibilities is inversely proportional to the oscillation frequency to the fourth power, and is proportional to the density of carriers and the superlattice periodicity to the second power. We applied the formula to the case of GaAs/AlGaAs, InAs/GaSb and HgTe/CdTe superlattices, and found that typical values of the third order susceptibilities are of the order of  $10^{-2}$  esu at 250 GHz and doping density of  $10^{16}\text{cm}^{-3}$ . These large third order millimeter wave susceptibilities indicate that semiconductor superlattice can support strong nonlinear effects with small intensity requirements. Second, we were able to solve exactly the equation of motion for the case of a single input millimeter wave beam, and found that the nonlinear polarization density is proportional to  $J_0(R) + J_2(R)$ ; where  $R$  is the ratio of the superlattice Rabi flopping to radiation frequencies, and  $J_0$  and  $J_2$  are the Bessel functions of zeroth and second order, respectively. The sum of the Bessel functions have a null for  $R=3.8$  using 250 GHz radiation and superlattice period of 150 Å. At this point, the millimeter wave field can propagate in the superlattice without loss in energy or beam spreading due to diffraction. That is, the phenomenon of self-induced transparency is intrinsic to

these materials. A numerical estimate of the condition for the observation of the self-induced transparency gives a critical field strength of 3.9 kV/cm at 250 GHz. And last, we calculated the conditions for the generation of third harmonic signals. We found that the third harmonic signal achieves a maximum at the point of self-induced transparency, provided that phase matching condition is satisfied. These results indicate that appropriate choices of nonlinear interaction length can render either nonlinear optical phenomena negligible. Hence selectivity of each of the phenomena can be achieved through material growth. The efficiency of the third harmonic signal is approximately 0.1 % for an interaction length of 0.04 mm. A practical obstacle to the realization of these predictions is the limitation in size imposed by the present state-of-the-art growth techniques of the superlattice structures. To test the limits of the MBE technique, we have successfully grown a 10 micron structure consisting of Si-doped 100-A-period GaAs/AlGaAs superlattice using Hughes in-house MBE system (funded by Hughes IRD). The photoluminescence of the samples showed unique features attributed to the 2-dim behavior. Hence, the growth technique appeared to be practical if extended to larger samples. More detailed descriptions are to be found in Appendix A.

### **2.3 NONLINEAR OPTICS AND LASING PROPERTIES OF SEMICONDUCTOR QUANTUM DOTS**

We carried out detailed analyses of the optical properties of semiconductor quantum dots. These unique 0-Dim systems are characterized by the delta function dependence on energy of the density-of-states. Hence they behave much like atoms or molecules. That is, the oscillator strength is concentrated at discrete energies, unlike the case of bulk semiconductors. We exploited the similarities of quantum dots and atomic systems to obtain the nonlinear response functions of the former.

The results of our calculations are summarized as follows. First, there exists three distinct regimes of quantization for the dots. If the Bohr radii of the electron and hole are larger than the dot size, then the energy of the carriers are determined by the particle-in-the-box quantization. If either of the Bohr radius of the electron or hole is larger than the dot size, then there exists an effective Coulombic potential that changes the particle-in-the-box quantization energy. However if the Bohr radii of both electron and hole are less than the dot size, then an exciton is formed inside the dot. The energy of the exciton is determined by the binding energy and the quantum confinement of the center of mass motion of the exciton. We found that enhancement of optical nonlinearities can occur only in the last regime. Second, applying the effective mass approximation to the band structure of the quantum dots in the presence of near resonant radiation fields, we found that the

exciton experiences dynamic Stark shift. We calculated the dressed atom energy levels and showed that the saturation intensity is enhanced in the regime where the Bohr radii of the electron and hole is smaller than the dot size. These results are in agreement with recent experiments performed with CdS quantum dots, which satisfy the exciton confinement criterion<sup>26</sup> Third, we analyzed the possibility of coherent energy transfer between two optical beams in a medium composed of quantum dots. Using the density matrix equations we found that exciton confinement will enhance the two-beam coupling process. The energy transfer depends on the ratio of the frequency mismatch between the probe and the pump to the pump detuning from resonance. The strength of the gain coefficient is proportional to the magnitude of the exciton-phonon coupling constant. No experiments have been done to confirm these predictions. The details of the analysis are attached in Appendices B, C and D

A major effort was undertaken in order to understand the impact of quantum dots on optoelectronics. The operating characteristics of a quantum dot laser were analyzed in the regime where the radii of the electron and hole were large compared to the dot size. Using the quantum transport equations for the population and optical coherence, we calculated the threshold condition for lasing as a function of dot size, for specific values of the decay constants and cavity losses. We found that the threshold current density decreases for smaller dots. For example, the threshold current density of 16 A/cm<sup>2</sup> for dot size of 150 Å was reduced to 10 A/cm<sup>2</sup> for dot size of 50 Å. The oscillation wavelength at the latter dot dimension will be in the 6000 Å range, indicating the possibility of producing visible radiation using quantum dots as the gain media. Furthermore, the gain profile is symmetric around the transition frequency due to the delta function dependence of the zero-dimensional density-of-states. We also found that the threshold current density is independent of the temperature, which is a major improvement in comparison with quantum well and bulk semiconductor lasers. Hence quantum dot lasers, if fabricated in the future, will provide a quantum jump in the field of optoelectronics by lowering the threshold current and relaxing the temperature requirements which limits the performance of current state-of-the art systems. A detailed description is to be found in section 4 of this report.

## **2.4 OPTICAL PHYSICS OF PHOTOREFRACTIVE MATERIALS**

We found a solution to the controversial problem of sublinear intensity dependence of the erasure rate in barium titanate. We attribute the origin of the sublinear behavior to the presence of shallow traps in the insulating material. The current model of Kukhtarev et al <sup>22</sup> does not give results consistent with experiments, in spite of its seemingly good quantitative (with suitable large

number of fitting parameters) explanation of macroscopic nonlinear optical processes in photorefractive materials.

Assuming a shallow impurity band profile, we calculated the space charge field in the presence of shallow level recombination and detrapping processes. Rate equations for the free carrier, shallow impurity band and deep level recombination centers are used to obtain the change in the index of refraction mediated by the electro-optic effect. The results can be summarized as follows. First, the decay rate is proportional to the light intensity raised to a rational fraction of magnitude less than unity, in qualitative agreement with all published optical experimental data. This behavior arises solely from the structure of the shallow impurity band, in contradiction with recent theoretical model based on a single shallow impurity level. The single impurity-level model requires a many-parameter fit to the experimental data. The formation of the impurity band arises from the overlapping of the Bohr radii of adjacent shallow impurities. A simple calculation indicated that the density of impurities required for the band formation is of the order of  $10^{16}\text{cm}^{-3}$ . This numerical estimate is in agreement with recent data obtained from detailed characterization of barium titanate. Second, The rational fraction or exponent is linearly proportional to the temperature of the sample and is a function of the spatial grating wavenumber. The latter arises from the work done by the space charge field on the free carriers. This result agrees with the experiments of Chang.<sup>27</sup> And last, the analytical solutions predict that the response time is an exponentially decreasing function of temperature. This behavior is due to the Fermi-Dirac distribution and the density of states of the impurity band. This theoretical model also predicts that the effective width of the impurity band is approximately 0.5 eV for barium titanate, although no identification of the shallow impurity is allowed in the model. This result reproduces the experimental data of Rytz et al.<sup>28</sup>

We also explored the origin of self-starting temporal oscillation in self-pumped photorefractive mirrors. We attribute the origin of oscillation to the induced photovoltaic field inside the barium titanate crystal. Typical measured values of the photovoltaic field are of the order of 100 V/cm. Using the charge transport and Maxwell's equations, we solved for the temporal response of the space charge field as a function of the input laser intensity. The photovoltaic effect is included in the rate equations as the product of the electron and deep-level recombination center densities. The results indicated that the backscattered phase conjugate signal oscillates as a function of time. The oscillation period decreases as the laser intensity is increased, in agreement with recent experiments.<sup>29,30</sup>

The details of the work are given in Appendices E and F.

## 2.5 RESONANTLY ENHANCED SELF-PUMPED PHASE CONJUGATION

An analysis of the mechanism that produces self-pumped phase conjugation in resonant materials was made using the coupled density matrix and Maxwell's equations. The results of our analysis identified the start-up conditions for the formation and coherent amplification of scattered noise. The starting mechanism is the production of resonance fluorescence, which is coherent with the input radiation field. The build up of the fluorescence or noise field is achieved through the formation of a traveling wave grating produced by the interference between the fluorescence and input fields, and followed by the coherent scattering of the pump field from the traveling wave grating. The generation of the phase conjugate field can be achieved in two distinct manner. The first one involves the stimulated backscattering of the input field from the traveling wave grating, and this mechanism does not require the presence of an optical cavity. The second scheme uses a linear optical cavity to take advantage of the forward going energy transfer process. The purpose of the optical cavity is to store the fluorescence radiation in a standing wave pattern. Coherent scattering of one of the standing wave component from the traveling wave grating produces a phase conjugate field. The latter is just the standard degenerate four-wave mixing configuration.

The solution of the density matrix equations provides the macroscopic polarization density, which is used in the wave equation to obtain a self-consistent, new radiation field. The density matrix equations are solved in two steps. First, we found the exact solution for the input field alone. Then these solutions are used to obtain the polarization density and gain condition in the presence of noise fields. We found that the coherent amplification of the noise field can only occur provided that the intensity of the input field is large compared with the medium saturation intensity. If the input field is tuned to resonance, the gain profile of the noise as a function of the difference frequency between the input field and noise has two symmetrical sidelobes, whose separation is equal to the Rabi flopping frequency. If the input field is detuned from resonance, the gain profile is asymmetrical such that amplification of the noise only occurs for either frequency upshift or downshift, but not both. The physical explanation of this result lies in the dynamical behavior of atomic states induced by strong radiation field. That is, the input field produces a dressed state of the system of atoms and radiation field, and gain occurs from a near degenerate four-wave mixing process taking place among each component of the dressed atom. Hence amplification of noise can occur provided that the input field is above saturation. The gain profile determines the frequency shift acquired by the phase conjugate field.

In order to verify the physical mechanism responsible for the production of phase conjugate fields, we demonstrated the first self-pumped phase conjugate mirror in cesium vapor at 0.852 micron. We used a linear cavity configuration which consists of a cesium cell enclosed between two

curved high reflecting mirrors. The incoming CW laser beam was directed into the cesium cell at an angle on the order of half a degree, leading to a large overlap between the input beam and resonator modes. A measured but un-optimized reflectivity of approximately 0.1% and a threshold intensity of  $35 \text{ W/cm}^2$  were observed. This elegant experiment confirmed the key mechanism in resonantly enhanced self-pumped phase conjugation. That is, energy transfer between the input beam and the induced resonance fluorescence provides a means of setting up the gratings from which coherent scattering of the radiation fields can take place. It just needs one single input aberrated beam to achieve such a nonlinear optical process.

Furthermore, we have extended our calculation beyond the two-level model in order to study the generation of self-pumped phase conjugate fields in rhodamine 6G. Experimental studies by Ivakin et al<sup>31</sup> and Lam et al<sup>32</sup> indicated the presence of phase conjugate fields when the organic dye was illuminated by an intense laser pulse. The experimental studies was performed with a mode locked 10-ns pulse emitted from a double YAG laser system, and a focused intensity at the dye cell of approximately  $1 \text{ MW/cm}^2$ . In order to understand the experimental data, we modelled the organic dye in terms of a 3-level system. Following the procedure stated above for the 2-level system, we calculated the nonlinear polarization density, and found that the gain profile of the amplified signal is consistent with the wide bandwidth (300 Å) obtained from the experiments.

The results of this work open up the distinct practical application of self-pumped phase conjugation using semiconductor lasers. A scenario will be the implementation of satellite-to-satellite secure communication links using high power semiconductor lasers. This unique phase conjugate mirror can be modulated at gigahertz rate, has a low threshold intensity (tens of  $\text{W/cm}^2$ ) for start-up operation, and possesses a negligible frequency shift (within the laser linewidth).

The details of the analysis and experiments are compiled in Appendices G, H, I and J.

## 2.6 OPTICAL NONLINEARITIES IN HgTe/CdTe SUPERLATTICES AND THEIR APPLICATIONS TO $10.6 \mu\text{m}$ SENSOR PROTECTION

An analysis of the mechanism responsible for optical nonlinearities in HgTe/CdTe superlattices was carried out. Using the heat equation, we calculated the change in the electron temperature and the associated change in the dielectric constant due to the action of radiation fields in the nearly degenerate four-wave mixing geometry. The results indicate that the third order optical nonlinearity is inversely proportional to the radiation frequency to the second power, effective mass and electronic specific heat. The nearly degenerate four-wave mixing spectral linewidth is determined by the larger of the electron thermalization or diffusion rate. Exploiting the small effective mass ( $m^* < 0.001 m_0$ ) of HgTe/CdTe, one finds that the third order susceptibilities are

approximately of the order of  $10^{-3}$  esu at  $10.6\text{ }\mu\text{m}$ . This large value makes it feasible to observe optical nonlinearities using low power lasers. An experiment was performed at Hughes (funded by Hughes IRD) using in-house grown samples of HgTe/CdTe superlattices (tailored for  $\text{CO}_2$  laser). The experiments involved the detection of phase conjugate signal at  $10.6\text{ }\mu\text{m}$  in the degenerate four-wave mixing geometry. The estimated value of the susceptibilities is of the order of  $10^{-4}$  esu for sample of HgTe/CdTe superlattices, in reasonable agreement with theory. The speed of response of these materials has not been measured. However they are expected to be fast (subnanosecond time scale) due to the electronic relaxation process.

HgTe/CdTe superlattices show a linear absorption spectral profile that is nearly flat extending from  $9.0$  to  $12.0\text{ }\mu\text{m}$ . This feature could provide a significant advantage if they can be used in a sensor protection scenario. We proposed the use of laser beam bending in HgTe/CdTe superlattices as a possible scheme for protecting FLIR against laser threats. The concept of laser beam bending relies on the formation of a light induced prism in a nonlinear optical material. The formation of a prism is possible provided that the laser beam has an asymmetric intensity distribution. The proposed device is assumed to be located at the focal point of the optical train in the sensor. Although the input optical power at the aperture could be small, the intrinsic magnification (approximately  $10^6$ ) of the sensor will provide a high intensity beam at the focal spot. We used the value of the third order optical susceptibilities in superlattices to calculate the operating characteristics of such a device. We found that the sensor protection device has the following features. It has a dynamic range of  $10^4$ , a threshold intensity at the input aperture plane of few tens of milliwatts per centimeter squared, a wide field of view, an operating bandwidth extending from  $9$  to  $12\text{ }\mu\text{m}$ , and a response time of less than one nanosecond. However the main drawback of the HgTe/CdTe superlattice material is the large absorption coefficient which puts a limit on the allowed transmitted intensity of the image to the detector.

## 2.7 FOUR-WAVE MIXING SPECTROSCOPY OF GaAs/AlGaAs QUANTUM WELLS

We explored the role of longitudinal optic phonon coupling to a Wannier exciton in GaAs/AlGaAs quantum wells. In spite of the magnitude of the LO phonon interaction energy of  $34\text{ meV}$ , current theoretical models do not include its effect in the dynamics of the excitonic transitions, except for a phenomenological decay rate in the exciton population. We used the Davydov Hamiltonian to study the four-wave mixing spectra in the weak optical signal regime. A perturbation calculation to third order in the radiation field was carried out from the coupled exciton-phonon-field equations. The results of our preliminary studies point to the following

conclusions. If only one phonon mode is considered, then the nearly degenerate four-wave mixing spectrum shows a symmetric profile as a function of the frequency difference between the pump and the probe. However if a multiple phonon structure is inserted in the calculation, the four-wave mixing spectra exhibits an asymmetric profile similar to that found in the Fano effect of atomic spectra. A simple physical explanation can be given. In the presence of multiple phonon modes, there exists a configurational mixing leading to a competition between different phonon modes. In a nutshell, the competition leads to an interference effect that cancels all contributions in certain portions of the spectra profile.

Furthermore, we were able to solve analytically the strong pump/weak probe regime. The results indicate that intrinsic optical bistability is present. The phase conjugate reflectivity should exhibit cavity-free optical bistability for a critical value of the pump intensity. Current four-wave mixing experiments are performed in the regimes where all input radiation fields are either below or above saturation. However, there exists no observation of the intrinsic bistable behavior.

The physics and analytical solutions have been communicated to the experimental group of Prof. Duncan Steel at the University of Michigan.



### SECTION 3

#### U.S. ARMY LABORATORY, CONFERENCE AND UNIVERSITY PRESENTATIONS

1. Theory of four-wave mixing processes in quantum dots  
Juan F. Lam  
Gordon Research Conference on Nonlinear Optics and Lasers  
Brewster Academy, Wolfeboro, New Hampshire  
July 1987
2. Theory of Transient self-pumped phase conjugation in photorefractive materials  
Juan F. Lam  
OSA Topical Meeting on Photorefractive Materials, Effects and Devices  
Juan F. Lam  
University of California, Los Angeles  
August 1987
3. Four-wave mixing spectroscopy of stat-selective collisions in gases and solids  
Juan F. Lam  
Third International Laser Science Conference  
Atlantic City, New Jersey  
November 1987
4. Theory of enhanced optical nonlinearities in quantum dots  
Juan F. Lam  
SPIE Conference on Quantum Wells and Superlattices II  
Newport Beach, California  
March 1988
5. Nonlinear optics of semiconductor in zero- and one-dimensional systems  
Juan F. Lam  
The IBM Seminar of the Center for Electronic Materials  
Pennsylvania State University  
April 1988
6. Enhanced optical nonlinearities in quantum dots: theory and applications  
Juan F. Lam  
CLEO 88  
Anaheim, California  
April 1988
7. Theory of self-pumped phase conjugation  
Juan F. Lam  
International Conference on Nonlinear Optical Phenomena  
Ashford Castle, Ireland  
May 1988

8. Millimeter wave nonlinearities in superlattices  
J.F. Lam, B.D. Guenther, R.A. McFarlane and D.D. Skatrud  
IQEC'88  
Tokyo, Japan  
July 1998
9. Nonlinear optics of semiconductor in zero- and one-dimensional systems  
Juan F. Lam  
Departments of Physics and Electrical Engineering  
The University of Michigan  
September 1988
10. Nonlinear Optics in quantum dots  
Juan F. Lam  
Department of Physics  
Duke University  
March 1989
11. Optical properties of quantum dots  
Juan F. Lam  
CECOM Electronic and Device Laboratory  
Fort Monmouth, New Jersey  
March 1989
12. Optical properties of quantum dots  
Juan F. Lam  
U.S. ARMY Harry Diamond Laboratories  
Adelphi, Maryland  
March 1989
13. On the origin of sublinear intensity dependence in photorefractive materials  
Juan F. Lam  
CLEO'89  
Baltimore, Maryland  
April 1989
14. Laser spectroscopy of semiconductor quantum dots  
Juan F. Lam  
9th International Conference on Laser Spectroscopy  
Bretton Woods, New Hampshire  
June 1989
15. Physics and Applications of novel nonlinear optics  
Juan F. Lam  
Department of Electrical Engineering  
UCLA  
September 1989

16. Temporal oscillation of two-wave mixing gain in pressure broadened sodium vapor  
C.J. Gaeta and J.F. Lam  
IQEC'90  
Anaheim, California  
May 1990
17. Optical response in photorefractive materials  
Juan F. Lam  
CLEO'90  
Anaheim, California  
May 1990
18. Self-pumped phase conjugation in cesium vapor  
C.J. Gaeta and J.F. Lam  
IEEE/LEOS Conference on Nonlinear Optics  
Kauai, Hawaii  
July 1990

## **SECTION 4**

### **INVENTION DISCLOSURE: QUANTUM DOT LASERS**

During the course of our theoretical studies, an invention disclosure on the operating characteristics and fabrication technique of quantum dot lasers was submitted. A detailed description is attached to this section. Hughes Aircraft Company decided not to file for patent protection.

## 1. TITLE OF INVENTION

QUANTUM DOT LASERS

## 2. INVENTOR(S)

NAME	PAYROLL NO	SOURCE CODE	LOC	BLDG	MS	PHONE	DEPARTMENT HEAD
Juan F. Lam	65683	30   27   30	MA	250	RL65	317-5929	Giuliano

## 3. PROOF OF CONCEPTION

A. BY WHOM WAS FIRST DRAWING MADE?	DATE	TIME SPENT	ACCT. CHARGED	LOCATION OF FIRST DRAWING
Juan F. Lam	8-25-88	8 hrs	BD10LT	
B. BY WHOM WAS FIRST DESCRIPTION WRITTEN?	DATE	TIME SPENT	ACCT. CHARGED	LOCATION OF FIRST DESCRIPTION
Juan F. Lam	8-24-88	8 hrs	BD10LT	
C. TO WHOM WAS INVENTION FIRST DISCLOSED?	DATE			
B.D. Guenther, ARO	1-30-88			

## 4. REDUCTION TO PRACTICE

A. WAS A DEVICE EMBODYING THE INVENTION CONSTRUCTED AND TESTED OR THE PROCESS PRACTICED?	YES ( ) NO (X)	BY WHOM	DATE STARTED	DATE COMPLETED	TIME SPENT
B. ACCT. CHARGED - TIME	ACCT. CHARGED - MATERIAL				
C. PRESENT LOCATION OF DOCUMENTS (DATE SIGNED AND WITNESSED), INCLUDING PHOTOS, DWGS. AND DATA SHEET: SHOWING REDUCTION TO PRACTICE.					

NOTE: ALL EVIDENCE OF CONCEPTION (FIRST DRAWING AND FIRST WRITTEN DESCRIPTION) AND EVIDENCE OF REDUCTION  
TO PRACTICE (DEVICE EMBODYING THE INVENTION AND TEST DATA) MUST BE RETAINED.

## 5. WORK ASSIGNMENT

INDICATE BY ACCT. NO. AND TITLE PROJECTS TO WHICH YOU CHARGED TIME DURING THE PERIOD WHEN YOU WORKED ON THIS DEVELOPMENT.	
ACCT. NO.: BD10LT	PROJECT NAME: Nonlinear Optical Properties of Novel Materials
ACCT. NO.:	PROJECT NAME:

## 6. RELATED DOCUMENTS

A. IS THERE A PUBLICATION RELATED TO THE INVENTION?	YES (X) NO ( )	DATE	IDENTIFY PRINTED PUBLICATION
B. ARE THERE ANY RELATED INVENTION DISCLOSURES OR PATENT APPLICATIONS	YES ( ) NO ( )	DATE	IDENTIFY PD NO. ETC.
C. ARE THERE ANY PROPOSALS OR REPORTS OR OTHER DOCUMENTS RELATING TO THIS INVENTION?	YES (X) NO ( )	DATE	IDENTIFY PROPOSAL, REPORT OR DOCUMENT

Semi-annual ARO Report 1-30-

## 7. SALE

HAS PRODUCT EMBODYING INVENTION OR MADE BY INVENTION BEEN SOLD OR OFFERED FOR SALE?	YES ( ) NO (X)	ORDER NO.	ORDER DATE	DELIVERY DATE	DATE OFFERED
--	-------------------	-----------	------------	---------------	--------------

## 8. DEVELOPMENT

A. IDENTIFY COMPANY PRODUCT DEVELOPMENT BY NAME AND/OR NUMBER, IF ANY.
B. IDENTIFY SUPPORTING GENERAL R AND D ENGINEERING BY NAME, PROJECT NO. AND YEAR, OR BID AND PROPOSAL EXPENSE, IF ANY.
C. IDENTIFY SUPPORTING CONTRACT BY TITLE AND CONTRACT NUMBER, IF ANY.

## HUGHES PROPRIETARY

THIS DOCUMENT CONTAINS PROPRIETARY INFORMATION, AND EXCEPT WITH WRITTEN PERMISSION OF  
HUGHES AIRCRAFT COMPANY, SUCH INFORMATION SHALL NOT BE PUBLISHED, OR DISCLOSED TO  
OTHERS OR USED FOR ANY PURPOSE, AND THE DOCUMENT SHALL NOT BE DUPLICATED IN WHOLE OR IN  
PART. THIS LEGEND SHALL BE APPLIED TO ALL DOCUMENTS CONTAINING THIS INFORMATION. IF  
REPORTED UNDER A CONTRACT, THE TERMS AND CONDITIONS THEREOF SHALL APPLY.  
SIGNATURE INVENTOR8/25/88  
DATE

236 CS JUN 81

SIGNATURE INVENTOR

DATE

PATENT DOCKET NO.

## 9. SUMMARY OF THE INVENTION

SHEET 2 OF 17

A. GIVE A BRIEF DESCRIPTION OF YOUR INVENTION, PARTICULARLY POINTING OUT WHAT IS BELIEVED TO BE NOVEL (THE "HEART" OF WHAT IS NEW)

A set of quantum dots, fabricated by means of focused ion beam induced interdiffusion technique, is the gain medium inside an optical cavity. Application of external current sources through a pn junction system leads to oscillation and coherent emission of radiation. The materials that make up the quantum dots are from III-V, II-VI and quaternary compound semiconductors.

B. EXPLAIN PURPOSE AND ADVANTAGES OF YOUR INVENTION (WHAT WILL THE INVENTION DO BETTER THAN DONE PREVIOUSLY?)

The advantages of this laser over the current semiconductor bulk and quantum well lasers are;

1. ultralow threshold current density for oscillation, typically few amperes per centimeter square.
2. symmetric gain profile due to the 0-Dim density of states.
3. the threshold current density is insensitive to the operating temperature ( due to the 0-Dim density of states ).
4. Artificially controlled frequency of oscillation of the emitted radiation.

The advantage of this quantum dot laser over the current quantum dot laser concepts is the use of a novel fabrication technique, that is, focused ion beam induced interdiffusion. This technique does not require the use of reactive ion etching, followed by epitaxial re-growth. Focused ion beam induced interdiffusion was pioneered by Y. Hirayama, Y. Suzuki, S. Tarucha and H. Okamoto, Japan. J. Appl. Phys. 24, L516 (1985)

## HUGHES PROPRIETARY

THIS DOCUMENT CONTAINS PROPRIETARY INFORMATION, AND EXCEPT WITH WRITTEN PERMISSION OF HUGHES AIRCRAFT COMPANY, SUCH INFORMATION SHALL NOT BE PUBLISHED, OR DISCLOSED TO OTHERS, OR USED FOR ANY PURPOSE, AND THE DOCUMENT SHALL NOT BE DUPLICATED IN WHOLE OR IN PART. THIS LEGEND SHALL BE APPLIED TO ALL DOCUMENTS CONTAINING THIS INFORMATION. IF REPORTED UNDER A CONTRACT, THE TERMS AND CONDITIONS THEREOF SHALL APPLY.



SIGNATURE INVENTOR

8/25/88  
DATE

PATENT DOCKET NO.

SIGNATURE INVENTOR

DATE

READ AND UNDERSTOOD BY:

WITNESS NAME (TYPE)

SIGNATURE

DATE

WITNESS NAME (TYPE)

SIGNATURE

DATE

EACH PAGE UPON WHICH INFORMATION IS ENTERED SHOULD BE SIGNED AND WITNESSED.

## 9. SUMMARY OF THE INVENTION (Continued)

SHEET 3 OF 17

C STATE THE IMPACT OF YOUR INVENTION ON COMPANY BUSINESS OR PRODUCT LINES OR ON POTENTIAL COMMERCIAL APPLICATIONS OR USE BY OTHERS. PLEASE FEEL FREE TO INCLUDE ANY OTHER INFORMATION WHICH YOU THINK MAY HELP THE INVENTION EVALUATION COMMITTEE DECIDE WHETHER A PATENT APPLICATION SHOULD BE FILED.

Diode lasers are components in current and future communication systems. There exists a need to lower the energy consumption, in terms of the threshold current density required to achieve oscillation inside the cavity. The quantum dot lasers promises to have threshold density which is four orders of magnitude below that of bulk diode lasers, and two orders of magnitude below that of quantum well lasers. Furthermore, quantum dot lasers offer the flexibility of a tunable bandgap, leading to the design of lasers oscillating at different frequencies. The tunability is insured by the quantum confinement properties of such lasers.

D IDENTIFY THE PRIOR ART KNOWN TO YOU WHICH IS IMPROVED UPON OR DISPLACED BY YOUR INVENTION. AND STATE IN DETAIL, IF KNOWN, THE DISADVANTAGES OF THE CLOSEST PRIOR ART.

The concept of quantum dot lasers have been the subject of discussion in the last coupled of years, with no practical implementation of a real quantum dot system. Listed below are the publications related to this device,

1. Y. Arakawa and H. Sasaki, Appl. Phys. Lett. 40, 939 (1982). A theoretical analysis of quantum confined lasers, i.e. bulk, well, wire and dot. First analysis of temperature dependence.
2. M. Asada, Y. Miyamoto and Y. Suematsu, IEEE J. Quantum Electron. QE-22, 1915 (1986). A theoretical discussion of gain and threshold properties of quantum dot lasers.
3. Y. Miyamoto, M. Cao, Y. Shingai, K. Furuya, Y. Suematsu, K.G. Ravikumar and S. Arai, Japan. J. Appl. Phys. 26, L225 (1987) First attempt to make a quantum dot laser.

## HUGHES PROPRIETARY

THIS DOCUMENT CONTAINS PROPRIETARY INFORMATION, AND EXCEPT WITH WRITTEN PERMISSION OF HUGHES AIRCRAFT COMPANY, SUCH INFORMATION SHALL NOT BE PUBLISHED, OR DISCLOSED TO OTHERS, OR USED FOR ANY PURPOSE, AND THE DOCUMENT SHALL NOT BE DUPLICATED IN WHOLE OR IN PART. THIS LEGEND SHALL BE APPLIED TO ALL DOCUMENTS CONTAINING THIS INFORMATION. IF REPORTED UNDER A CONTRACT, THE TERMS AND CONDITIONS THEREOF SHALL APPLY

  
SIGNATURE INVENTOR

8/25/88  
DATE

PATENT DOCKET NO

SIGNATURE INVENTOR

DATE

READ AND UNDERSTOOD BY

WITNESS NAME (TYPE)

SIGNATURE

DATE

WITNESS NAME (TYPE)

SIGNATURE

DATE

EACH PAGE UPON WHICH INFORMATION IS ENTERED SHOULD BE SIGNED AND WITNESSED

# 10. DETAILED DESCRIPTION

SHEET 4 OF 17

DESCRIBE YOUR INVENTION IN DETAIL, USING NECESSARY ADDITIONAL SHEETS.

A. BE SURE THAT EACH SHEET IS DATED AND SIGNED BY EACH INVENTOR AND TWO WITNESSES.  
(HAC FORM 236 B CS SHOULD BE USED, IF PRACTICAL)

B. ATTACH PRINTS OF DRAWINGS OR SKETCHES HELPFUL IN UNDERSTANDING HOW YOUR INVENTION WORKS.

C. IF YOUR INVENTION HAS BEEN TESTED BRIEFLY SUMMARIZE THE TEST RESULTS WHICH CONFIRM THE  
FUNCTIONS AND ADVANTAGES LISTED IN (9B) ABOVE.

## PRINCIPLES OF QUANTUM DOTS

Quantum dots or quantum confined semiconductors in 0-Dim arise when the dimension of the box is less than the deBroglie wavelength of the charge carriers. For typical semiconductor materials, the deBroglie wavelength is of the order of few hundred angstroms. Under the condition of simultaneous confinement of the charge carriers along three dimensions, the motion of the charge carriers is determined by the law of quantum mechanics, i.e. particle confined to a box. The properties of quantum dots are,

1. The density of states is a sum of Dirac delta functions.
2. The energy levels of the electron or holes are determined by quantization in a box.
3. The transition moment and the selection rules for electric dipole allowed transtion are determined by the matrix elements of the electric dipole moment, and under certain design, they show enhanced values over that of the bulk materials.

These three properties are crucial to the operation of the quantum dot lasers.

## OPERATING CHARACTERISTICS OF THE QUANTUM DOT LASERS IN THE PARTICLE QUANTIZATION REGIME

By particle quantization regime, we imply that the kinetic energy of the charge carrier is large compared to the Coulomb binding energy. In this case, the allowed energy levels of the particle ( electron and hole ) are calculated by solving the Schroedinger equation in all three dimensions. Figure 1 indicates the allowed energy levels in both the conduction and valence bands of a direct transition.

## HUGHES PROPRIETARY

THIS DOCUMENT CONTAINS PROPRIETARY INFORMATION, AND EXCEPT WITH WRITTEN PERMISSION OF HUGHES AIRCRAFT COMPANY, SUCH INFORMATION SHALL NOT BE PUBLISHED, OR DISCLOSED TO OTHERS, OR USED FOR ANY PURPOSE, AND THE DOCUMENT SHALL NOT BE DUPLICATED IN WHOLE OR IN PART. THIS LEGEND SHALL BE APPLIED TO ALL DOCUMENTS CONTAINING THIS INFORMATION. IF REPORTED UNDER A CONTRACT, THE TERMS AND CONDITIONS THEREOF SHALL APPLY

  
SIGNATURE INVENTOR

8/25/88  
DATE

PATENT DOCKET NO.

SIGNATURE INVENTOR

DATE

READ AND UNDERSTOOD BY:

WITNESS NAME (TYPE)

SIGNATURE

DATE

WITNESS NAME (TYPE)

SIGNATURE

DATE

TEACH PAGE UPON WHICH INFORMATION IS ENTERED SHOULD BE SIGNED AND WITNESSED:



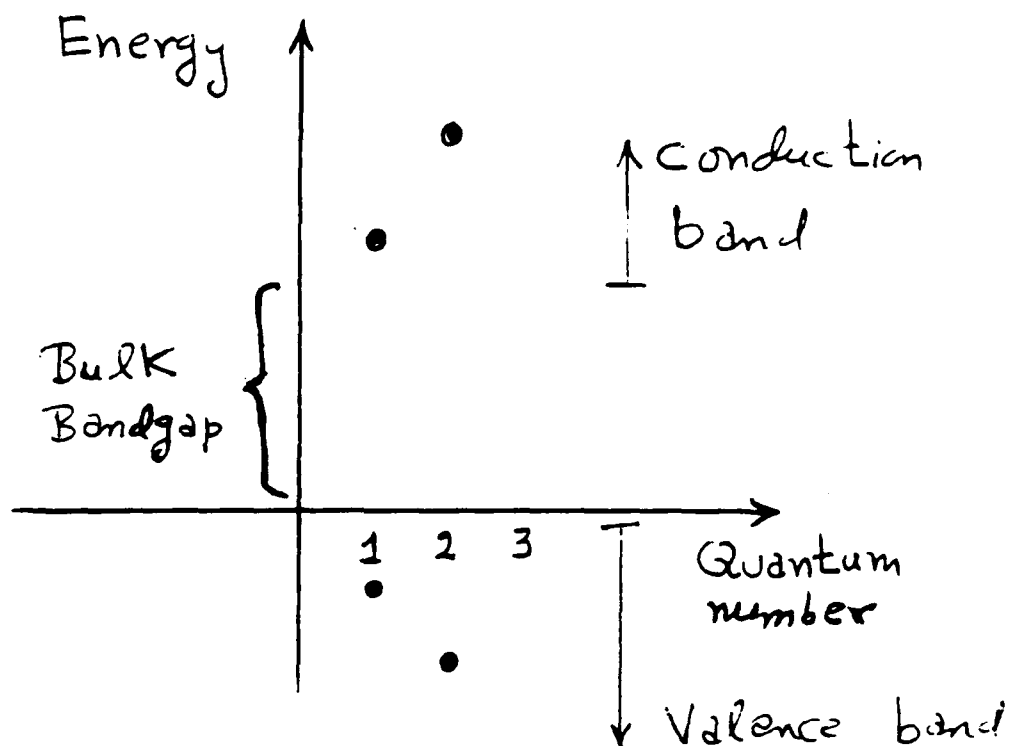


Figure 1. Allowed energy levels vs. quantum number for a quantum dot system. The black circles are the allowed energies for the conduction and valence bands

### HUGHES PROPRIETARY

THIS DOCUMENT CONTAINS PROPRIETARY INFORMATION, AND EXCEPT WITH WRITTEN PERMISSION OF HUGHES AIRCRAFT COMPANY, SUCH INFORMATION SHALL NOT BE PUBLISHED, OR DISCLOSED TO OTHERS, OR USED FOR ANY PURPOSE, AND THE DOCUMENT SHALL NOT BE DUPLICATED IN WHOLE OR IN PART. THIS LEGEND SHALL BE APPLIED TO ALL DOCUMENTS CONTAINING THIS INFORMATION. IF REPORTED UNDER A CONTRACT, THE TERMS AND CONDITIONS THEREOF SHALL APPLY.

*San L. Lam*  
SIGNATURE INVENTOR

8/25/85  
DATE

PATENT DOCKET NO.

SIGNATURE INVENTOR

DATE

READ AND UNDERSTOOD BY:

WITNESS NAME (TYPE)

SIGNATURE

DATE

WITNESS NAME (TYPE)

SIGNATURE

DATE

(EACH PAGE UPON WHICH INFORMATION IS ENTERED SHOULD BE SIGNED AND WITNESSED)

The calculated selection rules for electric dipole allowed transition is  $n \rightarrow n$ , where  $n$  is a quantum number. The energy separation is given by

$$E_{nm\ell} = E_{gap} + \frac{\hbar^2 \pi^2}{2\mu L^2} (n^2 + m^2 + \ell^2)$$

where  $\mu$  is the effective mass of the electron-hole system.  $n$ ,  $m$  and  $\ell$  are the quantum numbers along each of the direction in space. This formula assumes that the dot is a cube of size  $L$ .

An exact calculation has been performed to evaluate the operating characteristics of a laser composed of quantum boxes. This calculation uses the density matrix equation, and takes into account the band tailing effects and the Fermi-Dirac distribution. Figure 2 describes the model for the start of the analysis.

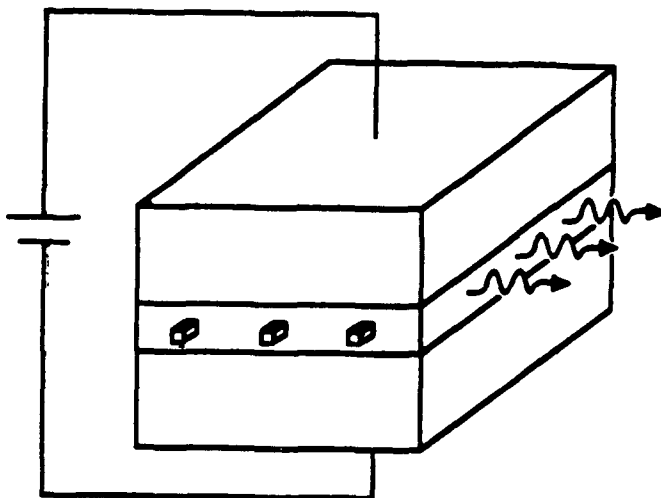


Figure 2. The model used for the analysis of the quantum dot laser

### HUGHES PROPRIETARY

THIS DOCUMENT CONTAINS PROPRIETARY INFORMATION, AND EXCEPT WITH WRITTEN PERMISSION OF HUGHES AIRCRAFT COMPANY, SUCH INFORMATION SHALL NOT BE PUBLISHED, OR DISCLOSED TO OTHERS, OR USED FOR ANY PURPOSE, AND THE DOCUMENT SHALL NOT BE DUPLICATED IN WHOLE OR IN PART. THIS LEGEND SHALL BE APPLIED TO ALL DOCUMENTS CONTAINING THIS INFORMATION. IF REPORTED UNDER A CONTRACT, THE TERMS AND CONDITIONS THEREOF SHALL APPLY.

*Lee T. Lam*  
SIGNATURE INVENTOR

8/25/88  
DATE

SIGNATURE INVENTOR

DATE

READ AND UNDERSTOOD BY:

WITNESS NAME (TYPE)

SIGNATURE

DATE

WITNESS NAME (TYPE)

SIGNATURE

DATE

(EACH PAGE UPON WHICH INFORMATION IS ENTERED SHOULD BE SIGNED AND WITNESSED)

PATENT DOCKET NO.

Figure 3 shows the results of the calculation of the gain vs the injected carrier ( electron ) density for the case of GaInAsP-GaAs dots. The physical parameters used for this calculation are

1. Quantum dots are separated by 1000 angstroms. The effective ratio of the surface area of the quantum dot to the area of the separation is given by  $L^2/(1000)^2$ .
2. The spontaneous emission time was set at 1 nsec.
3. The collision-dominated ( band tailing ) time is .1 psec
4. The net cavity loss ( including the facets ) is set at  $250 \text{ cm}^{-1}$ .

Figure 3 shows a family of curve, each labeled by two numbers. The first one is the size of the cube, and the second number is the threshold current density required for oscillation if the net loss is  $250 \text{ cm}^{-1}$ . One notes that the threshold current density is much lower than that of the bulk materials ( typically of the order of few hundreds kiloamperes per centimeter square ). The calculation was performed for one planar set of quantum dots.

Figure 4 shows the result of the calculation for the gain profile as a function of photon energy. As one can notice, the profile is symmetric about the resonance. The symmetry arises from the Dirac delta function for the density of states of the electrons and holes.

And last, an exact calculation of the threshold current density was performed and it shows that the threshold current density is independent of the operating temperature. This result is unlike the case of bulk lasers, where the threshold current density is exponentially dependent on the temperature. This implies that temperature stability is assured if a quantum dot laser can be fabricated.

## HUGHES PROPRIETARY

THIS DOCUMENT CONTAINS PROPRIETARY INFORMATION, AND EXCEPT WITH WRITTEN PERMISSION OF HUGHES AIRCRAFT COMPANY, SUCH INFORMATION SHALL NOT BE PUBLISHED, OR DISCLOSED TO OTHERS, OR USED FOR ANY PURPOSE, AND THE DOCUMENT SHALL NOT BE DUPLICATED IN WHOLE OR IN PART. THIS LEGEND SHALL BE APPLIED TO ALL DOCUMENTS CONTAINING THIS INFORMATION. IF REPORTED UNDER A CONTRACT, THE TERMS AND CONDITIONS THEREOF SHALL APPLY.

*Len F. Lam*  
SIGNATURE INVENTOR

8/25/83  
DATE

PATENT DOCKET NO.

SIGNATURE INVENTOR

DATE

READ AND UNDERSTOOD BY:

WITNESS NAME (TYPE)

SIGNATURE

DATE

WITNESS NAME (TYPE)

SIGNATURE

DATE

EACH PAGE UPON WHICH INFORMATION IS ENTERED SHOULD BE SIGNED AND WITNESSED

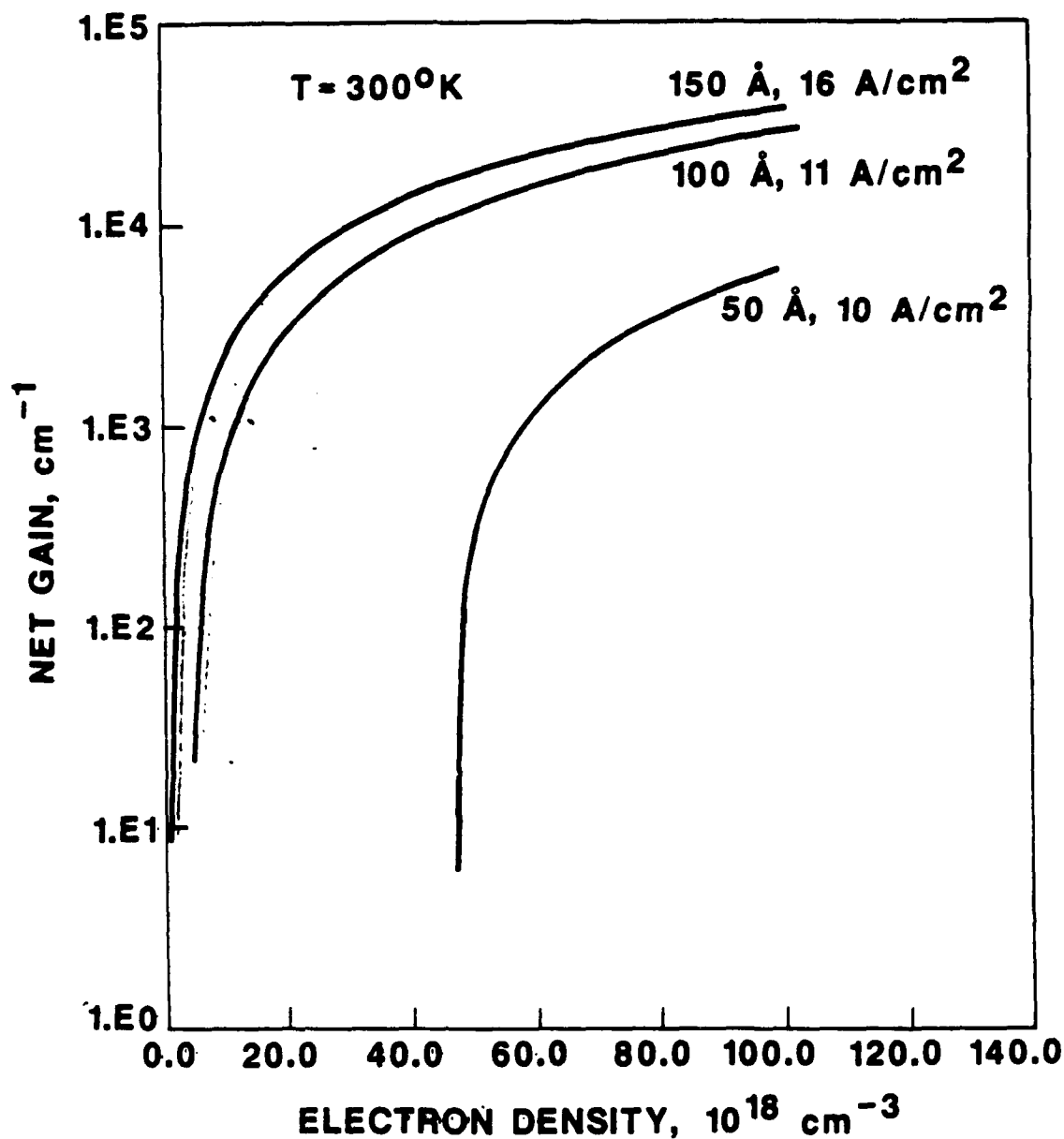



Figure 3. The gain profile as a function of the injected electron density

### HUGHES PROPRIETARY

THIS DOCUMENT CONTAINS PROPRIETARY INFORMATION, AND EXCEPT WITH WRITTEN PERMISSION OF HUGHES AIRCRAFT COMPANY, SUCH INFORMATION SHALL NOT BE PUBLISHED, OR DISCLOSED TO OTHERS, OR USED FOR ANY PURPOSE, AND THE DOCUMENT SHALL NOT BE DUPLICATED IN WHOLE OR IN PART. THIS LEGEND SHALL BE APPLIED TO ALL DOCUMENTS CONTAINING THIS INFORMATION. IF REPORTED UNDER A CONTRACT, THE TERMS AND CONDITIONS THEREOF SHALL APPLY.

 SIGNATURE INVENTOR		8/25/88 DATE
_____ SIGNATURE INVENTOR		_____ DATE
READ AND UNDERSTOOD BY:		
_____ WITNESS NAME (TYPE)	_____ SIGNATURE	_____ DATE
_____ WITNESS NAME (TYPE)	_____ SIGNATURE	_____ DATE

(EACH PAGE UPON WHICH INFORMATION IS ENTERED SHOULD BE SIGNED AND WITNESSED)

PATENT DOCKET NO.

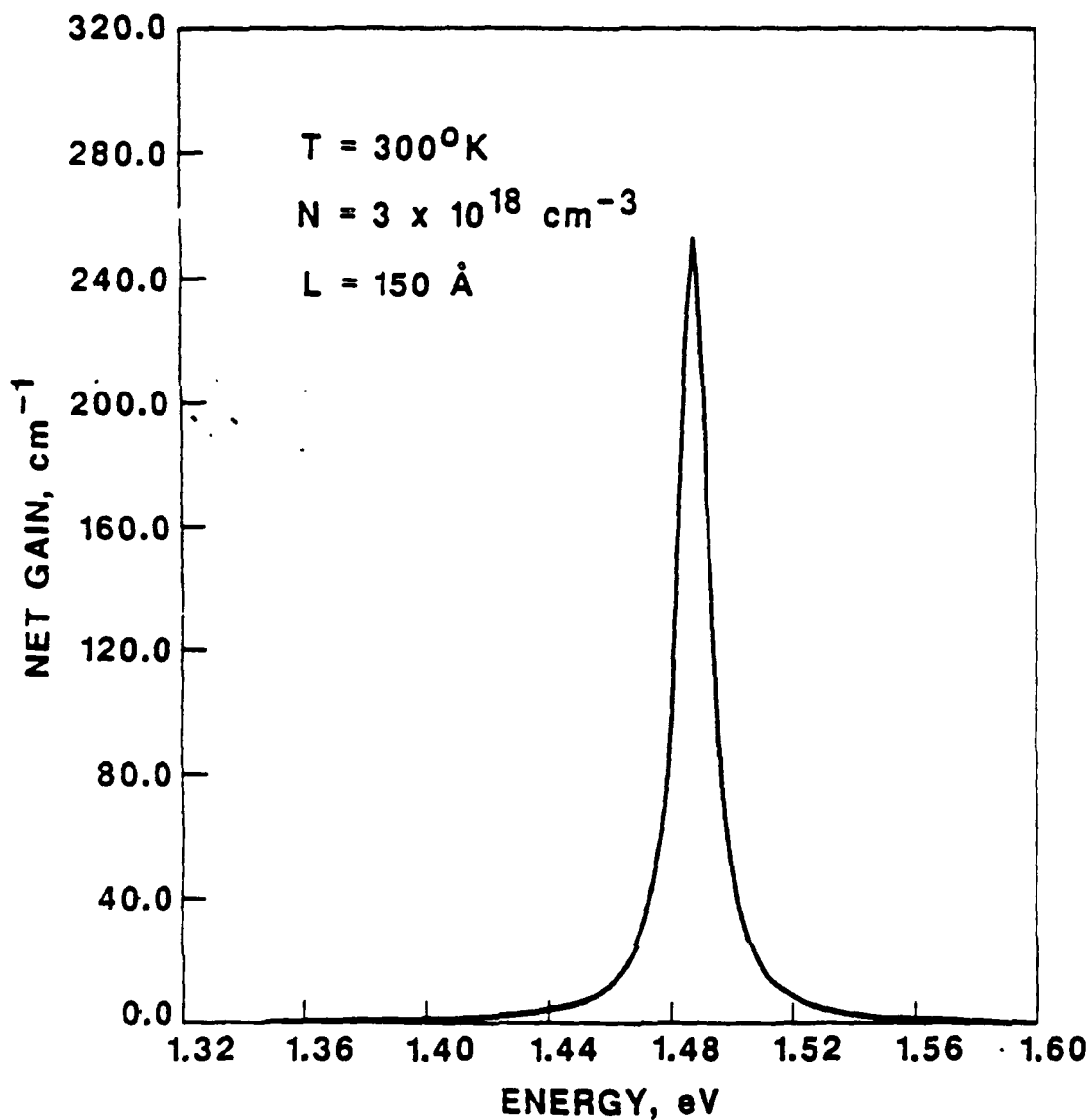


Figure 4. Gain profile as a function of the photon energy

### HUGHES PROPRIETARY

THIS DOCUMENT CONTAINS PROPRIETARY INFORMATION, AND EXCEPT WITH WRITTEN PERMISSION OF HUGHES AIRCRAFT COMPANY, SUCH INFORMATION SHALL NOT BE PUBLISHED, OR DISCLOSED TO OTHERS, OR USED FOR ANY PURPOSE, AND THE DOCUMENT SHALL NOT BE DUPLICATED IN WHOLE OR IN PART. THIS LEGEND SHALL BE APPLIED TO ALL DOCUMENTS CONTAINING THIS INFORMATION. IF REPORTED UNDER A CONTRACT, THE TERMS AND CONDITIONS THEREOF SHALL APPLY.

*[Signature]*  
SIGNATURE INVENTOR

*8/25/88*  
DATE

PATENT DOCKET NO.

SIGNATURE INVENTOR

DATE

READ AND UNDERSTOOD BY:

WITNESS NAME (TYPE)

SIGNATURE

DATE

WITNESS NAME (TYPE)

SIGNATURE

DATE

(ON EACH PAGE UPON WHICH INFORMATION IS ENTERED SHOULD BE SIGNED AND WITNESSED)

SHEET 10 OF 11

## PRACTICAL IMPLEMENTATION OF THE QUANTUM DOT LASER

This section proposes a way of fabricating the quantum dot laser. One of the steps involves the use of the technique of focused ion beam induced interdiffusion. Besides the reference to Hirayama et al, two important works performed by R.L. Kubena of HRL and P. Petroff of UCSB ( supported by the Microelectronics Program of HAC ) deserve mention. They are,

1. Focused ion beam implantation of GaAs-GaAlAs quantum well structures, by P.M. Petroff, X. Qian, P. Holtz, R.J. Simes, J.H. English, J. Merz and R.L. Kubena ( to be published in the Proceedings of the Materials Research Society, 1988)
2. Enhanced interdiffusion in deep quantum wells by focused ion beam implantation, by X. Qian, P.M. Petroff and R.L. Kubena ( to be published in the Applied Physics Letters, 1988 )


The steps involved in the fabrication of the quantum dot laser can be described in the following manner.

STEP 1. Grow a single quantum well layer using molecular beam epitaxy on an n-type GaAs substrate as shown in Figure 5.

STEP 2. Use the technique of focused ion beam induced interdiffusion to generate a planar set of quantum dots. In concise discussion, the technique involves the following processing, as shown in Figure 6. The effects of the Ga focused ion beam is to induce defects on the top AlGaAs layer and the GaAs quantum well layer, provided that the energy of the focused ion beam is controlled. Next the diffusion of Al and Ga are quite distinct. Since the Al ions tend to get trapped by the defects, subsequent annealing produces a diffusion of the Al-trapped defects into the GaAs quantum well region, as shown in Figure 6b ( This description is known from the work per-

## HUGHES PROPRIETARY

THIS DOCUMENT CONTAINS PROPRIETARY INFORMATION, AND EXCEPT WITH WRITTEN PERMISSION OF HUGHES AIRCRAFT COMPANY, SUCH INFORMATION SHALL NOT BE PUBLISHED, OR DISCLOSED TO OTHERS, OR USED FOR ANY PURPOSE, AND THE DOCUMENT SHALL NOT BE DUPLICATED IN WHOLE OR IN PART. THIS LEGEND SHALL BE APPLIED TO ALL DOCUMENTS CONTAINING THIS INFORMATION. IF REPORTED UNDER A CONTRACT, THE TERMS AND CONDITIONS THEREOF SHALL APPLY.

 _____ SIGNATURE INVENTOR		8/25/88 _____ DATE
_____ SIGNATURE INVENTOR		_____ DATE
READ AND UNDERSTOOD BY:		
_____ WITNESS NAME (TYPE)	_____ SIGNATURE	_____ DATE
_____ WITNESS NAME (TYPE)	_____ SIGNATURE	_____ DATE
(EACH PAGE UPON WHICH INFORMATION IS ENTERED SHOULD BE SIGNED AND WITNESSED)		

PATENT DOCKET

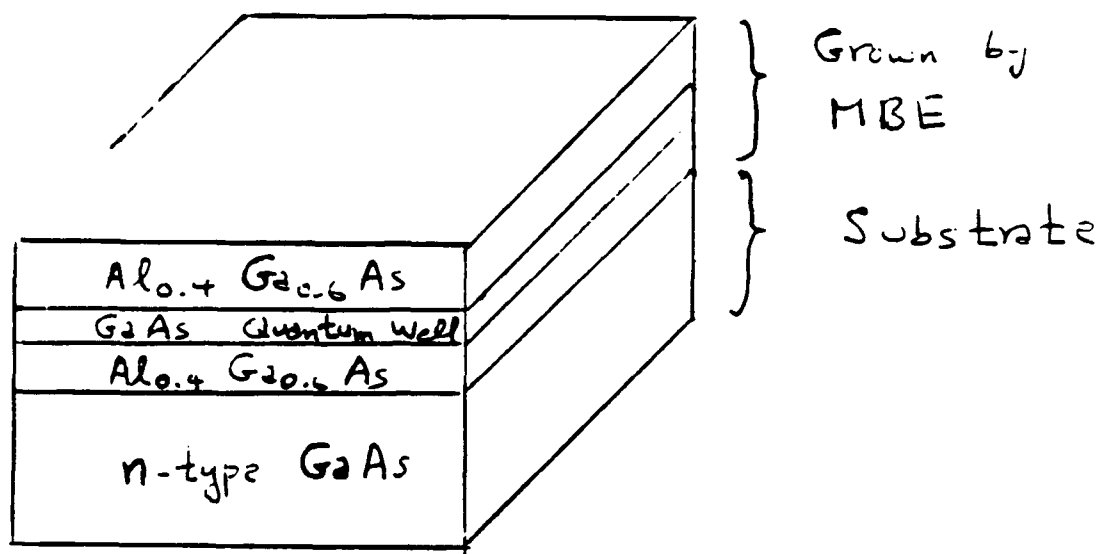
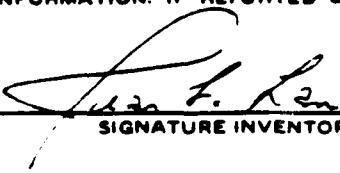


Figure 5. The MBE grown sample for the processing using focused ion beam

### HUGHES PROPRIETARY

THIS DOCUMENT CONTAINS PROPRIETARY INFORMATION, AND EXCEPT WITH WRITTEN PERMISSION OF HUGHES AIRCRAFT COMPANY, SUCH INFORMATION SHALL NOT BE PUBLISHED, OR DISCLOSED TO OTHERS, OR USED FOR ANY PURPOSE, AND THE DOCUMENT SHALL NOT BE DUPLICATED IN WHOLE OR IN PART. THIS LEGEND SHALL BE APPLIED TO ALL DOCUMENTS CONTAINING THIS INFORMATION. IF REPORTED UNDER A CONTRACT, THE TERMS AND CONDITIONS THEREOF SHALL APPLY.

  
 \_\_\_\_\_  
 SIGNATURE INVENTOR

8/25/88  
 \_\_\_\_\_  
 DATE

\_\_\_\_\_  
 SIGNATURE INVENTOR

\_\_\_\_\_  
 DATE

READ AND UNDERSTOOD BY:

_____	_____	_____
WITNESS NAME (TYPE)	SIGNATURE	DATE
_____	_____	_____
WITNESS NAME (TYPE)	SIGNATURE	DATE

(EACH PAGE UPON WHICH INFORMATION IS ENTERED SHOULD BE SIGNED AND WITNESSED)

PATENT DOCKET NO.

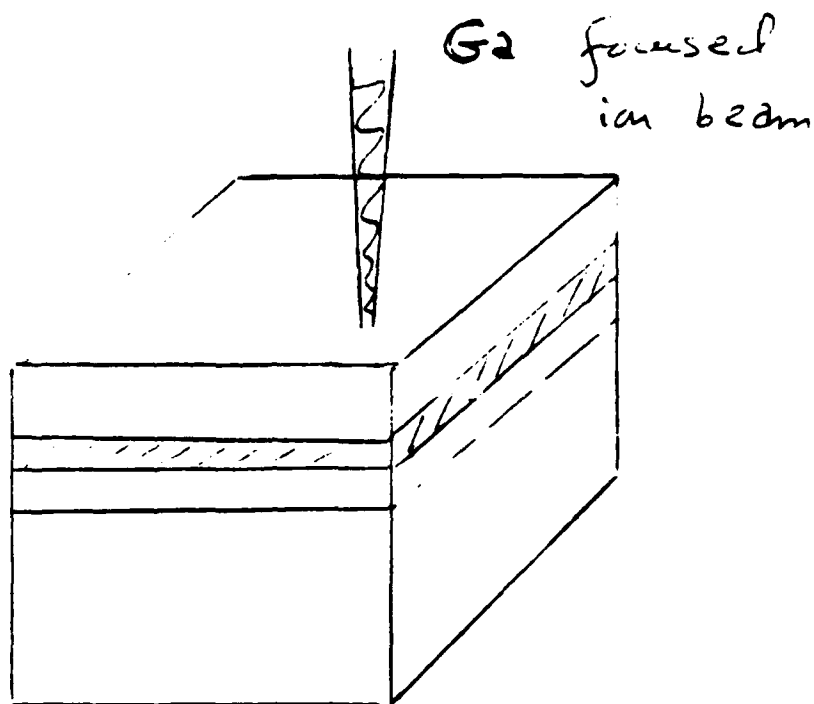
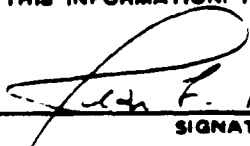


Figure 6a. Application of focused ion beam to a small spot of the MBE grown sample.

### HUGHES PROPRIETARY

THIS DOCUMENT CONTAINS PROPRIETARY INFORMATION, AND EXCEPT WITH WRITTEN PERMISSION OF HUGHES AIRCRAFT COMPANY, SUCH INFORMATION SHALL NOT BE PUBLISHED, OR DISCLOSED TO OTHERS, OR USED FOR ANY PURPOSE, AND THE DOCUMENT SHALL NOT BE DUPLICATED IN WHOLE OR IN PART. THIS LEGEND SHALL BE APPLIED TO ALL DOCUMENTS CONTAINING THIS INFORMATION. IF REPORTED UNDER A CONTRACT, THE TERMS AND CONDITIONS THEREOF SHALL APPLY.

		8/25/88
SIGNATURE INVENTOR		DATE
_____		DATE
SIGNATURE INVENTOR		DATE
READ AND UNDERSTOOD BY:		
_____	_____	_____
WITNESS NAME (TYPE)	SIGNATURE	DATE
_____	_____	_____
WITNESS NAME (TYPE)	SIGNATURE	DATE
_____	_____	_____

PATENT DOCKET NO.



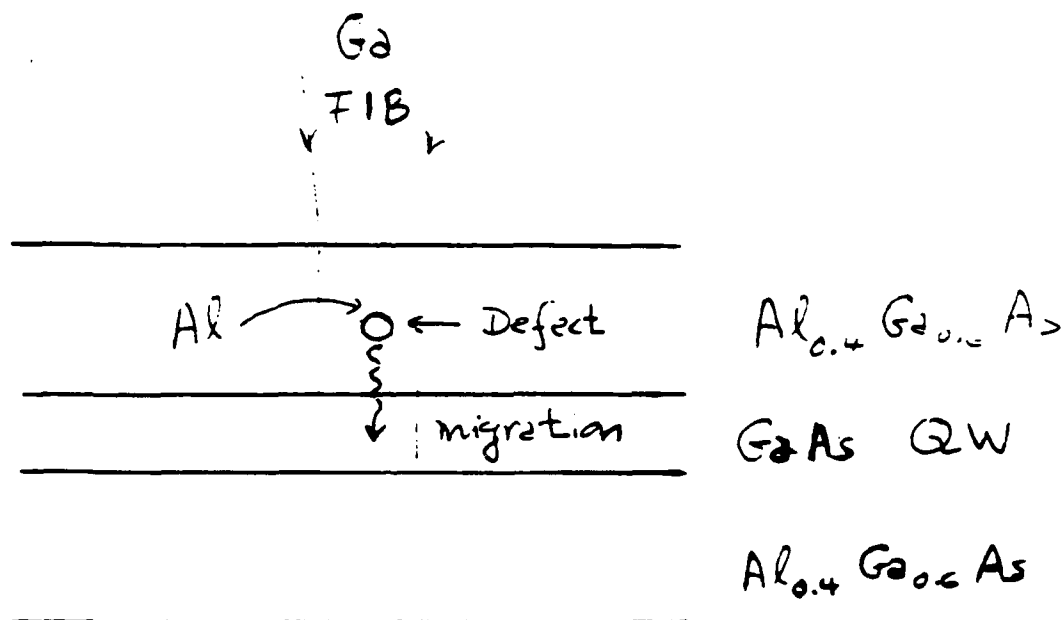


Figure 6b. The physical process of Ga induced damage ( defect formation ), followed by trapping of  $Al$  ions, and diffusion from the  $AlGaAs$  layer to the  $GaAs$  layer upon annealing at high temperature.

### HUGHES PROPRIETARY

THIS DOCUMENT CONTAINS PROPRIETARY INFORMATION, AND EXCEPT WITH WRITTEN PERMISSION OF HUGHES AIRCRAFT COMPANY, SUCH INFORMATION SHALL NOT BE PUBLISHED, OR DISCLOSED TO OTHERS, OR USED FOR ANY PURPOSE, AND THE DOCUMENT SHALL NOT BE DUPLICATED IN WHOLE OR IN PART. THIS LEGEND SHALL BE APPLIED TO ALL DOCUMENTS CONTAINING THIS INFORMATION. IF REPORTED UNDER A CONTRACT, THE TERMS AND CONDITIONS THEREOF SHALL APPLY.

[Signature]  
SIGNATURE INVENTOR

2/25/88  
DATE

\_\_\_\_\_  
SIGNATURE INVENTOR

\_\_\_\_\_  
DATE

READ AND UNDERSTOOD BY:

\_\_\_\_\_  
WITNESS NAME (TYPE)

\_\_\_\_\_  
SIGNATURE

\_\_\_\_\_  
DATE

\_\_\_\_\_  
WITNESS NAME (TYPE)

\_\_\_\_\_  
SIGNATURE

\_\_\_\_\_  
DATE

(EACH PAGE UPON WHICH INFORMATION IS ENTERED SHOULD BE SIGNED AND WITNESSED)

PATENT DOCKET NO.


SHEET 4 OF 17

ormed by R. Kubena at HRL. Stepping the focused ion beam along the horizontal direction allows one to form a quantum line. Turning the sample 90 degree, and repeating the process of implanting the Ga ions, followed by annealing, one obtains a set of planar quantum dots, as shown in Figure 6c and 6d.

STEP 3. Growth a p-type GaAs substrate on top of the focused ion beam processed sample. One then obtains a pn junction which is the crucial element for the quantum dot laser. Application of metal coating and wire for the top and bottom of the pn junction allows the final configuration for the quantum dot laser, as shown in Figure 7.

## HUGHES PROPRIETARY

THIS DOCUMENT CONTAINS PROPRIETARY INFORMATION, AND EXCEPT WITH WRITTEN PERMISSION OF HUGHES AIRCRAFT COMPANY, SUCH INFORMATION SHALL NOT BE PUBLISHED, OR DISCLOSED TO OTHERS, OR USED FOR ANY PURPOSE, AND THE DOCUMENT SHALL NOT BE DUPLICATED IN WHOLE OR IN PART. THIS LEGEND SHALL BE APPLIED TO ALL DOCUMENTS CONTAINING THIS INFORMATION. IF REPORTED UNDER A CONTRACT, THE TERMS AND CONDITIONS THEREOF SHALL APPLY.

  
\_\_\_\_\_  
SIGNATURE INVENTOR

8/25/82  
\_\_\_\_\_  
DATE

PATENT DOCKET NO.

\_\_\_\_\_  
SIGNATURE INVENTOR

\_\_\_\_\_  
DATE

READ AND UNDERSTOOD BY:

\_\_\_\_\_  
WITNESS NAME (TYPE)

\_\_\_\_\_  
SIGNATURE

\_\_\_\_\_  
DATE

\_\_\_\_\_  
WITNESS NAME (TYPE)

\_\_\_\_\_  
SIGNATURE

\_\_\_\_\_  
DATE

(EACH PAGE UPON WHICH INFORMATION IS ENTERED SHOULD BE SIGNED AND WITNESSED)

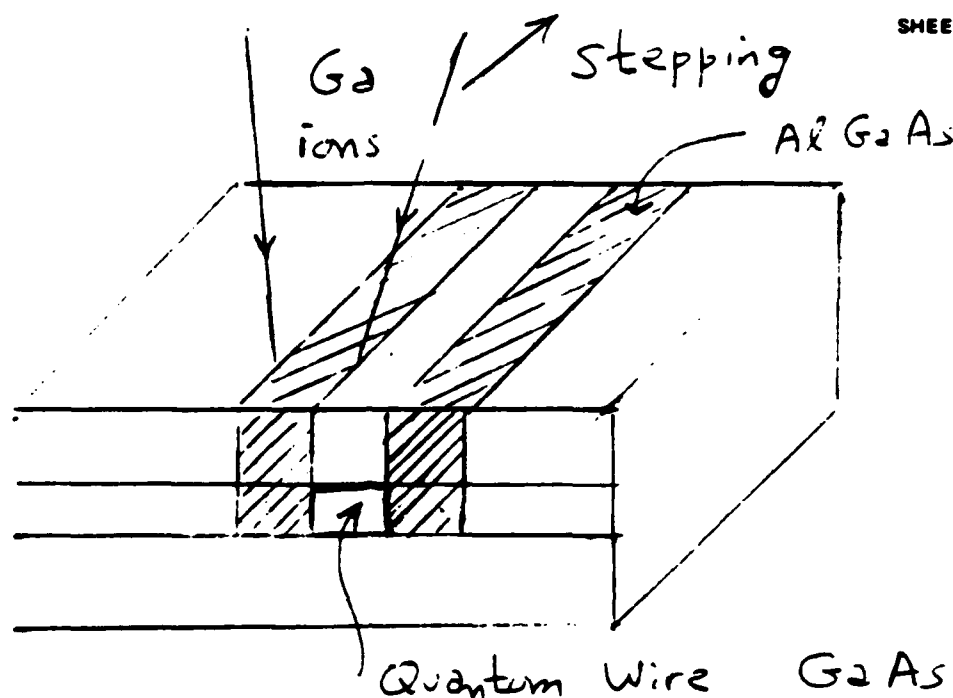
SHEET 16 OF 17

Figure 6c. Formation of a quantum wire by means of focused ion beam induced interdiffusion

## HUGHES PROPRIETARY

THIS DOCUMENT CONTAINS PROPRIETARY INFORMATION, AND EXCEPT WITH WRITTEN PERMISSION OF HUGHES AIRCRAFT COMPANY, SUCH INFORMATION SHALL NOT BE PUBLISHED, OR DISCLOSED TO OTHERS, OR USED FOR ANY PURPOSE, AND THE DOCUMENT SHALL NOT BE DUPLICATED IN WHOLE OR IN PART. THIS LEGEND SHALL BE APPLIED TO ALL DOCUMENTS CONTAINING THIS INFORMATION. IF REPORTED UNDER A CONTRACT, THE TERMS AND CONDITIONS THEREOF SHALL APPLY.

*Juan L. Lam*  
SIGNATURE INVENTOR

*8/21/38*  
DATE

PATENT DOCKET NO.

SIGNATURE INVENTOR

DATE

READ AND UNDERSTOOD BY:

WITNESS NAME (TYPE)

SIGNATURE

DATE

WITNESS NAME (TYPE)

SIGNATURE

DATE

(EACH PAGE UPON WHICH INFORMATION IS ENTERED SHOULD BE SIGNED AND WITNESSED)

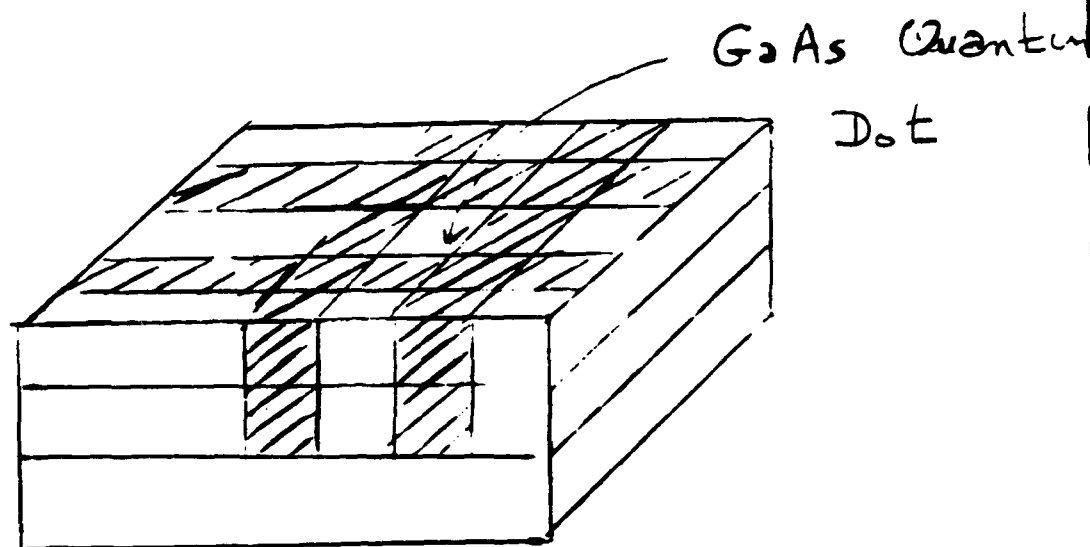
SHEET 16 OF 17

Figure 6d. Generation of quantum dots by cross processing using focused ion beam induced interdiffusion

## HUGHES PROPRIETARY

THIS DOCUMENT CONTAINS PROPRIETARY INFORMATION, AND EXCEPT WITH WRITTEN PERMISSION OF HUGHES AIRCRAFT COMPANY, SUCH INFORMATION SHALL NOT BE PUBLISHED, OR DISCLOSED TO OTHERS, OR USED FOR ANY PURPOSE, AND THE DOCUMENT SHALL NOT BE DUPLICATED IN WHOLE OR IN PART. THIS LEGEND SHALL BE APPLIED TO ALL DOCUMENTS CONTAINING THIS INFORMATION. IF REPORTED UNDER A CONTRACT, THE TERMS AND CONDITIONS THEREOF SHALL APPLY.

*[Signature]*  
SIGNATURE INVENTOR

*8/25/88*  
DATE

PATENT DOCKET NO.

SIGNATURE INVENTOR

DATE

READ AND UNDERSTOOD BY:

WITNESS NAME (TYPE)

SIGNATURE

DATE

WITNESS NAME (TYPE)

SIGNATURE

DATE

(EACH PAGE UPON WHICH INFORMATION IS ENTERED SHOULD BE SIGNED AND WITNESSED)

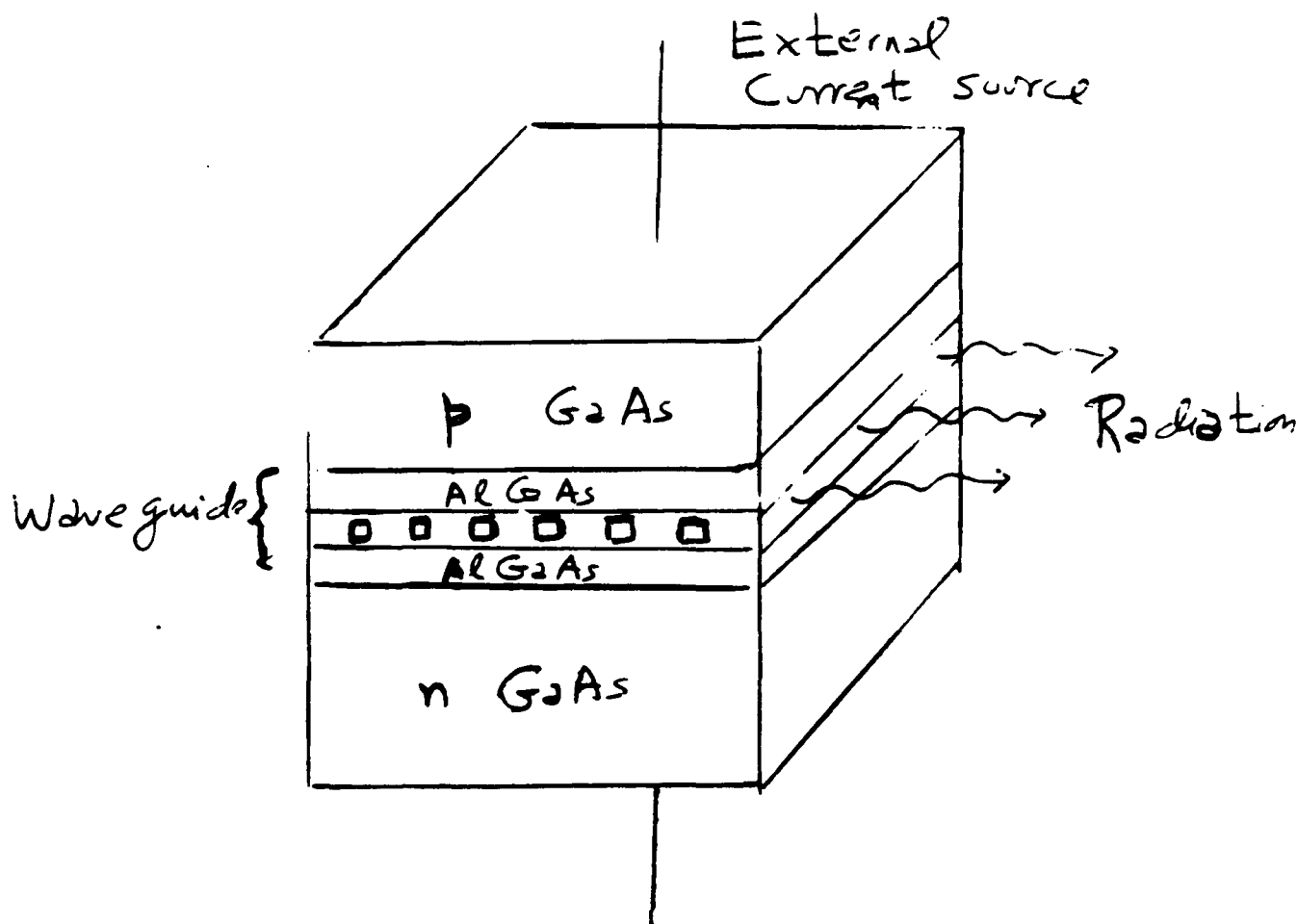
SHEET 17 OF 17

Figure 7. The quantum dot laser

## HUGHES PROPRIETARY

THIS DOCUMENT CONTAINS PROPRIETARY INFORMATION, AND EXCEPT WITH WRITTEN PERMISSION OF HUGHES AIRCRAFT COMPANY, SUCH INFORMATION SHALL NOT BE PUBLISHED, OR DISCLOSED TO OTHERS, OR USED FOR ANY PURPOSE, AND THE DOCUMENT SHALL NOT BE DUPLICATED IN WHOLE OR IN PART. THIS LEGEND SHALL BE APPLIED TO ALL DOCUMENTS CONTAINING THIS INFORMATION. IF REPORTED UNDER A CONTRACT, THE TERMS AND CONDITIONS THEREOF SHALL APPLY.

*Juan L. Ramirez*  
SIGNATURE INVENTOR

8/25/88  
DATE

PATENT DOCKET NO.

SIGNATURE INVENTOR

DATE

READ AND UNDERSTOOD BY:

WITNESS NAME (TYPE)

SIGNATURE

DATE

WITNESS NAME (TYPE)

SIGNATURE

DATE

(EACH PAGE UPON WHICH INFORMATION IS ENTERED SHOULD BE SIGNED AND WITNESSED)

## **SECTION 5**

### **TECHNOLOGY TRANSFER RESULTING FROM WORK PERFORMED UNDER U.S. ARMY RESEARCH OFFICE CONTRACT DAAG29-81-C-0008**

The objective of the contract was concerned with the understanding of the optical properties of Rydberg atoms using the technique of degenerate four-wave mixing. Some of the results of our studies were used in the understanding of the operating characteristics of an atmospheric compensation demonstration experiment over a 2 km range.

The accomplishment was the understanding of the spectral response of the degenerate four-wave mixing signal in an alkali vapor. In the low intensity regime, the spectral response is given by the spontaneous emission decay rate of the excited state. The spectrum broadens up significantly in the high intensity regime due to Rabi flopping. This work, experimental and theoretical, was supported by the Army Research Office during the period 1981-1984. This result was used in the interpretation of an atmospheric compensation demonstration experiment using pulsed lasers, supported by AFWAL. In a nut shell, the experiment involves the optical illumination of a retro-reflective mirror located 2 kms away from the phase conjugate mirror. The phase conjugate mirror is a sodium cell operating in the nearly degenerate four-wave mixing mode. The optical system was able to record a grating generated by two distinct laser pulses. Hence a phase conjugate signal was generated by means of degenerate four-wave mixing, leading to the propagation of the signal back to the retro-reflective mirror, despite the existing atmospheric aberration. Our understanding of the spectral response of the sodium phase conjugate mirror aided in the interpretation of the results of the experiments.

## REFERENCES

1. Woodbury, E.J. and W.K. Ng, Proc. IRE 50, 2367 (1962)
2. Zeldovich, B. Ya, V.J. Popovichev, V.V. Ragulskii and F.S. Faisullov, JETP Lett. 15, 109 (1972)
3. Askaryan, G.A., Sov. Phys. JETP 15, 1088 (1962); Talanov, V.I., Izv. VUZ-Radiofizika 7, 564 (1964); Chiao, R.Y., E. Garmire and C.H. Townes, Phys. Rev. Lett. 13, 479 (1964)
4. Hasegawa, A. and F. Tappert, Appl. Phys. Lett. 23, 171 (1973)
5. Photorefractive Materials and Their Applications I and II, edited by P. Gunter and J.-P. Huignard, (Springer-Verlag, 1989)
6. Optical Nonlinearities and Instabilities in Semiconductors, edited by Hartmut Haug (Academic Press, 1988)
7. Herman, M.A. and H. Sitter, Molecular Beam Epitaxy (Springer-Verlag 1989)
8. Chang, L.L., R. Tsu and L. Esaki, Appl. Phys. Lett. 24, 593 (1974)
9. Weiner, J.S., D.A.B. Miller, D.S. Chemla, T.C. Damen, C.A. Burrus, T.H. Wood, A.C. Gossard and W. Wiegmann, Appl. Phys. Lett. 47, 1148 (1985)
10. Miller, D.A.B., U.S. Patent 4,546,244
11. Chemla, D.S., D.A.B. Miller, P.W. Smith, A.C. Gossard and W. Wiegmann, IEEE J. Quantum Electron. QE-20, 265 (1984)
12. Mysyrowicz, A. D. Hulin, A. Antonetti, A. Migus, W.T. Masselink, and H. Morkoc, Phys. Rev. Lett. 56, 2748 (1986); Von Lehmen, A., D.S. Chemla, J.E. Zucker, J.P. Heritage, Opt. Lett. 11, 609 (1986)
13. Cibert, J., P.M. Petroff, G.J. Dolan, S.J. Pearton, A.C. Gossard and J.H. English, Appl. Phys. Lett. 49, 1275 (1986)
14. Kapon, E., S. Simhony, R. Bhat and D.M. Hwang, Appl. Phys. Lett. 55, 2715 (1989)
15. Craighead, H.G., in Physics of Quantum Electron Devices, edited by Federico Capasso (Springer-Verlag, 1990)
16. Bawendi, M.G, M.L. Steigerwald and L.E. Brus, Annu. Rev. Phys. Chem. 41, 477 (1990)
17. Roussignol, P. D. Ricard, C. Flytzanis and N. Neuroth, Phys. Rev. Lett. 62, 312 (1989)
18. Ekimov, A.I. and A.A. Onushchenko, Sov. Phys. Semicond. 16, 775 (1982); Efros, A.I. and L. Efros, Sov. Phys. Semicond. 16, 772 (1982)
19. Ashkin, A., G.D. Boyd, J.M. Dziedzic, R.G. Smith, A.A. Ballmann, and K. Nassau, Appl. Phys. Lett. 9, 72 (1966)

20. Chen, F.S., J. Appl. Phys. 40, 3389 (1969)
21. Vinetskii, V.L. and N.V. Kukhtarev, Sov. Phys. Solid State 16, 2414 (1975)
- 22.. Kukhtarev, N.V., V.B. Makov, S.G. Odulov, M.S. Soskin, and V.L. Vinetskii, Ferroelectrics 22, 949 (1979)
23. Ducharme, S. and J. Feinberg, J. Appl. Phys. 56, 839 (1984); Mahgerefteh, D. and J. Feinberg, Opt. Lett. 13, 1111 (1989)
24. Lam, J.F., CLEO'89 (Baltimore 1989)
25. Gaeta, C.J., J.F. Lam and R.C. Lind, Opt. Lett. 14, 245 (1989)
26. Efros, Al.L. and L. Efros, Sov. Phys. Semicond. 16, 772 (1982)
27. Chang, T., Doctoral Dissertation, (University of Southern California 1986)
28. Rytz, D., M.B. Klein, R.A. Mullen, R.N. Schwartz, G.C. Valley and B.A. Wechsler, Appl. Phys. Lett. 52, 1759 (1988)
29. Gunter, P., et. al Opt. Commun. 55, 210 (1985)
30. Smout, A.M.C., et al Opt. Commun. 59, 77 (1986)
31. Ivakin, E.V., V.G. Koptev, A.M. Lazaruk, I.P. Petrovich and A.S. Rubanov, JETP Lett. 30, 614 (1979)
32. Lam, J.F. et al, IQEC'87 ( San Francisco 1986)



# Theory of millimeter wave nonlinearities in semiconductor superlattices

Juan F. Lam

Hughes Research Laboratories, Malibu, California 90265

Bob D. Guenther and David D. Skatrud

Department of Physics, Duke University, Durham, North Carolina 27706

(Received 3 July 1989; accepted for publication 12 December 1989)

A study of the impact of semiconductor superlattices on millimeter wave nonlinearities is reported.  $\chi^{(3)}$  as large as  $10^{-2}$  esu can be achieved by using 250 GHz radiation. Self-induced transparency is also predicted, and its competition with the third-harmonic generation process is quantified.

Current research in nonlinear optics has been concentrated in the wavelength regimes that extend from the infrared to the UV. However, little effort has been devoted to the understanding of nonlinear materials in the millimeter wave regime in spite of the fact that coherent sources are currently available. Recently, several experiments<sup>1-3</sup> have been performed that probe the material requirements and their suitability for use in the far-infrared regime. For example, the demonstration of difference frequency generation in Si/Ge superlattices and the measurement of the nonlinear index of refraction in graphite suspensions indicated that nonlinearities in the millimeter range could be quite large, in comparison to those found in the optical regime. Due to the importance of millimeter wave technology in future information processing applications, we report on a detailed study of millimeter wave nonlinearities in semiconductor superlattices.

The perturbative analysis of the nonlinear optical response function of conduction electrons in superlattices was first reported by Tsu and Esaki.<sup>4</sup> Their work indicated that nonlinear optical phenomena occurring in superlattices were stronger than those found in bulk semiconductors. More detailed analyses by Bloss and Friedman<sup>5</sup> and by Chang<sup>6</sup> arrived at the same results.

The starting point in our analysis is the coupled charge transport and crystal momentum equations for the motion of the Bloch carriers directed along the direction of the superlattice growth (labeled by the subscript  $z$ ).

$$\frac{dv_z}{dt} + \frac{v_z}{\tau} = \frac{d}{dt} \left( \frac{1}{\hbar} \frac{\partial U}{\partial k_z} \right), \quad (1)$$

$$\hbar \frac{dk_z}{dt} = qE(t), \quad (2)$$

where  $v_z$  is the carrier velocity,  $\tau$  is the carrier momentum relaxation time<sup>7</sup> along  $z$ ,  $k_z$  is the crystal momentum,  $E(t)$  is the radiation field with polarization state oriented along  $z$ ,  $q$  is the charge of the carrier, and  $U$  is the superlattice band structure.

The validity<sup>8</sup> of the semiclassical approximation rests on the following assumptions. First, the wavelength of the radiation field must be larger than the lattice constant. Second, the energy of the radiation field must be smaller than the band gap. Third, the work done by the applied field in a distance equal to the lattice constant must be less than  $U_{gap}^2/U_F$ , where  $U_{gap}$  and  $U_F$  are the band gap and Fermi

energies, respectively. Furthermore, at low dopant density, the electron-electron interaction is assumed to be negligible.<sup>9</sup>

In the one-band or Kronig-Penney model,  $U$  takes a simple form

$$U = U_0(1 - \cos k_z d), \quad (3)$$

where  $d$  is the superlattice period. Equations (1), (2), and (3) can be combined together to yield the following expression:

$$\frac{dv}{dt} + \frac{v}{\tau} = \frac{qE(t)}{m_z}, \quad (4a)$$

where the superlattice effective mass  $m_z$  is given by

$$\frac{1}{m_z} = \frac{U_0 d^2}{\hbar^2} \cos \frac{qd}{\hbar} \int E(t') dt'. \quad (4b)$$

Equations (4) describe the physical origin of the nonlinearity in semiconductor superlattices. That is, the nonlinearities arise from the artificially induced nonparabolicity, through the superlattice effective mass. In the absence of  $E(t)$ ,  $m_z$  becomes the superlattice mass,  $m_0$ , at the high symmetry point. The nonlinear current density is given by

$$J = nqv_z, \quad (5)$$

where  $n$  is the carrier concentration. Nonlinearities also arise for the charge carriers moving in the plane of the superlattices. The origin of the nonlinearity has been studied extensively, and is attributed to the bulk band nonparabolicity in doped semiconductors.<sup>10</sup>

Several important conclusions can be deduced from the variety of solutions that can be obtained from Eqs. (4) and (5). First, the third-order susceptibilities can be obtained from the Taylor series expansion of the superlattice effective mass. The expansion is valid provided that the superlattice Rabi flopping frequency is less than the radiation frequency. For radiation oscillating at 250 GHz and a superlattice period of 150 Å, the maximum field strength is 690 V/cm in order that the Taylor series expansion is valid. A direct calculation gives the following result for the third-order susceptibilities:

$$\chi^{(3)} = -i \frac{nq^4 d^2}{8m_0 \hbar^2} \frac{1}{\omega^3(1/\tau - i\omega)}, \quad (6)$$

with  $m_0$  being the superlattice effective mass. Equation (6) indicates that the periodicity  $d$  and the superlattice mass  $m_0$  determine the magnitude of the nonlinear response function, for given values of  $\omega$ , in agreement with previous studies.

The interesting conclusion to be drawn is its frequency dependence, which indicates that the use of coherent millimeter radiation will lead to a substantial increase of the third-order susceptibilities in comparison to those obtained in the optical regimes. In order to illustrate the importance of Eq. (6) for millimeter wave operation, Table I shows typical values of  $\chi^{(3)}$  for several semiconductor superlattices. The assumed frequency of oscillation is 250 GHz, and the lattice periodicity is 100 Å. The relatively large value of the third-order susceptibility indicates that semiconductor superlattices, when properly configured can have potential applications in the millimeter wave regime.

Second, the nonlinear polarization density induced by a radiation field  $E(r,t) = E_0 \cos(kx - \omega t + \phi)$  can be obtained from the exact solution of Eqs. (4), and it is given by

$$P = -(\omega_p/\omega)^2 [J_0(R) + J_2(R)] \times \{ \omega\tau/[1 + (\omega\tau)^2] E_0 \sin(kx - \omega t + \phi) + (\omega\tau)^2/[1 + (\omega\tau)^2] E_0 \cos(kx - \omega t + \phi) \}, \quad (7)$$

where  $\omega_p = 4\pi nq^2/m_0$  is the plasma frequency, and  $R = qdE_0/\hbar\omega$  is the superlattice Rabi flopping frequency normalized to the frequency of the applied radiation field.  $J_0$  and  $J_2$  are the zeroth and second orders of the Bessel functions, respectively. The expression for the polarization density has a simple physical interpretation. The first factor,  $(\omega_p/\omega)^2$ , on the right-hand side describes the degree of linear opacity of the medium. That is, radiation will propagate inside the semiconductor superlattices provided that  $\omega_p < \omega$ , since the linear dielectric constant of the superlattice is equal to  $1 - (\omega_p/\omega)^2$ . The second factor,  $J_0(R) + J_2(R)$ , describes the effect of the nonlinear motion of the charge carriers in the presence of radiation fields. This term approaches unity for weak radiation fields, and modifies the dielectric constant for high radiation fields. The third factor has two components. The first component, proportional to the sine function of the radiation phase, is responsible for the absorption coefficient; while the second one, proportional to the cosine function of the radiation phase, accounts for the index of refraction of the material.

Figure 1 depicts the functional dependence of the factor,  $J_0 + J_2$ , of Eq. (7) versus  $R$ . It decreases monotonically until it reaches 0 for  $R = 3.8$ . This behavior implies that for a given set of material parameters, there exists a specific value of  $E_0$  such that the radiation field travels through the super-

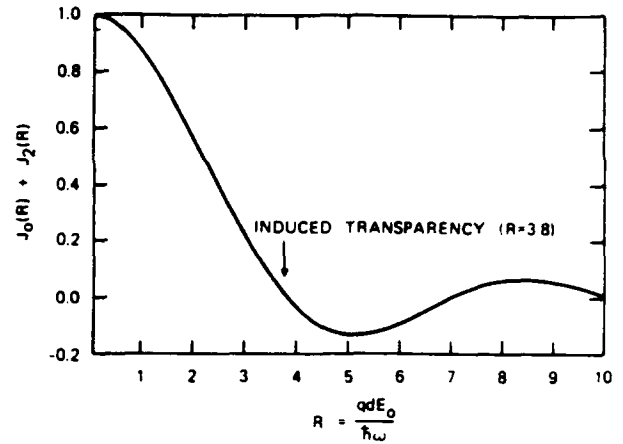


FIG. 1. Plot of  $J_0(R) + J_2(R)$  as a function of  $R$ , the normalized superlattice Rabi frequency. At  $R = 3.8$ , induced transparency of the radiation field occurs.

lattice material as if it were a vacuum. At this critical point, the radiation field does not experience energy absorption nor optical phase dispersion. This effect has been discussed previously by Ignatov and Romanov.<sup>11</sup> Their results differ from ours by the term  $J_2(R)$ . As an example, given a radiation field that oscillates at 250 GHz and incident upon a semiconductor superlattice of periodicity  $d = 100$  Å, the condition for induced transparency implies that the critical amplitude of the radiation field is 3.9 kV/cm. This phenomenon is analogous to self-induced transparency that occurs in resonant optical materials. It is interesting to note that since  $J_0(R) + J_2(R)$  becomes negative for some values of  $E_0$ , "apparent" amplification of the amplitude of the input radiation field will occur. This result has a simple physical interpretation, without violating the law of conservation of energy, when one considers the interaction between a strong radiation field  $E_0$  oscillating at  $\omega_0$  and a weak radiation field  $E_1$  oscillating at frequency  $\omega_1$ . Their nonlinear interaction mediated by the superlattice produces a traveling-wave excitation oscillating at frequency  $\omega_1 - \omega_0$ . The scattering of the strong radiation from the traveling-wave excitation couples back to the weak radiation field  $E_1$ . The coupling coefficient from such a coherent scattering process is calculated using Eqs. (1) and (2), and the spatial evolution of the complex amplitude,  $A$ , of  $E_1$  is governed by the following expression:

$$\frac{dA}{dx} = -A \frac{\omega_p^2 \tau}{2n_\omega c} \times \frac{1 + i\omega_1 \tau}{1 + (\omega_1 \tau)^2} \times \left[ J_0(R) + \frac{R^2}{2} \left( \frac{\omega_0}{\omega_1} \right) [J_0(R) + J_2(R)] \right]. \quad (8)$$

Equation (8) has a very transparent interpretation. For small values of  $R$ , the first term inside the bracket is the linear absorption coefficient, and the second term is the traveling grating contribution to the absorption coefficient. For values of  $R$  exceeding 3.8, the amplitude of the weak radiation field is amplified at the expense of the strong radiation field. That is, there is a net energy transfer from the strong to the weak radiation field.<sup>12</sup>

Third, a fundamental limitation to the observation of the self-induced transparency effect in semiconductor super-

TABLE I. Operation at 250 GHz and  $\tau \sim 10^{-11}$  s.

Superlattices $d = 100$ Å	$m_0/m$	$\chi^{(3)}$ (esu)
GaAs-AlGaAs	0.1 <sup>a</sup>	$1.88 \times 10^{-2}$
InAs-GaSb	0.035 <sup>b</sup>	$5.37 \times 10^{-2}$
HgTe-CdTe	0.01 <sup>c</sup>	$1.88 \times 10^{-1}$

<sup>a</sup> N. F. Johnson, H. Ehrenreich, K. C. Hass, and T. C. McGill, Phys. Rev. Lett. 59, 2352 (1987).

<sup>b</sup> G. Bastard, Phys. Rev. B 25, 7584 (1982).

<sup>c</sup> G. Bastard, in *NATO Advanced Study Institute on Molecular Beam Epitaxy in Heterostructures*, edited by L. L. Chang and K. Ploog (Martinus-Nijhoff, Dordrecht, 1984), p. 381.

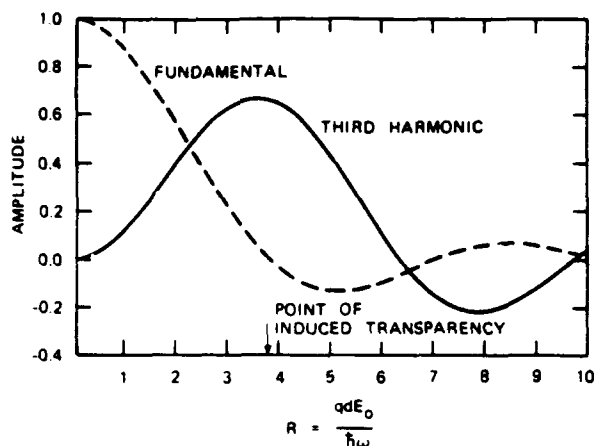


FIG. 2. Plots of the third harmonic and fundamental signals as a function of  $R$ . For properly configured superlattices, the third-harmonic generation depletes the fundamental signal to avoid induced transparency.

lattices is the generation of third-harmonic signal. A calculation of the third-harmonic signal, in the undepleted pump approximation, gives

$$\frac{I_{3\omega}(L)}{I_{\omega}(0)} = \left( \frac{\omega_p^2 L}{2cn_{3\omega}} \right)^2 \frac{[J_2(R) + J_4(R)]^2}{(1/\tau)^2 + (3\omega)^2} \left( \frac{\sin x}{x} \right)^2, \quad (9)$$

where  $L$  is the transverse dimension (in the plane of the superlattice) of the sample,  $n_{3\omega}$  is the linear index of refraction at the third-harmonic frequency,  $J_4$  is the fourth-order Bessel function, and  $x = (k_{3\omega} - k_{\omega})L/2$  is the phase mismatch. The term  $\sin x/x$  is just the window function that arises from the phase mismatch. Figure 2 plots the ratio of the third-harmonic intensity to the input intensity as a function of  $R$ , which is shown as a solid line. In the same figure and in dotted lines, we plot the slowly varying component of the polarization density. It is assumed that the window function does not alter the third-harmonic signal. Figure 2 shows that the third-harmonic generation takes energy away from the incident beam; hence it leads to a suppression of the self-induced transparency phenomenon. It is important to calculate the efficiency of the third-harmonic generation process for typical semiconductor superlattices such as GaAs-AlGaAs. Reasonable phase matching is achieved provided that  $\Delta kL < 2\pi$ . Assuming an average index of refraction of

3.5 at 250 and 750 GHz, one finds that  $L = 0.04$  mm, with the third-harmonic generation efficiency of 0.1%.

And last, nonlinear processes will take place in the superlattice provided that the radiation field can be propagated inside the medium; i.e., is the medium underdense and weakly absorbing at the frequency of oscillation? A calculation of the linear dielectric constant and the linear absorption coefficient indicates that for charge carrier density of  $10^{16} \text{ cm}^{-3}$  and oscillation frequency of 250 GHz, the superlattice is underdense and has a linear absorption coefficient of  $\sim 3/\text{mm}$  for GaAs-based materials.

In conclusion, we have carried out a study of the millimeter wave nonlinearities in semiconductor superlattices, and found that these materials possess large third-order susceptibilities, can be modified so that induced transparency will be present, and is a possible source for third-harmonic generation. However, the practical implementation of a suitable large size semiconductor superlattice still remains an obstacle for the demonstration of the predictions proposed in this letter.

This work is supported by the Army Research Office. The authors extend their sincere thanks to the referee for the constructive criticisms that led to a better exposition of the results.

<sup>1</sup>A. A. Kostenko, O. A. Kuznetsov, V. A. Tolomasov, O. N. Filatov, G. I. Khlopov, and V. P. Shestopalov, *Sov. Phys. Dokl.* **28**, 670 (1983).

<sup>2</sup>M. M. Kechiev, A. A. Kostenko, V. D. Kurek, O. A. Kuznetsov, V. A. Tolomasov, O. N. Filatov, G. I. Khlopov, and V. P. Shestopalov, *Sov. Phys. Semicond.* **17**, 1024 (1983).

<sup>3</sup>B. Bobbs, R. Shih, H. R. Fetterman, and W. H. Ho, *Appl. Phys. Lett.* **52**, 4 (1988).

<sup>4</sup>R. Tsu and L. Esaki, *Appl. Phys. Lett.* **19**, 246 (1971).

<sup>5</sup>W. L. Bloss and L. Friedman, *Appl. Phys. Lett.* **41**, 1024 (1982).

<sup>6</sup>Y. C. Chang, *J. Appl. Phys.* **58**, 499 (1985).

<sup>7</sup>The use of the phenomenological relaxation time  $\tau$  assumes that the carrier scattering processes can be decomposed into two separate components. This simple argument is not generally correct, and might lead to different results. See E. Vass, *Z. Phys. B* **67**, 435 (1987).

<sup>8</sup>N. W. Ashcroft and N. D. Mermin, *Solid State Physics* (Saunders, Philadelphia, 1976), p. 219.

<sup>9</sup>Studies of dependence of the mobility of doped semiconductors on the electron densities showed that electron-electron scattering does not play a significant role in comparison to polar optical scattering. See K. Seeger, *Semiconductor Physics* (Springer, Berlin, 1982), p. 206.

<sup>10</sup>P. A. Wolff and G. A. Pearson, *Phys. Rev. Lett.* **17**, 1015 (1966).

<sup>11</sup>A. A. Ignatov and Yu. A. Romanov, *Sov. Phys. Solid State* **17**, 2216 (1976).

<sup>12</sup>Competing effects from other gratings might play an important role in the energy transfer process.

# Theory of enhanced optical nonlinearities in quantum dots

Juan F. Lam

Hughes Research Laboratories  
Malibu, California 90265

## ABSTRACT

A discussion of the exciton regime of quantum dots is presented. We predict the possibility of enhancement of the optical nonlinearities due to exciton quantization. Applications to the dynamic Stark effect and two-wave mixing processes are described.

## 1. INTRODUCTION

The initial experimental and theoretical studies of quantization effects in linear optical absorption of CuCl microcrystals by Ekimov and Onushchenko<sup>1</sup> and by Efros and Efros<sup>2</sup> demonstrated the phenomenon of blue shift due to size quantization. The first nonlinear optical experiment was performed by Jain and Lind<sup>3</sup> who showed the existence of phase conjugate degenerate four-wave mixing in CdS, Se<sub>1-x</sub>S<sub>x</sub> doped glasses. These experiments were confronted with the nonuniformity of the crystallite sizes, which led to a broadening of the observed spectra.

In the last year theoretical works by Schmitt-Rink, Miller and Chemla<sup>4</sup> and by Hanamura<sup>5</sup> have confirmed the results of Efros and Efros, and explored the possibility of size-induced enhancement of the nonlinear optical response of quantum dots. Furthermore, Banyai and Koch<sup>6</sup> showed the existence of radiation-induced blue shift due to Coulomb screening.

The objective of this work is to provide additional insights into the role of quantum dots in nonlinear optics. In the following, the preliminary results of quantum confinement on 1) Dynamical Stark Effect and 2) Two-wave mixing processes are presented. In addition a simple physical interpretation of optical enhancement is provided as well as a discussion on the limitation on the density of quantum dots that must be achieved in order for the quantum dots to be novel optical materials.

## 2. PHYSICAL MODEL

We consider the interaction of external radiation fields with a set of quantum boxes of dimension  $L$ . The band structure of the semiconductor material is assumed to consist of two isotropic bands. The optical transition is assumed to occur at the  $\Gamma$ -point. As described by Efros and Efros, there are three distinct regimes which depend on the relative order of magnitudes of  $L$ , the Bohr radius of the electron,  $a_e$ , and the Bohr radius of the hole,  $a_h$ .

The first regime corresponds to the case where  $L < a_e, a_h$ . This is the regime of size quantization of the individual charge carriers. The second regime corresponds to the case where  $a_h < L < a_e$ . This is the regime where only the electron experiences free particle size quantization. And the last regime corresponds to the case where  $L > a_e, a_h$ . This last case corresponds to the formation of an exciton and the size quantization of the center of mass of the exciton. We shall restrict our work to the last case. As will be demonstrated, this last regime gives rise to strong enhancement of the nonlinear optical processes in quantum boxes, in agreement with the studies of Hanamura.

We shall restrict the discussion to the low excitation regime. This regime entails the following physical simplifications. First, it does not take into account the role of band non-parabolicity. And second, quantum confinement effects due to plasma generation are unimportant. In the high excitation regime, non-parabolicity effects will play an important role in narrow gap semiconductors.

## 3. THE DYNAMIC STARK EFFECT

This section describes the phenomenon of the dynamic Stark effect in quantum dots. Using the appropriate Wannier wavefunctions for the ground and first excited states of a quantum confined structure, it is shown that the derivation of the Stark splitting can be accomplished in the framework of the dressed-atom picture a la Cohen-Tannoudji and Reynaud<sup>7</sup>. We would like to point out that the derivation is valid for all values of the laser detuning, contrary to the case of multiple quantum wells where on-resonant excitation lead to the formation of an electron-hole plasma due to phonon-induced ionization. Hence it invalidates the dressed-exciton picture for on-resonance excitation of multiple quantum wells, even in the lowest optical transition.

In the rotating frame associated with the photon field, the interaction of a radiation field with the first two quantum states of a dot is described by

$$\{ H_0 + \hbar\omega_L a^\dagger a - \mu \cdot E(R) \} |\Psi\rangle = U |\Psi\rangle \quad (1)$$

where  $H_0$  is the electronic Hamiltonian of the N-electron system,  $\omega_L$  is the frequency of the laser field,  $a$  and  $a^\dagger$  are the annihilation and creation operator for the laser field,  $-\mu \cdot E$  is the electric dipole interaction with the radiation field. The state vector  $|\Psi\rangle$  is given in terms of the superposition of the ground and excited state wavefunctions in the Wannier representation,

$$|\Psi\rangle = c_g |g\rangle |n\rangle + F_{b.o.x} c_e |exc\rangle |n-1\rangle \quad (2)$$

where  $|g\rangle$  describes the ground state of the N-electron system,  $|exc\rangle$  describes the first excited state with one electron in the conduction band and one hole in the valence band,  $|n\rangle$  describe the n-photon field.  $F_{b.o.x}$  is the envelope amplitude describing dot quantization. Hence the problem is identical to the case encountered in atomic systems. Similar approach was taken by Mysyrowicz et al to understand the results in GaAs-AlGaAs multiple quantum wells. However, in the latter the dressed-exciton picture only works provided that  $\hbar\omega_L < E_{g,p}$ .

Invoking the effective mass approximation, equation (1) leads to the following eigenvalue problem

$$\begin{bmatrix} \hbar\omega_L - U & -\mu_{eg} \cdot E \int dr F_{b.o.x} \\ -\mu_{ge} \cdot E \int dr F_{b.o.x} & E_{g,p} + E_{b.o.x} + (n-1)\hbar\omega_L - U \end{bmatrix} \begin{bmatrix} c_g \\ c_e \end{bmatrix} = \begin{bmatrix} 0 \\ 0 \end{bmatrix} \quad (3)$$

where we chose the ground state energy to be equal to zero. Equation (3) shows an important feature that distinguishes the problem of quantum dots from atomic systems and quantum wells. The electric dipole coupling to the radiation field has a proportionality constant  $\int dr F_{b.o.x}$ , which is just the size quantization condition. In the case where  $L > a_e, a_h$ , one finds that

$$\int dr F_{dot} = \text{constant} \times (L/R_{exciton})^{3/2} \times \frac{1}{n_x n_y n_z} \sin^2(n_x \pi/2) \sin^2(n_y \pi/2) \sin^2(n_z \pi/2) \quad (4)$$

where we have chosen quantization for the center of mass motion of the 1s exciton in a box of length  $L$ . The energy  $E_{b.o.x}$  is the sum of the energy of a single particle of mass  $m_e^* + m_h^*$  confined in a box of length  $L$  and the hydrogenic-like energy of the bulk exciton. The quantum numbers  $n_i$  ( $i=x,y,z$ ) varies for all integer values. One can conclude from Eq. (4) that strong enhancement of the electric dipole coupling to the radiation field can be achieved for  $L/R_{exciton}$  is greater than one, and for  $n_x=1=n_y=n_z$ .

The dressed energies are found from the determinant of Eq. (3) and they are

$$U_{\pm} = \alpha/2 \pm \hbar\Omega \quad (5)$$

where  $\alpha = (2n-1)\hbar\omega_L + E_{g,p} + E_{b.o.x}$  is the total energy of the system,  $\Omega = \{\Delta^2 + |\int dr F_{b.o.x} \mu_{eg} \cdot E|^2\}^{1/2}$  is the generalized Rabi frequency, and  $\Delta = \omega_L - (E_{g,p} + E_{b.o.x})/\hbar$  is the laser detuning from resonance.

The result of Eq. (5) is now transparent. In analogy to the atomic system, one has an infinite set of doublets of separation  $\hbar\Omega$ . The energy separation between two adjacent doublets is  $\hbar\omega_L$ . This result points to the distant possibility of observing size quantization in resonance fluorescence experiments in quantum dots, provided that interference effects due to adjacent levels can be kept at a minimum. Furthermore, the size quantization of the generalized Rabi frequency implies that the saturation intensity is decreased by a factor  $\{\int dr F_{b.o.x}\}^2$ .

#### 4. TWO-WAVE MIXING

This section describes the processes of energy transfer associated with two-wave mixing processes. Hence, it is important to adopt a theoretical formalism that will provide the third order polarization density. In view of the analogy of quantum dots with atomic systems, we shall introduce the quantum mechanical transport equation appropriate for discrete states.

The evolution of a system of quantum dots under the combined action of two radiation fields oscillating at frequency  $\omega_L$  and  $\omega_L + \delta$  is described rigorously by the quantum analog of the Liouville equation,

$$i\hbar \partial \rho / \partial t = [H_0, \rho] + [V, \rho] + i\hbar \partial \rho / \partial t |_{r.s.} \quad (6)$$

where  $\rho$  is the density operator.  $V = -\mu \cdot \{E(\omega_L) + E(\omega_L + \delta)\}$  is the electric dipole coupling to the radiation field. The last term in Eq. (6) describes the effects of radiative and non-radiative relaxation. The interpretation of the elements of  $\rho$  in the basis states  $|g\rangle$  and  $F_{b.o.x} |exc\rangle$  is as follows. The diagonal elements are just the probability of finding the N-electron system either in the ground or first excited state. The off-diagonal elements are the laser-induced optical coherences. We shall assume the physical condition in which the probability of state  $F_{b.o.x} |exc\rangle$  decays to state  $|g\rangle$  at the spontaneous emission rate  $\gamma\{\int dr F_{b.o.x}\}^2$ . While the off-diagonal elements experience dephasing due to spontaneous emission and phonon-induced coupling, at a rate  $\gamma\{\int dr F_{b.o.x}\}^2/2 + \Gamma$ . The phonon-induced dephasing rate  $\Gamma$  is assumed to be independent of  $k$  and experiences no size quantization effects. In the low excitation regime, the solution of Eq. (6) that describes the interaction of two radiation fields can be derived in a straightforward manner. The third order polarization density is

$$P = \text{constant } N\{\int dr F_{b.o.x}\}^4 L(\Delta, \delta) |E(\omega_L)|^2 E(\omega_L + \delta) \quad (7)$$

where  $N$  is the density of quantum dots,  $L(\Delta, \delta)$  is the lineshape factor. An important result is the enhanced polarization density due to size quantization.

The energy transfer between two radiation fields is described by the Maxwell equations. In the slowly varying envelope approximation, the spatial evolution of  $E(\omega_L + \delta)$  is governed by wave equation,

$$dE(\omega_L + \delta)/dz = \epsilon A\{\int dr F_{b.o.x}\}^4 L(\Delta, \delta) |E(\omega_L)|^2 E(\omega_L + \delta) \quad (8)$$

where  $\epsilon=1$  for co-propagating fields and  $\epsilon=-1$  for counter-propagating fields.  $A$  is just the normal gain coefficient. Two interesting features can be deduced from Eq. (8). First the two-wave mixing gain is enhanced by size quantization. And second, the relative direction of the gain process depends on the sign of the real part of  $L(\Delta, \delta)$ .

An interesting result can be deduced for the case when  $\Delta >$  optical dephasing rate. In this case  $L(\Delta, \delta)$  takes on a very simple expression

$$L(\Delta, \delta) = -(\delta/\Delta) \Gamma \frac{\gamma\{\int dr F_{b.o.x}\}^2}{|\gamma\{\int dr F_{b.o.x}\}^2 + i\delta|^2} \quad (9)$$

which implies that the gain of  $E(\omega_L + \delta)$  is controlled by the magnitude of the phonon-induced relaxation rate, and the directionality of the gain process is determined by the sign of  $\delta/\Delta$ . A similar process was predicted by Khitrova<sup>9</sup> and for atomic system embedded in a buffer gas. The experimental confirmation in sodium vapor was recently achieved by Grandclement, Grynberg and Pinard<sup>10</sup>.

## 5. SUMMARY

We presented some preliminary results concerning the role of size quantization on the nonlinear optical responses of quantum dots. The theoretical formulation of this work was restricted to the low excitation regime, where non-parabolicity and plasma effects can be neglected. In the context of this approximation, we found that size enhancement will occur for the following conditions:  $L > a_0, a_h$ . Hence, in this regime, the dynamic Stark splitting, and the two-wave mixing gain are enhanced by  $\{\int dr F_{b.o.x}\}^2$ , and  $\{\int dr F_{b.o.x}\}^4$ ; respectively. For the case of 1s exciton, the enhancement factor takes the following simple form  $(L/R_{exciton})^{3/2}$ .

Current theoretical studies are being performed in the transition regime between low and high excitation, with the objective of understanding size quantization under condition of saturation. Calculations are also being directed toward the understanding of the performance of quantum dot semiconductor lasers.

## 6. ACKNOWLEDGEMENTS

This work supported by the U.S. Army Research Office under contract No. DAAL03-87-C-0001

## 7. REFERENCES

1. Ekimov, A.I. and A.A. Onushchenko, Sov. Phys. Semicond. 16, 775 (1982).
2. Efros, Al.L. and L. Efros, Sov. Phys. Semicond. 16, 772 (1982).
3. Jain, R.K. and R.C. Lind, J. Opt. Soc. Am. 73, 647 (1983).
4. Schmitt-Rink, S., D.A.B. Miller and D.S. Chemla, Phys. Rev. B 35, 8113 (1987).
5. Hanamura, E., Solid State Commun. 62, 465 (1987).
6. Banyai, L. and S.W. Koch, Phys. Rev. Lett. 57, 2722 (1987).
7. Cohen-Tannoudji, C. and S. Reynaud, in MULTIPHOTON PROCESSES, edited by J.H. Eberly and P. Lambropoulos, John Wiley and Sons, (1978).
8. Mysyrowicz, A., D. Hulin, A. Antonetti, A. Migus, W.T. Masselink and H. Morkoc, Phys. Rev. Lett. 56, 2748 (1986).
9. Khitrova, G. Ph. D. Thesis, New York University (1987)
10. Grandclement, D., G. Grynberg and M. Pinard, Phys. Rev. Lett. 59, 40 (1987).

AMERICAN INSTITUTE OF PHYSICS  
CONFERENCE PROCEEDINGS NO. 172

# OPTICAL SCIENCE AND ENGINEERING SERIES 9

---

## ADVANCES IN LASER SCIENCE-III

ATLANTIC CITY, NJ 1987

EDITORS: ANDREW C. TAM, JAMES L. GOLE  
& WILLIAM C. STWALLEY

---



# FOUR-WAVE MIXING SPECTROSCOPY OF STATE SELECTIVE COLLISIONS IN GASES AND SOLIDS\*

Juan F. Lam  
Hughes Research Laboratories  
Malibu, California 90265

## ABSTRACT

The quantum evolution from a closed to an open system, induced by collisional processes, is presented in the framework of nearly degenerate four-wave mixing (NDFWM) spectroscopy. We show that an open system manifests itself by the appearance of a subnatural linewidth in the spectrum of the phase conjugate signal. Examples are described for sodium vapor in the presence of buffer gases and in  $\text{Nd}^{3+}$  doped  $\beta$ -Na-Alumina for high concentration of  $\text{Nd}^{3+}$  ions.

## INTRODUCTION

The discovery of real time phase conjugate optics by Stepanov et al<sup>1</sup> and Woerdman<sup>2</sup> has provided the foundation for the use of four-wave mixing processes as novel spectroscopic tools. The inherent advantages of backward degenerate four-wave mixing over saturated absorption techniques are the existence of Doppler-free spectrum combined with their nearly background-free signals, and the simultaneous measurement of the longitudinal and transverse relaxation times in a single spectral scan. The Doppler free feature was first pointed out by Liao and Bloom<sup>3</sup> in their investigation of resonantly enhanced phase conjugate mirrors. While the simultaneous presence of the longitudinal and transverse relaxation times in the spectrum were described by Lam et al<sup>4</sup>.

Recent studies of collisional processes using four-wave mixing techniques have shed new insights on how collisional processes affect the spectral lineshape<sup>5</sup>. A point in question was the measurement of ground state behavior in spite that the laser was resonant to an optical transition. This fact illustrates the complexity involved in our understanding of collision-induced lineshapes. The objective of this review is to provide an up-to-date account of how the technique of nearly degenerate four-wave mixing probes the evolution of a quantum system in the presence of perturbers<sup>6</sup>.

### THE TECHNIQUE OF NDFWM SPECTROSCOPY

The technique of NDFWM spectroscopy<sup>4</sup> involves the generation of a travelling wave excitation in the medium (with an atomic resonance  $\omega_0$ ) by the interference of two nearly co-propagating radiation fields oscillating at frequency  $\omega$  and  $\omega+\delta$ ; respectively. The nearly phase conjugate field is produced by the scattering of a counter-propagating read-out beam off the travelling wave excitation. The nearly conjugate field oscillates at frequency  $\omega-\delta$  and travels in opposite direction to the input beam oscillating at  $\omega+\delta$ .

The small signal spectrum of the phase conjugate fields takes on distinct behavior depending on whether the resonant medium is homogeneously or inhomogeneously broadened. For the case of a two-level homogeneously broadened system, the theoretical spectral lineshape<sup>7</sup> for  $\omega=\omega_0$  exhibits a resonance at  $\delta=0$  with linewidth given by  $.41\gamma$ , where  $\gamma$  is the spontaneous decay rate, in the absence of a buffer gas. In the presence of a buffer gas, the NDFWM lineshape shows an effective narrowing in the linewidth. This phenomenon arises from the formation of a long-lived ground-state population excitation formed by the interference of two input radiation fields. The limiting factor is ultimately determined by the transit time of an atom traveling across a laser beam.

The spectral lineshape takes on a similar behavior for the case of an inhomogeneously broadened system when  $\omega=\omega_0$ . It describes the evolution of the spectral lineshape as buffer gas is added to the quantum system. For  $\omega=\omega_0$ , the lineshape contains two resonances located at  $\delta=-2\Delta$  and  $\delta=0$ . However the linewidths have different behavior in the presence of buffer gases<sup>4</sup>. The resonance line located at  $\delta=-2\Delta$  experiences phase interrupting collision, which tends to broaden the linewidth. The resonance line at  $\delta=0$  experiences a decoupling of the ground state from the excited state and the width of the line is determined by the lifetime of the ground state (in this case it is the transit time).  $\Delta$  is the detuning of the pump from resonance.

The spectral behavior of the nearly phase conjugate field illustrates two important points. First, the spectrum contains simultaneous information on the energy and dipole relaxation times, when  $\omega=\omega_0$ . And second, the spectrum provides a direct measurement of the ground state lifetime in the presence of a buffer gas.

## COLLISION-INDUCED RESONANCES IN SODIUM VAPOR

Sodium vapor provides a testing ground for the concept outlined above. We consider the excitation of the  $D_2$  line of sodium using two correlated cw lasers having a bandwidth of approximately 1 MHz. Since the spectral lineshape depends on the difference of frequency between the two correlated lasers, phase fluctuations are automatically eliminated and the fundamental limitation to the sensitivity of our measurement technique is the time of flight of the atom across the optical beam or the laser linewidth, whichever is larger. Figure 1a shows the spectral behavior of the nearly phase conjugate field for equally polarized input fields and for  $\omega$  tuned to the  $3 S_{1/2}$  ( $F=2$ ) to  $3 P_{3/2}$  ( $F=3$ ) transition<sup>4</sup>. It depicts a

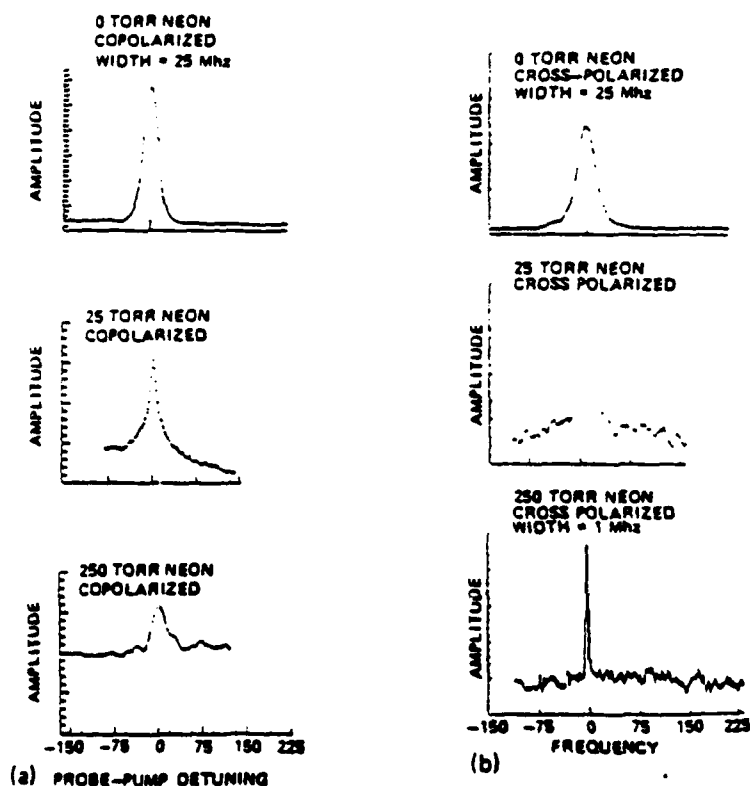


Figure 1. Spectral lineshape of the NDFWM of sodium for (a) co-polarized radiation fields, (b) cross-polarized radiation fields.

narrowing of the linewidth, from 20 Mhz to 1 Mhz, as argon buffer gas is added to the sodium cell. It can also be interpreted as the appearance of a new resonance with a much narrower linewidth. Hence it provides a direct measurement of the effective lifetime of the  $3S_{1/2}$  state. As the buffer gas pressure increases to 250 torr, the linewidth broadens up due to the excited state.

Figure 1b shows the spectral lineshape for the case where the counterpropagating fields, oscillating at  $\omega$ , is orthogonally polarized with respect to the field oscillating at  $\omega + \delta$ . Again as the buffer gas pressure increases, the linewidth decreases from 20 Mhz to 1 Mhz, even beyond the 250 torr regime. The use of cross polarized radiation fields induces a Zeeman coherence grating rather than a population grating<sup>8</sup>. The collision cross section for Zeeman coherences is relatively small, which accounts for the 1 Mhz linewidth even at a pressure of 250 torr. These data provides a glimpse of the simplicity of collisional processes on the NDFWM spectrum. However, Khitrova and Berman<sup>9</sup> has predicted that additional ultranarrow features are also present even in the absence of buffer gases. These features are the result of optical pumping processes that exist when the atomic multipoles are produced by the interference of two orthogonally polarized light beam. A detail account of the theory and experiment related to these novel features are presented by Steel et al.<sup>10</sup>.

#### OPTICAL PAIR INTERACTION IN $\text{Nd}^{3+}$ - $\beta$ -Na-Alumina

The study of cooperative processes in solids has been a subject of great interest since they determine the practical limitations of solid state optical devices. The technique of NDFWM spectroscopy has provided an initial step toward understanding the role of ion-ion interaction in the spectral lineshape<sup>11</sup>. An interesting candidate material is  $\text{Nd}^{3+}$  doped  $\beta$ -Na-Alumina<sup>12,13</sup>. For this material, the four-wave mixing process takes place at 575 nm between the  $^4I_{9/2}$  and  $^4G_{7/2}$  states. However due to the fast nonradiative relaxation rate of the excited state  $^4G_{7/2}$ , the NDFWM spectrum shows a ultranarrow resonance whose width is determined by radiative decay rate at 1.06  $\mu\text{m}$  ( which is of the order of few hundreds  $\mu\text{sec}$  ). The transition at 1.06  $\mu\text{m}$  is between the  $^4F_{3/2}$  and  $^4I_{11/2}$  states of  $\text{Nd}^{3+}$ .

Figure 2a depicts the spectral lineshape of the nearly phase conjugate field for three different pump

intensities. The curve labeled by 25 mW provides a direct measurement of the spontaneous decay rate at  $1.06 \mu\text{m}$  even though the laser used in the experiments has a wavelength of 575 nm. At higher value of the laser intensity, the linewidth broadens up due to pump-induced saturation. Rand et al<sup>11</sup> showed that the intensity behavior of the NDFWM linewidth is consistent with the system being inhomogeneously broadened. Figure 2b describes the dependence of the saturation intensity and the linewidth as a function of  $\text{Nd}^{3+}$  concentration. For densities larger than  $5 \times 10^{21} \text{ cm}^{-3}$ , both physical parameters experience a decrease. Lam and Rand<sup>14</sup> has shown that this behavior arises from the increase in the pair interaction which creates an additional channel for the electron located in  $^4F_{3/2}$  to escape, leading to such a behavior.

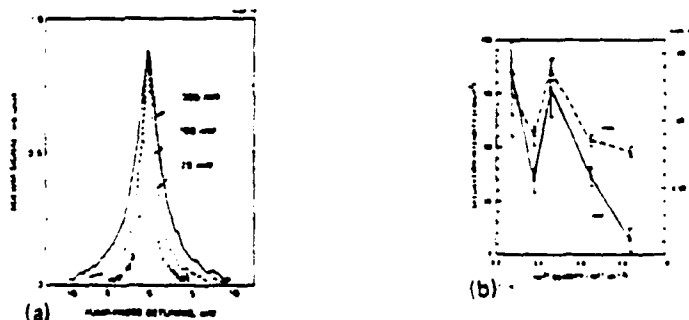


Figure 2. (a) Spectral lineshape for different intensities. (b) Behavior of the saturation intensity and linewidth as a function of dopant density.

#### SUMMARY

We have described some of the subtle issues associated with spectral lineshape of NDFWM in the presence of collisional processes. The results have demonstrated that collisions do indeed provide a means of separating the ground state from the excited state. The ultranarrow linewidth of the NDFWM spectrum is a manifestation of the ground state effective lifetime.

Work supported by the United States Army Research Office under contract #DAAL03-87-C-0001 and by the Air Force Office of Scientific Research under contract #F49620-85-C-0058

#### ACKNOWLEDGEMENT

The author gratefully acknowledges the important contributions made by Drs. Duncan Steel, Steve Rand, Ross McFarlane, Steve Turley and Oscar Stafsudd.

#### REFERENCES

1. Stepanov, B.I., E.V. Ivakin and A.S. Rubanov,, Sov. Phys. Dokl. Tech. Phys. 15, 46 (1971)
2. Woerdman, J.P., Opt. Commun. 2, 212 (1971)
3. Liao, P.F., and D.M. Bloom, Opt. Lett. 3, 4 (1978)
4. Lam, J.F., D.G. Steel and R.A. McFarlane, Phys. Rev. Lett. 49, 1628 (1982)
5. Rothberg, L., in PROGRESS IN OPTICS, ed. by E. Wolf, North Holland, Amsterdam (1987)
6. Berman, P.R., in NEW TRENDS IN ATOMIC PHYSICS, Les Houches, ed. by G. Grynberg and R. Stora, North Holland, Amsterdam (1984)
7. Lam, J.F., D.G. Steel and R.A. McFarlane, in LASER SPECTROSCOPY VII, ed. by T.W. Hansch and Y.R. Shen, Springer Verlag, Berlin (1985)
8. Lam, J.F., D.G. Steel and R.A. McFarlane, Phys. Rev. Lett. 56, 1679 (1986)
9. Khitrova, G. and P.R. Berman, to be published (1988)
10. Steel, D.G., J. Liu, G. Khitrova and P.R. Berman, unpublished (1988).
11. Steel, D.G. and S.C. Rand, Phys. Rev. Lett. 55, 2285 (1985)
12. Boyd, R.W., M.T. Gruneisen, P. Narum, D.J. Simkin, B. Dunn and D.L. Yang, Opt. Lett. 11, 162 (1986)
13. Rand, S.C., J.F. Lam, R.S. Turley, R.A. McFarlane and O.M. Stafsudd, Phys. Rev. Lett. 59, 597 (1987)
14. Lam, J.F. and S.C. Rand, ( unpublished 1988 )

# Laser Spectroscopy of Semiconductor Quantum Dots

J.F. Lam

Hughes Research Laboratories  
Malibu, CA 90265, USA

Recent advances in nanofabrication techniques have opened the door for the study of quantum confined semiconductor structures. The first observation of quantum dots was reported by Ekimov and Onushchenko<sup>1</sup> who measured the blue shift of the absorption lines of CuCl as the dimension of the dot decreases. The experimental data confirmed the theoretical model of Efros and Efros<sup>2</sup>. Theoretical studies in both the strongly<sup>3</sup> and weakly quantized<sup>4,5</sup> regimes indicated that semiconductor quantum dots might have enhanced optical nonlinearities. Hence applications of quantum dots in optical devices such as lasers<sup>6</sup> and modulators<sup>7</sup> appear to be promising, provided that the technology is sophisticated enough to produce well characterized samples of quantum dots.

In spite of its potential applications, little is understood concerning the spectroscopy of semiconductor quantum dots. Roussignol et al<sup>8</sup> have recently observed spectral hole burning in CdSSe microcrystallites using a pump-probe technique. Furthermore their measurements indicated that the phonon broadening dominated the spectral behavior of these materials. This article describes the optical Stark effect in these materials, and proposes that the technique of nearly degenerate two-wave mixing has the potential of providing a direct measurement of the energy relaxation and dipole dephasing times of semiconductor quantum dots.

In order to appreciate the regimes that are being considered, Table I gives typical semiconductor parameters, together with the estimates of the de Broglie wavelengths of the electron,  $\lambda_D$ , and the Bohr radius of the exciton,  $R_B$ . For example, a GaAs quantum dot with dimension of 200 Å will enclose a quantum confined exciton. If the dimension decreases to 100 Å, the quantum dot consists of electron and hole confined inside a box, independent of each other. Note that a 50 Å GaAs quantum dot will possess optical transition in the visible regime. And if such a set of such dots can be inserted inside a pn junction, it will generate, in principle, coherent radiation at approximately 6000 Å. This intriguing idea indicates that the optical properties of quantum dots require careful examination.

The study of optical processes in semiconductors relies upon the solution of the bi-local quantum transport equations, which takes into account both the coherent amplitude of the electron-hole pair and the number densities. We will restrict our studies to the case where excitonic processes are important. In this case the dot size is assumed to be large compared to the excitonic Bohr radius but its is limited by the de Broglie wavelength of the electron.

The ground state is determined by the Slater determinant of one-electron Bloch states, all located in the valence band

TABLE I

	$\epsilon$	$m^*/m_0$	$E_g$ (eV)	$\lambda_D$ (Å)	$R_B$ (Å)
Ga In As P $x=0.27$ $y=0.60$	12.4	0.053	0.95	276	137
In P	12.4	0.077	1.35	229	96
Ga As	13.1	0.067	1.42	245	118
Cd S	5.4	0.21	2.42	139	17
Cd Se	10.0	0.13	1.70	176	53

The first excited state is determined by the Slater determinant of one-electron Bloch states, in which one electron and one hole have been created in the conduction and valence bands; respectively.

In the effective mass approximation, the interaction of light with excitons can be described in terms of

$$H = E_C (-i \nabla_e) - E_V (-i \nabla_h) + V(\vec{r}_e - \vec{r}_h) \quad (1)$$

$$- \vec{\mu} \cdot \vec{E}(\vec{R}, t)$$

The state  $|1\rangle$  is the eigenstate of the "unperturbed" effective mass Hamiltonian,  $H_0$ .

One can construct density matrix equations in the same manner as those found in atomic systems. That is,

$$i \hbar \frac{\partial \rho}{\partial t} = [H, \rho] + i \hbar \left. \frac{\partial \rho}{\partial t} \right|_{\text{Relaxation}} \quad (2)$$

where the elements of the density matrices have simple physical interpretation.  $\langle 1 | \rho | 1 \rangle$  is the probability of finding an exciton, and  $\langle 0 | \rho | 1 \rangle$  is the optical coherence amplitude. This is the starting point for the analysis of four-wave mixing processes in semiconductor quantum dots.

The diagonalization of the exciton Hamiltonian is achieved by finding the determinant of the following matrix

$$\begin{bmatrix} -U & -\vec{\mu}_R \cdot \vec{E} \left( \frac{L}{R_B} \right)^{3/2} \\ -\vec{\mu}_R \cdot \vec{E} \left( \frac{L}{R_B} \right)^{3/2} & U_{\text{exc}} - U \end{bmatrix} \quad (3)$$



TABLE II

$\Delta = 20 \text{ meV}$	$L \text{ (Å)}$	$I \text{ (W/cm}^2\text{)}$	Stark Shift (meV)
GaAs-AlGaAs MQW	100	106	0.2
CdS dot	139	$6 \times 10^2$	0.2

which gives the following result for the energy level of the exciton in the presence of a detuned light field

$$U = U_{\text{exc}} + \frac{|\vec{\mu}_B \cdot \vec{E}|^2}{U_{\text{exc}} - \hbar\omega_L} \left( \frac{L}{R_B} \right)^3 \quad (4)$$

The first two terms are just the exciton binding energy and the last term is the A.C. Stark shift. Note that the Stark shift contains a geometric factor which gives the ratio of the dot size to the exciton Bohr radius. In order to appreciate the significance of this result, Table II provides a comparison of the intensities of the light field for the case of a GaAs Multiple Quantum Well and a CdS quantum dot. One sees that in order to achieve the same Stark shift, the power density for the multiple quantum well is four orders of magnitude higher than that of the quantum dot. This is intimately related to the geometric factor.

The application of the density matrix equations to the case of two-wave mixing can be carried out using perturbation theory. The result of the analysis provides an expression for the small signal gain coefficient

$$g = \alpha \cdot \left\{ 1 + \frac{\Gamma}{\gamma} \times \frac{\delta}{\Delta} \times \frac{\Omega^2}{\gamma^2 + \delta^2} \right\} \quad (5)$$

where  $\alpha_0$  is the linear absorption coefficient,  $\Gamma$  is the exciton dephasing rate,  $\gamma$  is the exciton energy relaxation rate,  $\delta$  is the frequency mismatch between the two input beam,  $\Delta$  is the detuning of the strong pump from exciton resonance, and  $\Omega$  is the exciton Rabi flopping frequency. This result is identical to the one obtained from resonant two-level systems.

Figure 1 gives the dependence of the gain-length factor as a function of the frequency mismatch  $\delta$ , for the case of CdS quantum dot. In a manner identical to that encountered in resonant atomic system, amplification of the signal is achieved under certain conditions. The maximum of the gain coefficient gives a direct measurement of the exciton energy relaxation rate. While the amplitude gives a direct measurement of the exciton dephasing rate.

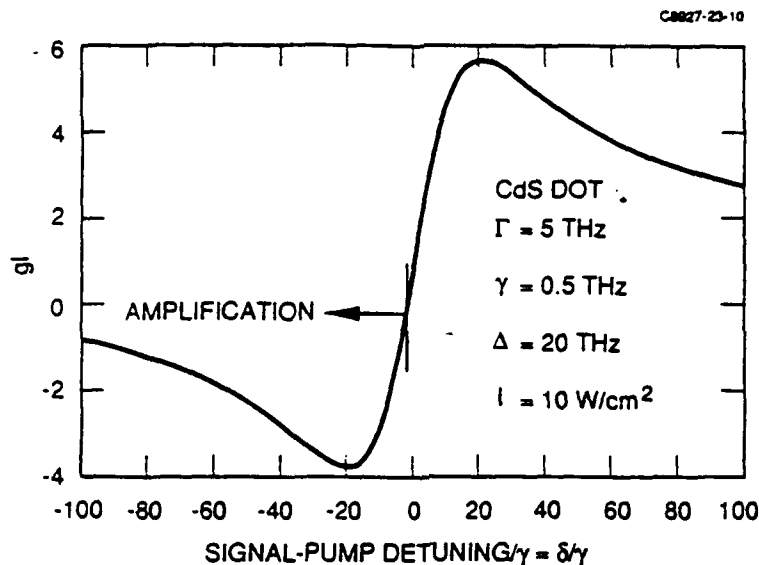


Figure 1. Gain length product as a function of the normalized frequency mismatch.

\* This work is supported by the ARO.

#### REFERENCES

1. A.I. Ekimov and A.A. Onushchenko, Sov. Phys. Semicond. 16, 775 (1982)
2. Al. L. Efros and A. L. Efros, Sov. Phys. Semicond. 16, 772 (1982)
3. S. Schmitt-Rink, D.A.B. Miller and D.S. Chemla, Phys. Rev. B 35, 8113 (1987)
4. E. Hanamura, Phys. Rev. B 37, 1273 (1988)
5. F. Henneberger, U. Woggon, J. Puls and Ch. Spiegelberg, Appl. Phys. B 46, 19 (1988)
6. Y. Miyamoto, M. Cao, Y. Shingai, K. Furuya, Y. Suematsu, K.G. Ravikumar and S. Arai, Jpn. J. Appl. Phys. 26, L225 (1987)
7. See Reference 3
8. P. Roussignol, D. Ricard, C. Flytzanis and N. Neuroth, Phys. Rev. Lett. 62, 312 (1989)

THEORY OF TRANSIENT SELF-PUMPED PHASE CONJUGATION  
IN  
PHOTOREFRACTIVE MATERIALS \*

Juan F. Lam  
Hughes Research Laboratories  
Malibu , CA 90265

Abstract

A self-consistent solution of the coupled charge transport-Maxwell equations has been obtained in the transient regime for self-pumped photorefractive mirrors. The theory predicts the existence of self-pulsation and frequency chirping of the phase conjugate signal.

Theory of Transient Self-pumped Phase Conjugation  
in  
Photorefractive Materials

Juan F. Lam  
Hughes Research Laboratories  
Malibu , CA 90265

The discoveries of self-pumped phase conjugation in barium titanate by White et al<sup>1</sup> and by Feinberg<sup>2</sup> have provided the impetus for the practical implementation of loaded phase conjugate resonators<sup>3</sup>, demonstration of optical convolution and correlation<sup>4</sup>, and application of the thresholding property to associative memories<sup>5</sup>.

During the last few years, a substantial understanding of the physical mechanism giving rise to self-pumped phase conjugation has been achieved<sup>6,7</sup>. However, the origin of the frequency shift reported by several authors has been the source of current controversy. The objective of this paper is to attempt to provide an understanding of the temporal evolution of the self-pumped phase conjugation process, for the purpose of explaining some of the frequency shift data<sup>8,9</sup>.

The formulation of the transient problem is based on the solutions of the coupled charge transport and Maxwell equations, in the limit of small modulation parameter and in the presence of a temporal step incident intensity. The crucial assumption is the existence of a photo-excited photovoltaic current, directed along the c-axis of the electro-optic crystal. This current was postulated to be responsible for the origin of frequency shift<sup>7</sup>. Since the formation of the phase conjugate beam is sensitive to the boundary conditions inside the crystal, two distinct geometries were analyzed. The first geometry involves the spontaneous generation of counterpropagating pump waves from the side walls of the crystal, in a manner identical to the experiments of Gunter et al<sup>8</sup>. Using Laplace transform techniques, the temporal evolution of the internal space charge field was obtained and used to generate the nonlinear polarization density. In the small signal limit, the phase conjugate signal is shown to possess two interesting contributions.

The first one involves the temporal dependence of the intensity, as shown in Figure 1. It depicts the evolution of the phase conjugate intensity (normalized to the steady state value) for two distinct values of the input intensity. This oscillatory behavior is a direct consequence of the photo-excited photovoltaic effect. The dielectric relaxation rate ( $\Gamma_0$ ) and the photovoltaic frequency shift ( $\delta_n$ ) are the two important

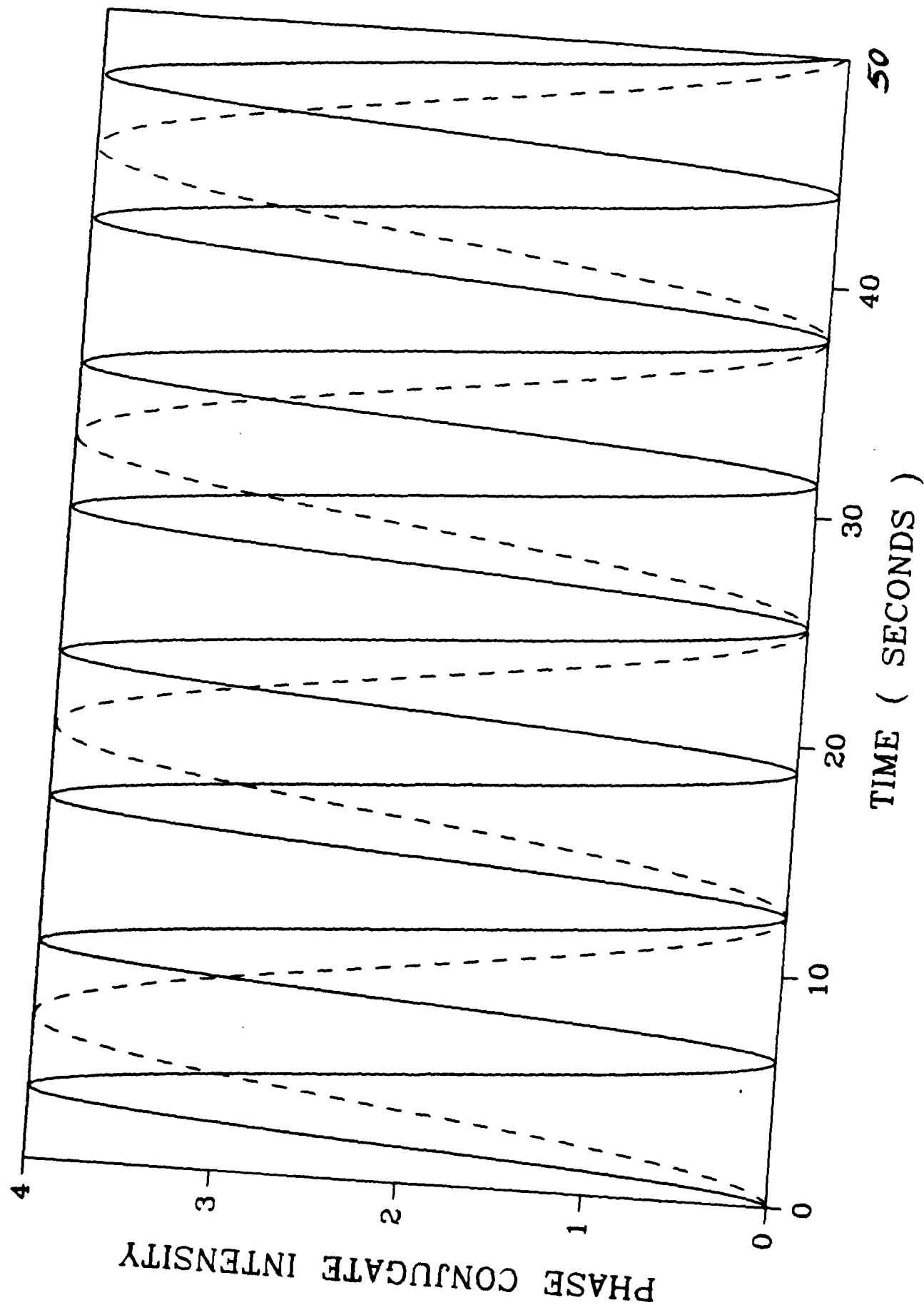
physical parameters in the calculation. We have chosen  $\Gamma_0 = 10^{-4}$   $I_0$  Hz and  $\delta_n = 1 \times I_0$  Hz. As the intensity increases by a factor of 2, the oscillation also increases by the same factor. This behavior, called self-pulsation, has been reported by Gunter et al. The second one involves the temporal evolution of the optical phase. The solution of the problem shows that there exists a frequency chirping, which decays in time at a rate given by  $\Gamma_0$ . This phenomenon may provide a clue to the origin of the self-scanning property of a barium titanate phase conjugate resonator.

\* Supported by the Army Research Office under contract No.

DAAL03-87-C-0001

1. J.O. White et al, Appl. Phys. Lett. 40 , 450 (1982)
2. J. Feinberg, Opt. Lett. 7 , 486 (1982)
3. R.A. McFarlane and D.G. Steel, Opt. Lett. 8 , 208 (1983)
4. R.A. Fisher, OPTICAL PHASE CONJUGATION, Academic Press (1983)
5. B.H. Soffer et al, Opt. Lett. 11 , 118 (1986)
6. K.R. McDonald and J. Feinberg, JOSA B 73 , 548 (1983).  
T.Y. Chang and R.W. Hellwarth, Opt. Lett.
7. J.F. Lam, Appl. Phys. Lett. 46 , 909 (1985)
8. P. Gunter et al, Opt. Commun. 55 , 210 (1985)
9. A.M.C. Smout et al, Opt. Commun. 59 , 77 (1986)

—  $1 \text{ W/cm}^2$       - - -  $0.5 \text{ W/cm}^2$



# ORIGIN OF ANOMALOUS DIELECTRIC RELAXATION TIME IN PHOTOREFRACTIVE MATERIALS \*

Juan F. Lam

Hughes Research Laboratories

Malibu, California 90265

## ABSTRACT

A solution to the sublinear intensity dependence of the photorefractive response is proposed. The theory predicts that the shallow traps are responsible for the  $I^{-1/2}$  behavior of the response time, in agreement with current experiments. The parameter  $\alpha$  is found to be a function of the temperature, the grating spacing and the width of the energy distribution of the shallow traps. The theory suggests a novel approach toward improving the room temperature response time of these materials by two orders of magnitude.



The initial understanding of the photorefractive effect in insulators was pioneered by Vinetskii and Kukhtarev <sup>1</sup>. They used the classical charge transport equations in a two band model to describe the interaction of light with the insulating material. Assuming that the generation of carriers take place via the photoionization of deep level impurities, followed by band transport mediated by diffusion, they arrived at an elegant expression for the change of the index of refraction due to the first order electro optic effect. This model has been very successful in predicting the majority of the macroscopic nonlinear optical phenomena such as two-wave mixing gain <sup>2</sup>, degenerate four-wave mixing <sup>3</sup>, and self pumped phase conjugation <sup>4</sup>.

In the last few years, there have been several attempts made to provide a deeper understanding of the fundamental physics underlying the photorefractive effect. Careful experiments <sup>5</sup> have been performed which showed that the charge transport model might be incomplete, and possibly unsuitable, for the measurement of critical physical parameters. These experiments indicated that the response time of these materials is not inversely proportional to the light intensity, as has been claimed from the simple solution of the charge transport equations.

The experiments involve (1) the writing of a spatial grating by the interference of two optical beams, whose propagation wave vectors are incident on the photorefractive material with an angle  $\theta$  relative to each other; (2) the erasure of this grating by either a coherent or incoherent optical beam; and (3) the coherent scattering of a fourth optical beam from the spatial grating, which acts as a read out process.

The results of the experiments indicate the following facts:

- A. The spatial grating decays exponentially at a rate which is proportional to the erase beam intensity to the  $x$  power, where  $x$  has been found to be less than 1.
- B.  $x$  increases toward unity as the temperature of the sample increases.

- C.  $\alpha$  depends on grating spacing.
- D. The spatial grating decay rate increases by two orders of magnitude when the temperature of the sample increases from 20 C to 120 C.

These results can not be explained from the current charge transport model. The results also indicate that the use of the original charge transport equations for the determination of mobility coefficient, deep level photoionization rates and deep level recombination rates might lead to significant errors. Current deduced values are based upon the linearity of the response time on the light intensity.

In view of the lack of understanding of the fundamental physics of photorefractive effect, this article proposes a solution, based on the existence of shallow traps, of the sublinear intensity dependence of the erasure rate. The predictions of the theory will be shown to be in qualitative agreement with all available experimental data.

The photorefractive effect arises from the change in the index of refraction  $n$  due to the generation of an internal space charge field  $E$  in an electro-optic crystal. That is,

$$\Delta\left\{\frac{1}{n}\right\} = r \cdot E \quad (1)$$

where  $r$  is the electro-optic tensor.

The space charge field,  $E$ , is produced by the diffusion process that is inherent in a spatial varying distribution of photo-ionized charge carriers, of density  $n$ , which in turn is generated by the interference of two optical beams, whose wave vectors make an angle  $\theta$  with respect to each other. The photo-ionized carriers originate from deep level impurities, having density  $N$ . The random motion in the band coupled with the spatial inhomogeneity of the distribution function leads to a charge separation between the ionized deep level impurities and the carriers. The ensuing Coulomb interaction sets up a space charge field which is stationary provided that the frequency of both optical beams are identical. The mechanism of diffusion is responsible for the nonlocal behavior of the index of refraction.

That is, the space charge field is  $90^\circ$  out of phase with respect to the photo-ionized carrier distribution.

The dynamics of the charge transport process takes an added but important complexity if shallow traps,  $N_t$ , are present in the material. The photogenerated carriers will hop in the shallow traps for a certain period ( as determined by their capture rate,  $\omega_t$ , and ejection rate  $r_t$  ) until they find deep levels to recombine. It is this the hopping process in the shallow traps that determine the intensity dependence of the photorefractive response time.

The dynamics of the charge carriers are described in terms of the following equations of motion

$$\frac{\partial n}{\partial t} + \frac{1}{q} \times \frac{\partial J}{\partial x} = S - \sum_i n\omega_i + \sum_i N_t r_i \quad (2a)$$

$$\frac{\partial N_t}{\partial t} = n\omega_i - N_t r_i \quad (2b)$$

$$\frac{\partial N}{\partial t} = S \quad (2c)$$

$$\frac{\partial E}{\partial x} = \frac{q}{\epsilon\epsilon_0} \times \{n + \sum_i N_t - N\} \quad (2d)$$

where  $J = q\mu E - D\partial n/\partial t$  and  $S = g - r$ . The notation  $g$  and  $r$  stands for the deep level photogeneration and recombination rates; respectively.

Equations (2) can be combined to arrive at the following exact expression for the time evolution of the space charge field:

$$\frac{\partial E}{\partial t} = -\left\{\frac{q\mu n}{\epsilon\epsilon_0}\right\}E + \left\{\frac{qD}{\epsilon\epsilon_0}\right\} \times \frac{\partial n}{\partial x} \quad (3)$$

The first term in Equation (3) describes the temporal response of the space charge field, while the second term describes its spatial diffusion. Hence the critical problem is to find an expression for the carrier density  $n$ . This task can be accomplished by using the method of statistical mechanics<sup>6</sup>. That is, the carrier density is directly related to the

probability,  $p(n)$ , of finding  $n$  carriers, in the presence of photogeneration, shallow trap hopping and deep level recombination. This fact can be written as

$$n = \int_0^{\infty} dn p(n) \quad (4)$$

The probability is given in terms of the density of states of the shallow trap levels as well as the number of photo-generated carriers. That is,

$$p(n) = \int_0^{\infty} dU g(U) \delta[n - n(U - qEd)] \quad (5)$$

where  $n = \sigma I(N_D - N_o)/\gamma N_o$  is the photo-generated carrier density from the deep traps,  $n(U)$  is the Fermi-Dirac distribution taking into account the internal space charge field and the effective hopping distance  $d$ ; and  $g(U) = A \exp[-(U - U_D)/kT_o] H(U - U_D)$  is the density of states of the shallow traps.  $H(U - U_D)$  is the Heavyside function. The physical parameters are the photoionization cross section,  $\sigma$ , the deep level recombination rate per unit volume,  $\gamma$ , the donor density,  $N_D$ , the acceptor density,  $N_o$ , the minimum shallow trap level,  $U_D$ , and the growth temperature of the sample,  $T_o$ . Inserting the respective quantities in Equation (4), one finds the following exact analytical expression for the optical response time of the photorefractive materials,

$$\tau = \frac{\epsilon \epsilon_o}{q \mu n_o^{1-x}} \times n^{-x} \times \exp(\Delta E/kTf) \quad (6)$$

where the exponent  $x$  is defined by

$$x = \frac{T}{T_o} \times \left\{ 1 - \frac{m \Delta k d}{1 + (\Delta k/k_o)^2} \right\} \quad (7)$$

and  $f = T_o x/T$  describes the action of the space charge field on the carriers moving in the band and hopping in the shallow traps.  $\Delta E$  is the difference between the Fermi energy and  $E_D$ .  $n_o$  is the dark carrier density,  $m$  is the modulation index arising from the two wave mixing process.  $\Delta k$  is the wavenumber of the generated spatial grating,  $k_o$  is the Debye wavenumber. Equation (6) is the key result of our work.

Several important conclusions can be derived from Equation (6). First, the optical response or erasure time is inversely proportional to the light intensity to the  $x$  power. In order to illustrate this point, Figure 1 depicts the erasure rate ( the inverse of the erasure time ) as a function of the erase beam intensity. The open triangle corresponds to the experimental data of Magerefteh and Feinberg<sup>5</sup>. And the solid line is the result of Equation (6). The theory is in qualitative agreement with the room temperature experimental data if  $T_o = 285K$  and  $\Delta E/k_B = 5000K$ . The computed theoretical value for  $x$  is .887, which is approximately equal to the experimental value of .88 . Hence the presence of shallow traps change the optical behavior of photorefractive materials in a very significant manner. Indeed estimates of optical response times, photoionization and recombination rates can be off by orders of magnitude, if the linear intensity dependence is used in the analysis.

Second, the exponent  $x$  is a function of the spatial grating wavenumber. This dependence arises from the work done the the space charge field on the carriers, leading to the change of their local effective temperature. Figure 2 compares the theoretical results with the experimental data of Chang<sup>7</sup>. The solid line is the result of the model, while the circles ( open and close ) are data taken from beam erasure experiments. The physical parameters used are  $m = .06$  for the modulation index,  $k_o^2 = 7 \times 10^9 cm^{-2}$  and  $\Delta k^2 = 7.60 \times 10^{10} cm^{-2}$ . The only variable in the theoretical fit was the hopping distance  $d$ , which was found to be approximately 370 nm. This numerical value is ten times larger than that estimated from the simple charge transport model. It appears to be consistent with the physical model that the carriers hops in the shallow traps before experiencing deep level recombination.

Third, Equation (6) predicts a response time which is exponentially decreasing with the equilibrium temperature of the sample. The dependence arises from the Fermi-Dirac distribution and the density of the shallow traps. Figure 3 compares the result of the theoretical model with the experimental data of Rytz et al<sup>8</sup>. Using their value of  $\Delta E/k_B = 5000K$ , we found that the results obtained from theory are in reasonably good agreement with experiments.

What can be predicted from the theoretical model? A key question in photorefractive nonlinear optics is the improvement of the optical response time of the material at room temperature. Figure 4 suggests an entirely new approach toward answering this important question. It shows that the optical response time can be decreased by at least three orders of magnitude at room temperature if  $\Delta E/k_b$  can be reduced from 5000 K to half its value. This can be accomplished by investigating techniques for reducing the difference between the Fermi-Dirac energy and  $E_D$ . It implies that the hopping processes that have slow capture rate and fast release rate in the shallow traps are key to the solution of this problem.

In conclusion, we presented, for the first time, a solution to the long-standing problem of sublinear intensity dependence of the optical response time of photorefractive materials. In addition, the theory predicts the distinct possibility of decreasing the optical response time of these materials by three orders of magnitude provided that the behavior of the shallow traps can be controlled properly.

- \* This work was first presented at the Conference on Lasers and Electro-Optics, Baltimore (April, 1989).

#### ACKNOWLEDGEMENT

The author extends his sincere thanks to Dr. Daniel Rytz and Dr. Tallis Chang for bringing into his attention the many subtleties of the experiments, and for their permission for using the experimental data in Figures 3 and 4. The support by the Army Research Office is gratefully acknowledged.

## REFERENCES

1. V.L. Vinetskii and N.V. Kukhtarev, Sov. Phys. Solid State **16**, 2414 (1975)
2. N.V. Kukhtarev, V.B. Markov, S.G. Odulov, M.S. Soskin, and V.L. Vintetskii, Ferroelectrics **22** , 949 and 961 (1979)
3. P. Gunter and F. Michelon, Ferroelectrics **18** 27 (1978); J.P. Huignard, J.P. Herriau, P. Aubourg and E. Spitz, Opt. Lett. **4** , 21 (1979); J.P. Huignard, J.P. Herriau, G. Rivet and P. Gunter, Opt. Lett. **5** 102 (1980)
4. J.O. White, M. Cronin-Golomb, B. Fischer and A. Yariv, Appl. Phys. Lett. **40** 450 (1982)
5. S. Ducharme and J. Feinberg, J. Appl. Phys. **56**, S39 (1984); D. Mahgerefteh and J. Feinberg, Opt. Lett. **13**, 1111 (1989).
6. There exists an equivalence between the charge transport equations (2) and the probabilistic interpretation proposed here. The equivalence arises from the energy dispersion of the shallow trap capture and eject rates. The physical interpretation is quite simple. The hopping mechanism is no more than the transport in a random medium, which consists of neutral traps having a range of activation energies. For an interesting discussion of this topic, the reader is referred to the important work of R.G. Palmer et al. Phys. Rev. Lett. **53**, 958 (1984).
7. T. Y. Chang, "Nonlinear optical studies of Barium titanate". Doctoral dissertation, University of Southern California (1986). This thesis contains the first careful experimental studies of the sublinear intensity dependence in barium titanate.
8. D. Rytz, M.B. Klein, R.A. Mullen, R.N. Schwartz, G.C. Valley, and B.A. Wechsler, Appl. Phys. Lett. **52** , 1759 (1988).

## FIGURE CAPTIONS

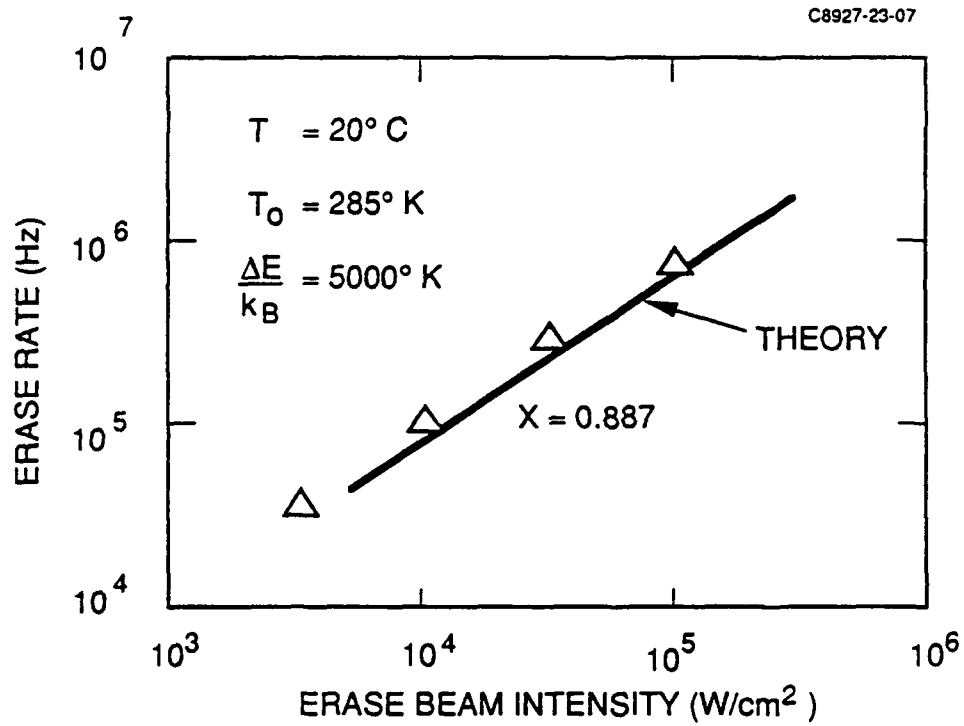
Figure 1 Intensity dependence of the erase rate at room temperature. The open triangle are taken from the experimental data of Reference 5. The solid curve is the result of the theory. The only fitting parameter is  $\Delta E/k_B$  and  $T_c$ .

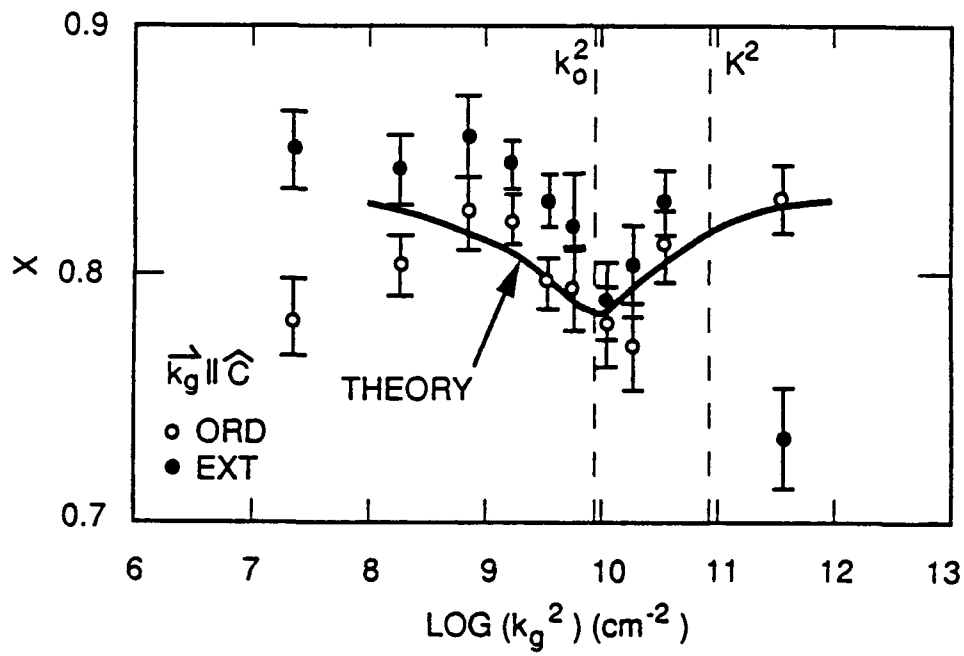
Figure 2 Dependence of the exponent  $x$  on the grating spacing. The solid curve is the result of the theory, while the open and closed circles are taken from the doctoral thesis of Chang. The only fitting parameter is the effective hopping length.

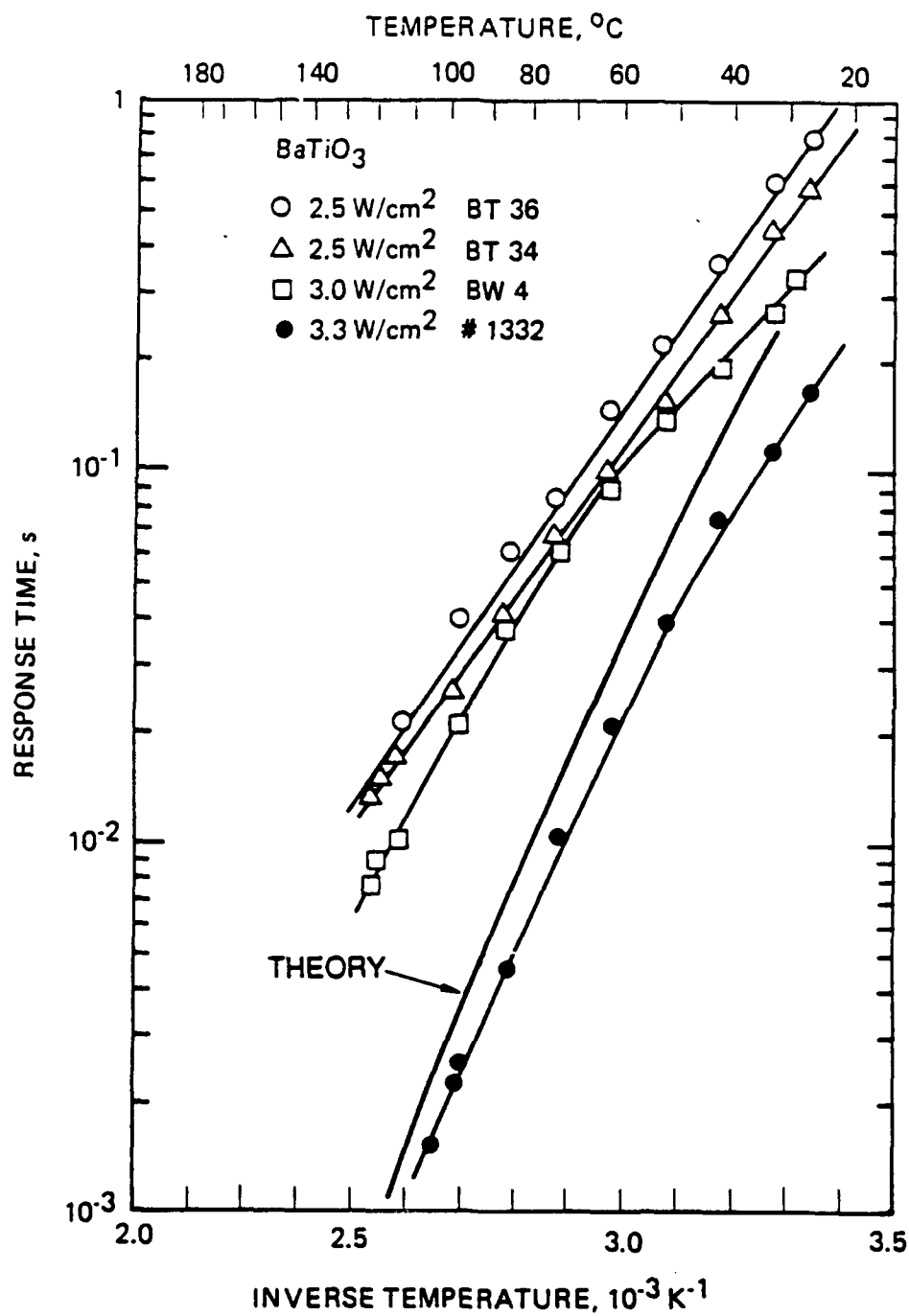
Figure 3 Dependence of the response time on the sample temperature. The solid line is the theory while the experimental data were taken from the work of Rytz et al.

Figure 4 The dielectric response time as a function of  $\Delta E/k_B$ , for room temperature operation.

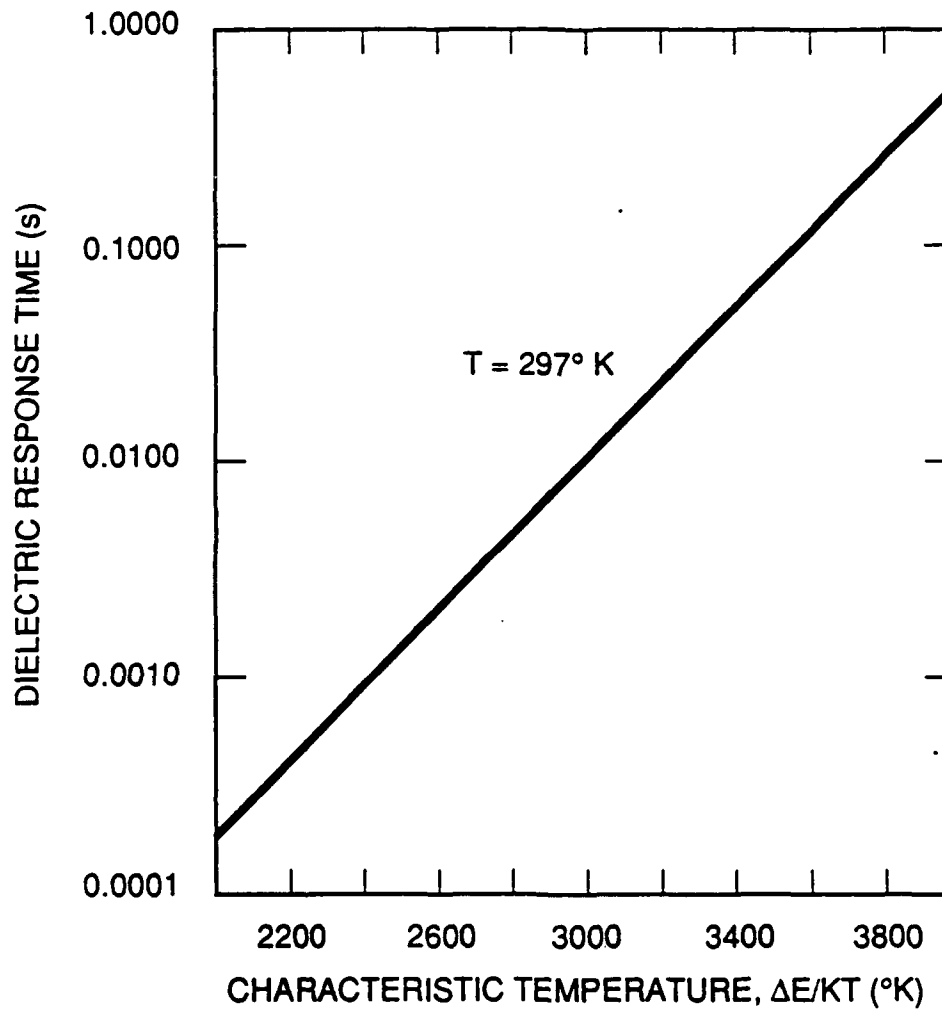








C8927-23-05



**THEORY OF STIMULATED SCATTERING PHASE CONJUGATION  
IN  
RESONANT SYSTEMS**

**Juan F. Lam  
Hughes Research Laboratories  
Malibu , California 90265**

**ABSTRACT**

A theory of self-pumped phase conjugation in resonant systems is presented. We postulate that stimulated backward two-wave mixing is the mechanism leading to the production of phase conjugate waves. We show that the conjugation process has a threshold behavior and the phase conjugate wave has an intrinsic frequency shift as a function of the pump intensity.

## I. INTRODUCTION

Self-pumped phase conjugation ( SPPC ) has been a subject of great interest due to its application in the area of optical signal processing<sup>1</sup>. The phenomenon of SPPC was first discovered when Stimulated Brillouin scattering was generated in a nonlinear medium <sup>2</sup>. They found surprisingly that the backscattered radiation had the property for correcting any artificial aberration imposed on the input pump field. This observation led to the development of phase conjugate optics as an integral part of quantum electronics. The success of SPPC lies in its simplicity for the implementation of phase conjugate mirrors. That is, a single input pump field can generate a backward propagating radiation field, whose optical phase is the negative of that of the input pump field provided specific energy and momentum conservation laws are satisfied. This general remark needs to be quantified dependent upon the circumstances of the experimental set-up. For example, experiments performed in a geometry where an optical cavity is present might also involve the process of four-wave mixing which will produce phase conjugate fields. However even in this case, given a single input pump field, stimulated scattering appears to play the dominant role in producing the additional two other coherent beams which are required for the four-wave mixing process to take place.

Subsequently , the same phenomenon has been replicated in photorefractive materials<sup>3</sup>, in Kerr media<sup>4</sup>, saturable absorbers<sup>5</sup> and lately in atomic vapor<sup>6</sup>. Self-pumped phase conjugation in photorefractive materials arises from the amplification of noise by means of coherent energy transfer between the incident pump field and the scattered field.<sup>7</sup> The mechanism responsible for net gain is the formation of a nonlocal traveling wave grating, arising from the diffusion and drift of charge carriers. An internal space charge field is produced by the spatial separation of the photo-ionized carriers from the defects present in the electro-optic crystals. The change of the index of refraction, which is proportional to the intrinsic space charge field, is 90 degree out of phase with respect to the intensity interference pattern. The scattering of the pump field from the refractive index generates

a coherent amplification of the scattered noise. Although this simple physical picture is acknowledged to be correct, there are complex behaviors such as intrinsic frequency shifts and instabilities that obscure the interpretation of the experimental data. The production of phase conjugate fields in a Kerr medium was observed in the presence of an optical cavity. In this case, the physics became clear. The pulsed laser induced stimulated Brillouin scattering which is allowed to bounce back and forth inside the resonator. Hence the counterpropagating beams in the resonator constitute the pump beams in the standard four-wave mixing configuration. Phase conjugate fields arise from the scattering of one of the counterpropagating beam from the interference pattern generated by the input pump and the other one of the intracavity beams. Intrinsic to the stimulated Brillouin scattering, there exists a large frequency shift of the order of one Ghz. In a similar manner, SPPC in sodium vapor was also observed in an intracavity configuration. Identical argument can be given to ascertain the origin of phase conjugate fields in the latter case.

In spite of these studies, little is understood concerning the role of stimulated scattering processes in the generation of phase conjugate fields in resonant materials. The experimental discovery of nearly phase conjugate wave in rhodamine 6 G by Koptev et al <sup>4</sup> led to the understanding that saturable absorbers impose a large frequency shift ( few hundreds angstroms ) between the input light and the scattered light. A preliminary theoretical model by Lam et al <sup>8</sup> appears to confirm the experimental findings. Furthermore, this theory predicted that even two-level systems do indeed generate gain in the absence of population inversion, leading to the appearance of phase conjugate fields. In addition, careful experiments<sup>8</sup> performed on rhodamine 6G indicated that the spectrum of the spontaneous emission noise was much wider than the spectrum arising from lasing action. And the phase conjugate spectrum mimics that of the spontaneous emission. These observations raise the question whether or not SPPC is a universal phenomenon; i.e. can this effect be generated in any nonlinear optical material ?. The objective of this work is to show that the fundamental physical mechanism giving rise to SPPC is stimulated two-wave

mixing. This is the same mechanism proposed to explain the origin of phase conjugate waves in photorefractive materials<sup>7</sup>. Furthermore, we shall show that the mechanism can be operative in any resonant systems. Hence, the objective of this work is to extend the results<sup>8</sup> and put into a coherent form a physical description of the fundamental physics of phase conjugate field generation arising from resonant systems.

Section II provides an intuitive physical description of the scattering mechanisms responsible for the generation of phase conjugate fields. This section discusses, in terms of simple physical arguments, criteria that are necessary for the stimulated two-wave mixing to occur. Utilization of the basic concepts such as conservation laws lead to a clear understanding of the scattering processes. The discussion set the stages for the detail calculation of the nonlinear response function, which is the objective of Section III. We assume that the resonant medium can be described in terms of a set of homogenously broadened two-level systems. We calculate the medium response using the density operator formalism, and couple the results with the wave equations in a self-consistent manner. Section III is included for sake of completeness. The results for the case of pump-probe interactions have been extensively analyzed previously<sup>9-15</sup>. Section IV provides a physical model for the generation of phase conjugate fields in resonant systems. This model gives additional insight into the nonlinear processes responsible for the origin of the phase conjugate field in stimulated scattering. A description of the nonlinear gain and dispersion functions for both the backward and forward scattered lights is presented. We will show that the optimum gain condition determines the frequency of the scattered field. A summary of our results is presented in section V.



## II. PHYSICAL PICTURE

The dynamics of backward stimulated two-wave mixing relies on the Rayleigh scattering to provide the noise source required in the formation of an interference pattern. Consider a pump field  $E_p$  incident upon an absorbing medium. The simultaneous absorption of the pump field and the generation of a fluorescence emission field produces an isotropic distribution of scattered fields. However only the component of the scattered field that is counterpropagating to that of the pump can generate, in general, a traveling wave grating ( assuming that they do not coincide in frequency ) . Subsequent scattering of the pump field reinforces and produces additional backscattered field  $E_s$ . Backward scattering possesses the advantage of achieving maximum spatial overlap between the incident and generated radiation fields. In analogy to the Zeldovich's argument of phase conjugation via stimulated Brillouin scattering, the component of the backscattered field that achieves maximum transverse spatial overlap with the input pump field is the phase conjugate field.<sup>2</sup>

The qualitative description given above can be quantified in the following manner. Consider the work done by the radiation field  $E(r,t)$  which is defined by  $W = \langle J \cdot E \rangle$ , where  $J$  is the nonlinear current density induced by the radiation field, and  $\langle \dots \rangle$  stands for the spatial average over one wavelength of light. The spatial averaging is required since macroscopic optical phenomena can only take place for interaction volume larger than one wavelength of light. Energy transfer between the incident pump field and the scattered field can only take place provided that  $W \neq 0$ . This fact can only be satisfied if there exists certain phase relationship between  $J$  and  $E$ . Figure 1 illustrates the essence of this discussion. At the top center of the figure is a picture of the intensity distribution for a period of one wavelength. On the left hand and right hand columns of the figure, the medium response, the current density and the work done by the field are illustrated from top to bottom. Now, the work done is just the total area under the curve. If the area is nonzero, then the work is finite. In this case energy transfer occur. As one can see nonzero

work is possible provided that the medium response is 90 degree out of phase with respect to intensity interference pattern, as seen from the figures in the left column. If the medium response is in phase with the intensity pattern, then the work done is identically equal to zero, as shown in the figures on the right column.

The important question to ask is how this simple picture relates with the problem encountered in resonant systems. These systems are known to possess two components in their optical responses to radiation fields. They are the absorption coefficient and the index of refraction. Gain does not occur except under conditions of population inversion or nonlinear wave mixing. The fundamental of energy transfer process can be understood in the framework of the dressed atom. The effect of a strong pump field is to induce changes in the eigenstates of the atom. Effectively the radiation field breaks the degeneracy of the eigenfunction in the following manner. The electric dipole interaction with the radiation field mixes the atomic eigenstates into a coherent superposition. Each atomic energy level acquires both a symmetric and an anti-symmetric wavefunctions, whose separation is the Rabi flopping frequency. Hence for an initial two-level system, the application of a strong radiation field gives rise to a 4-level system. The process of energy transfer can then be described in terms of a Raman-type interaction in which the absorption and reemission of the pump field gives rise to an amplification of the scattered field.

### III. FORMULATION OF THE PROBLEM

To quantify these ideas we carried out a calculation of the spectral lineshape gain for an ensemble of homogeneously broadened two-level atoms in the presence of an input pump field  $E_p$ , oscillating at a frequency  $\omega$ , and a backscattered field  $E_s$ , with a spectrum of oscillating frequencies  $\omega + \delta$ . The latter is due to the noise properties of scattered radiation, as remarked in the previous section. We shall allow  $\delta$  to vary in order to find out the condition under which the backscattered signal achieves an optimum gain, hence taking away energy from the pump. Furthermore it is assumed the magnitude of  $E_p$  is much stronger than that of  $E_s$ ; i.e. pump depletion is not taken into account. Starting from the density matrix equations, the strategy we shall follow is to solve exactly the response of the medium to  $E_p$  and then use the solutions to find the response of the medium to the wave mixing process due to  $E_p$  and  $E_s$ . The nonlinear wave mixing problem is then reduced to a self-consistent coupling between the density matrix equations and the Maxwell's equations.

The density operator  $\rho$  obeys the quantum transport equation

$$i\hbar \frac{d\rho}{dt} = [H_0, \rho] + [V, \rho] + i\hbar \left( \frac{d\rho}{dt} \right)_{rel} \quad (1)$$

where  $H_0$  is the unperturbed Hamiltonian,  $V = -\mu E$  is the electric dipole coupling to the radiation field, and the last term on the right hand side is the relaxation due to reservoir coupling. In a closed two-level system ( no state selective collisions present ), the last term takes on a very simple form for the case of a two-level system. If  $|1\rangle$  and  $|2\rangle$  are the ground and excited states of  $H_0$ ; then

$$\left( \frac{d\rho_{11}}{dt} \right)_{rel} = \gamma \rho_{22} \quad (2a)$$

$$\left( \frac{d\rho_{22}}{dt} \right)_{rel} = -\gamma \rho_{22} \quad (2b)$$

$$\left( \frac{d\rho_{12}}{dt} \right)_{rel} = -\frac{\gamma}{2} \rho_{12} \quad (2c)$$

where  $\gamma$  is the radiative decay rate of the excited state. Using the assumption that the incident pump field is much stronger than the scattered field, one can write the electric dipole coupling in the following manner

$$V = -\mu E_p(r, t) - \mu E_s(r, t) \quad (3)$$

We shall first solve the density operator equation for  $E_p$  exactly, and then use the solution to solve the density operator equation for  $E_s$ .

The components of the density operator equation for the pump field  $E_p$  are given by

$$\frac{d\rho_{11}^{(0)}}{dt} = \gamma\rho_{22}^{(0)} + \frac{1}{i\hbar}\{V_{12}^{(0)}\rho_{21}^{(0)} - \rho_{12}^{(0)}V_{21}^{(0)}\} \quad (4a)$$

$$\frac{d\rho_{22}^{(0)}}{dt} = -\gamma\rho_{22}^{(0)} - \frac{1}{i\hbar}\{V_{12}^{(0)}\rho_{21}^{(0)} - \rho_{12}^{(0)}V_{21}^{(0)}\} \quad (4b)$$

$$\left\{\frac{d}{dt} + \frac{\gamma}{2} - i\omega_o\right\}\rho_{12}^{(0)} = \frac{1}{i\hbar}V_{12}^{(0)}(\rho_{22}^{(0)} - \rho_{11}^{(0)}) \quad (4c)$$

where  $\omega_o$  is the two-level transition frequency and the superscript , (0), stands for the equations and solutions pertinent to  $E_p$ . That is,  $V_{12}^{(0)} = -\mu_{12}E_p(r, t)$  is the potential energy due to the electric dipole moment  $\mu_{12}$  coupled to  $E_p$ .

In a similar manner, the components of the density operator equation for the scattered field  $E_s$  are given as

$$\frac{d\rho_{11}^{(1)}}{dt} = \gamma\rho_{22}^{(1)} + \frac{1}{i\hbar}\{V_{12}^{(0)}\rho_{21}^{(1)} - \rho_{12}^{(1)}V_{21}^{(0)}\} + \frac{1}{i\hbar}\{V_{12}^{(1)}\rho_{21}^{(0)} - \rho_{12}^{(0)}V_{21}^{(1)}\} \quad (5a)$$

$$\frac{d\rho_{22}^{(1)}}{dt} = -\gamma\rho_{22}^{(1)} - \frac{1}{i\hbar}\{V_{12}^{(0)}\rho_{21}^{(1)} - \rho_{12}^{(1)}V_{21}^{(0)}\} - \frac{1}{i\hbar}\{V_{12}^{(1)}\rho_{21}^{(0)} - \rho_{12}^{(0)}V_{21}^{(1)}\} \quad (5b)$$

$$\left\{\frac{d}{dt} + \frac{\gamma}{2} - i\omega_o\right\}\rho_{12}^{(1)} = \frac{1}{i\hbar}V_{12}^{(0)}[\rho_{22}^{(1)} - \rho_{11}^{(1)}] + \frac{1}{i\hbar}V_{12}^{(1)}[\rho_{22}^{(0)} - \rho_{11}^{(0)}] \quad (5c)$$

where  $V_{12}^{(1)} = -\mu E_s(r, t)$  is the potential energy of the electric dipole moment  $\mu_{12}$  coupled to  $E_s$ .

The density operator equations have very simple physical interpretation. The right hand side of the equations for the population of the ground and excited states describe the work done by the field on the atoms. The right hand side of the equations for the optical coherence describe the coherent scattering of light from induced gratings in the population difference.

The polarization density that contributes to the evolution of  $E_s(r, t)$  is defined by

$$P(r, t) = \text{Trace}(\rho^{(1)} \mu) = \rho_{12}^{(1)} \mu_{21} + h.c. \quad (6)$$

where h. c. stands for the hermitean conjugate of the first term. The polarization density enters into the Maxwell's equations as a source term. The wave equation can be reduced into a simple form if one assumes that the envelope of the radiation field varies slowly on a spatial scale as compared to the wavelength of light. This is just the slowly varying envelope approximation. That is, if  $E(r, t) = (1/2) \int d\omega A(r, \omega) \exp i(kr - \omega t) + c.c.$ , then one can neglect the second order spatial derivative, along the direction of  $k$ , of  $A$  in the wave equation. Using this assumption, one obtains the following expression for the Fourier envelope

$$\frac{dA}{dr} = i\epsilon \left( \frac{\omega}{c} \right) < P(r, t) \exp(-i(kr - \omega t)) > \quad (7)$$

where  $\epsilon = 1$  for forward scattered light and  $\epsilon = -1$  for backward scattered light. The boundary conditions for the problem is the following. For the forward scattered light, a finite amplitude of the radiation field is given at the entrance to the material. For the case of backward scattered light, the amplitude of the scattered light is set to a constant at the back of the material. This constant is determined by the amount of resonance fluorescence present in the material.

#### IV. ANALYTICAL SOLUTIONS AND PHYSICAL INTERPRETATION

We shall assume that all physical quantities are the Fourier components, unless otherwise stated. Using the slowly varying envelope and rotating wave approximations, the steady state solutions are given as

$$\rho_{22}^{(0)} - \rho_{11}^{(0)} = - \frac{N_o}{1 + \text{Re}\{L(\Delta)\} \times (I/I_s)} \quad (8)$$

is the population difference between the excited and ground state of the two-level systems.  $\text{Re}$  stands for the real part of a complex quantity. The factor  $L(\Delta) = 1/(\gamma/2 + i\Delta)$  is the complex spectral lineshape.  $\Delta = \omega - \omega_o$  is the pump detuning from resonance.

$$\rho_{12}^{(0)} = iR_o^* L(\Delta) [\rho_{22}^{(0)} - \rho_{11}^{(0)}] \quad (9)$$

is the optical coherence induced by  $E_p$ .  $R_o = \mu E/2\hbar$  is the Rabi flopping frequency. These solutions are well known in the context of saturated absorption and dispersion of coherent light.

Equations (8) and (9) are used to find the nonlinear optical coherence which is obtained from an exact solution of Eqs. (1), and is given as

$$\rho_{12}^{(1)} = \left(\frac{1}{D}\right) \{ iR_1^* [\rho_{22}^{(0)} - \rho_{11}^{(0)}] + \frac{2R_1^* R_o^* \rho_{21}^{(0)}}{\gamma - i\delta} \} \quad (10)$$

with

$$D = \frac{\gamma}{2} + i(-\delta + \Delta) + (I/I_s) \times \frac{\gamma^2}{\gamma + i\delta}$$

where  $\delta$  is the frequency detuning of the scattered field with respect to the pump field. Equation (10) has the following physical interpretation. The first term is just the absorption coefficient of  $E_s$ , modified by the presence of  $E_p$ . That is, the population difference is altered by the action of the pump field. The second term gives rise to stimulated two-wave mixing processes, and its strength is attributed to the formation of a traveling wave grating. The grating contribution is reflected in the nonzero value of  $\delta$ .

The equation for the scattered field is derived with the help of Eq.( ), and the results is

$$\frac{1}{A_s} \frac{dA_s}{dt} = -\epsilon F(\Delta, \delta, I/I_s) \quad (11)$$

where the complex function  $F$  determines the condition for net gain or loss, as well as the nonlinear dispersion coefficient of the material. In specific,  $F$  is given as

$$F(\Delta, \delta, I/I_s) = \frac{\alpha}{2} \frac{1}{1 + \frac{I/I_s}{[1 - (2\Delta/\gamma)^2]}} \frac{1}{1 - i(\Delta - \delta) + \frac{(I/2I_s)}{(1 + i\delta/\gamma)}} \{1 - \frac{(I/2I_s)}{1 + i\delta/\gamma} \times L(\Delta)\}$$

where  $\alpha$  is the linear on-resonance absorption coefficient of  $A_s$ . The second factor on the right hand side is the saturation parameter due to the strong pump field. The third factor is the pump modified spectral response of  $A_s$ . And the last factor consists of two terms. The first one, which is proportional to 1, is just the linear loss and dispersion contribution. The second term describes the two-wave mixing interaction. Equation (12) has the following physical interpretation. Given a specific  $\Delta$  and  $I/I_s$ , there exists a range of  $\delta$  such that coherent energy transfer takes place from the input pump field to the scattered field. For example, if the real part of  $F$  is negative for certain range of  $\delta$ , then the backscattered field is coherently amplified. On equal footing, if the real part of  $F$  is positive for certain values of  $\delta$ , then the forward scattered field is amplified.

In order to appreciate the results obtained, we proceed to provide a pictorial description of the real and imaginary part of  $F$ . The real part describes the effect of absorption or amplification. The imaginary part is just the effective dispersion coefficient. Figure 2 represent the real part of  $F$  when the input pum field is tuned to resonance (  $\Delta = 0$  ). The results indicate that for low input pump field, no net two-wave mixing gain is ever achieved. Amplification of the scattered light occurs for  $I/I_s = 10$  as shown in Figure (2c). A double sideband amplification is achieved for the scattered field detuned from the

input pump field by about 2.5 times the linewidth. For higher values of  $I/I_s$ , one noticed a ring like structure for the scattered light. This phenomenon has been observed in high intensity experiments performed in Na vapor, and will occur provided that the spectrum of the scattered light has enough bandwidth in order to accomodate the gain spectrum.

Figure 3 describes the effect of detuning of the pump field from resonance. Again, for low intensity of the input pump field, gain does not take place. Gain is achieved as shown in Figure 3c, where  $I/I_s = 10$ . The spectrum acquires a skew symmetry, remminescence of dispersionlike lineshape. Gain is possible only for the low frequency component of the scattered light. The dispersionlike character is accentuated in Figure 3d where the input intensity is far above saturation. The origin of the dispersive character is easily understood as arising from the response of the material to the applied radiation field. When the input field is detuned, the two-level system has a tendency to follow the radiation field, and the lineshape is determined by the detuning parameter, and not by the linewidth, as is true in resonant situations.

Figure 4 describes an extreme case where the incident pump field is far detuned from resonance. Again, no gain is present for low intensity. Small amount of gain start to appear for  $I/I_s = 10$ . The gain feature becomes more pronounced when the intensity of the pump is far above saturation.

These spectral line features becomes more complicated when one factors in the flourescence spectrum of the atom. That is, if one takes into account the spectral width of the scattered radiation. An intuitive deduction can be obtained in the following manner. Suppose that the spectrum of the scattered light mimics that of the input pump field; assumed to have a bandwidth  $\Delta\Omega$ . Then the scattered radiation will be amplified provided that the spectral gain falls within the bandwidth of the pump field.

The nonlinear dispersion coefficient is displayed in Figure 5 and 6 for the case of on-resonance and far detuned from resonance. The dispersion line shapes are just the



derivatives of the nonlinear lineshape, as should be from the Kramers-Kronig relation. The dispersion lineshape determines the nonlinear index of refraction of the material.

A brief summary is in order. The Fourier component of  $F$  contains two terms. The first one in the numerator describes the effect of linear absorption and dispersion, modified by the wave mixing effects. The second term arises from the intrinsic two-wave mixing process. The sign of  $F$  determines the condition for the amplification of the scattered light. However, a condition must be satisfied. The spectrum of the input incident field must fall within the gain bandwidth in order for the scattered radiation to acquire energy without population inversion. This picture is consistent with the fundamental physics of resonance fluorescence. If the radiation field spectral bandwidth is narrower compared to the natural linewidth, then the scattered light spectral bandwidth is identical to that of the pump field.

Equation (11) has a simple exponential solution within the regime of our approximation. The occurrence of gain for the backscattered field depends entirely on the behavior of  $F$ . Several interesting features can be derived from Eq. (11). First,  $F$  has two contributions. The real part of  $F$  describes the gain or loss characteristics of the self-pumped wave mixing process. For a specific set of  $\Delta$  and  $\delta$ , the real part of  $F$  goes through a null as a function of  $I/I_s$ . It implies that the self-pumped process has a threshold behavior. This conclusion is shown in Figure 8 where the net absorption coefficient is plotted for the case of a model atomic vapor with density of  $10^{11} \text{ cm}^{-3}$  and the input pump field is tuned on resonance. It is assumed that there exists no frequency mismatch. For this case, threshold for gain is obtained at  $10 \text{ W/cm}^2$ . For input intensities higher than  $10 \text{ W/cm}^2$ , the backscattered field  $E_s$  is coherently amplified from the spontaneous noise. The second contribution is the imaginary part of  $F$  which gives rise to the nonlinear dispersive behavior of the backscattered wave.

## V. GENERATION OF PHASE CONJUGATE FIELDS: A SIMPLE MODEL

And last, although the analysis above shows the possibility of backward gain under the condition of achieving threshold, it is important to point out that the backscattered field is the phase conjugate of the pump field. This can be accomplished by applying the rudiments of scattering theory to wave mixing processes. The pump field can be written as

$$E_p = E_0 \exp(iKz) + \lambda \int d\kappa E_1(\kappa, z) \exp(i\kappa r_{\perp} + ikz) \quad (12)$$

where the first term is a plane wave propagating along the  $z$  axis and the second term contains all the distorted components of the pump field, after passing through an aberrator. The dummy parameter  $\lambda$  describes the relative magnitude of the second term with respect to the first term. In a similar manner, one can write the scattered field as

$$E_s = E_1 \exp(-iK'z) + \lambda \int d\kappa E_m(\kappa, z) \exp(i\kappa r_{\perp} - ik'z) \quad (13)$$

where the first term is again a plane wave propagating in the opposite direction to the pump field and the second term arises from the scattered component due to wave mixing processes. We shall assume in our analysis that  $\lambda < 1$  i.e. the magnitude of the scattered component in Eq.(13) is small compared to the plane wave component. Using Eq.(12) in Eq.(13), one obtains the following spatial evolution equation for the scattered field envelope  $E_m$

$$\frac{dE_m}{dz} = AE_m + B\{E_1 E_0 E_1^* + E_1 E_0^* E_1 \exp(i\Delta kz)\} \quad (14)$$

Where  $A = a F(I)$ ,  $B = -2 A G(I)/E_{sat}^2$ ,  $F(I) = (1-I)/(1+I)(1+2I)$ ,  $G = 1/(1+2I) + 1/(1-I)$ ,  $I = I_0/I_s$  and  $\Delta k = 2(k-K)$ . The on-resonance saturating field  $E_{sat}$  is equal to  $2I_s/c\epsilon_0^{1/2}$ . Equation (14) has a very simple physical interpretation. The first term on the right hand side is just the DC response of the medium. The second term has all the important information concerning the degree of phase conjugation. The first term inside the bracket represents the degenerate four-wave mixing process giving rise to phase conjugate fields.

i.e. proportional to  $E_1^*$ . The second term inside the bracket describes the existence of the non-conjugate field, i.e. proportional to  $E_1$ . However these two terms differ by a phase factor  $Wkz$ , which is a measure of the degree of distortion of the input pump field. The second term can be made negligible provided that the combination of distortion and/or the length of the medium is long enough to make  $\Delta kz > 2\pi$ . The appearance of the non-conjugate component in self-pumped phase conjugation is a consequence of the collinear geometry inherent in the problem. The same effect appears in collinear degenerate four-wave mixing. Hence for sufficiently long interaction length, the phase conjugate component of the backscattered field dominates. This result points out that if the pump intensity exceeds threshold for backscattering to take place and for long interaction length, the backscattered field is the phase conjugate of the input pump field.

## CONCLUSIONS

In summary, a theory of self-pumped phase conjugation in resonant media has been presented. We predict the existence of a threshold behavior for backward gain, we attribute the origin of frequency sidebands to the dynamic Stark effect and we found that the nonconjugate component of the backscattered field can be eliminated by using a long interaction length.

- \* Work supported by the Army Research Office under contract *No. DAAL03 - 87 - C - 0001* and by the Air Force Office of Scientific Research under contract *F49620 - 88 - C - 0042*

## REFERENCES

1. R.A. Fisher, OPTICAL PHASE CONJUGATION, Academic Press (1983)
2. B.Y. Zeldovich, V.J. Popovichev, V.V. Ragulskii and F.S. Faisullov, JETP Lett. 15 . 109 (1972)
3. J. Feinberg, Opt. Lett. 7 , 486 (1982);
4. V.G. Koptev, et al , Sov. Phys. JETP Lett. 28 , 434 (1978); E.V. Ivakin et al, Sov. Phys. JETP Lett. 30 , 613 (1978); Lazaruk, Sov. J. Quantum Electron. 9 , 1041 (1979).
5. J.F. Lam, S.C. Rand, R.C. Lind, R.A. McFarlane and A.L. Smirl, Proc. International Quantum Electronics Conference, San Francisco (1986).
6. J.F. Lam, Appl. Phys. Lett. 46 , 911 (1985). T.Y. Chang and R.W. Hellwarth, Opt. Lett. 10 , 408 (1985).
7. S.H. Autler and C.H. Townes, Phys. Rev. 100 , 703 (1955).
8. J.H. Marburger, in OPTICAL PHASE CONJUGATION, edited by R.A. Fisher , Academic Press ( 1983 ).
9. S.G. Rautian and I.I. Sobel'man, Sov. Phys. JETP 14, 328 (1961), Sov. Phys. JETP 17, 636 (1963)
10. E.V. Baklanov and V.P. Chebotaev, Sov. Phys. JETP 34, 490 (1972)
11. S. Haroche and F. Hartman, Phys. Rev. A6, 1280 (1972)
12. B.R. Mollow, Phys. Rev. A5, 2217 (1972)
13. M. Sargent III, and P.E. Toschek, Appl. Phys. 11, 107 (1976)
14. G. Khitrova, P.R. Berman, and M. Sargent III, JOSA B 5, 160 (1988)
15. M.T. Gruneisen, K.R. McDonald and R.W. Boyd, JOSA B 5, 123 (1988)

## FIGURE CAPTIONS

- Figure 1. The intensity modulation, medium response, current density, and the work done by the field, from top to bottom.
- Figure 2. The nonlinear lineshape or the real part of  $F$  as a function of pump-probe detuning, for distinct values of the input intensity. The case of resonant excitation is considered
- Figure 3. The nonlinear lineshape or the real part of  $F$  as a function of pump-probe detuning, for distinct values of the input intensity. The case of the pump detuned one linewidth away from resonance
- Figure 4. The nonlinear lineshape or the real part of  $F$  as a function of pump-probe detuning, for distinct value of the input intensity. The pump is detuned by 10 times the linewidth away from resonance
- Figure 5. The nonlinear dispersion coefficient for the on-resonance case, for distinct values of the input intensity
- Figure 6. The nonlinear dispersion coefficient for the case when the incident pump field is detuned by 10 times the linewidth away from resonance
- Figure 7. The net absorption coefficient as a function of the input pump intensity. Positive values of the net absorption coefficients represent losses while negative values represent gain.

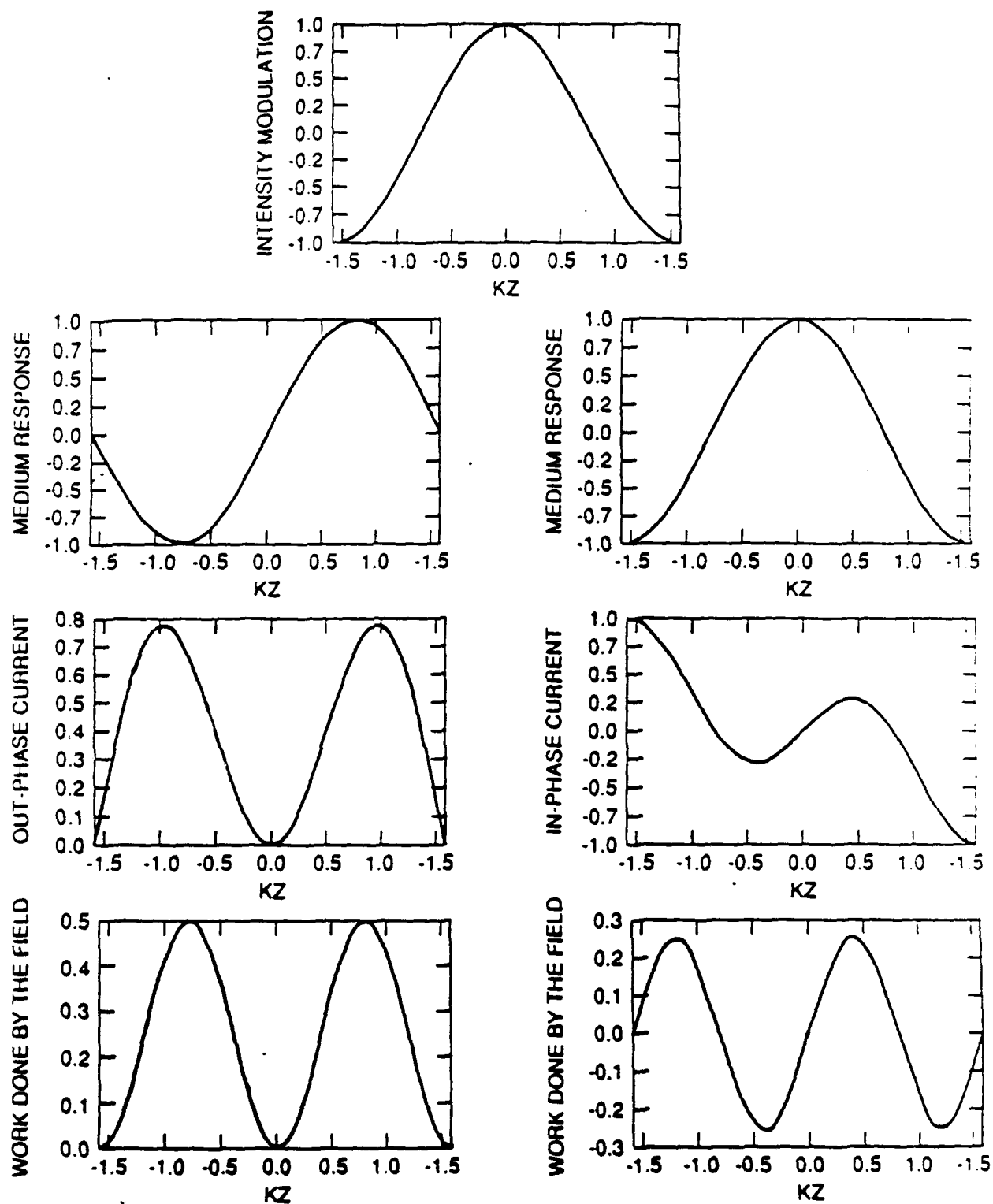


Figure G-1

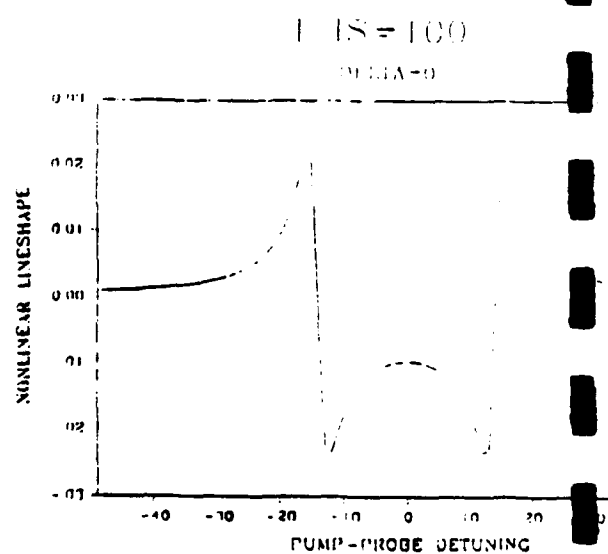
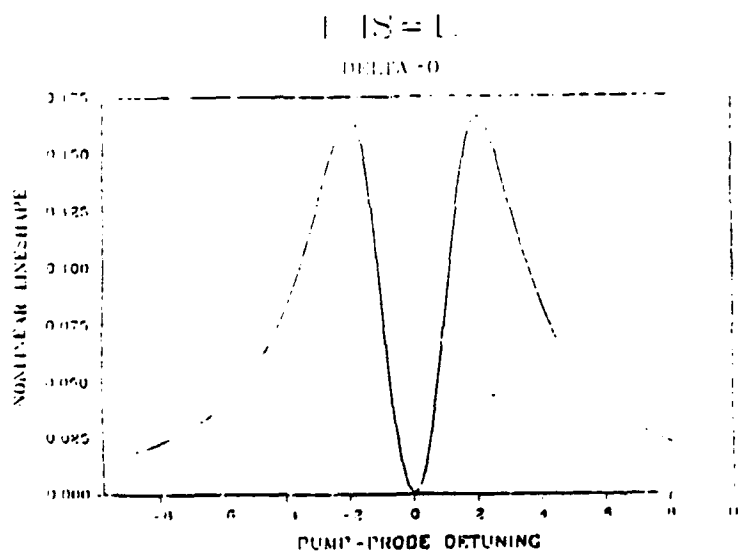
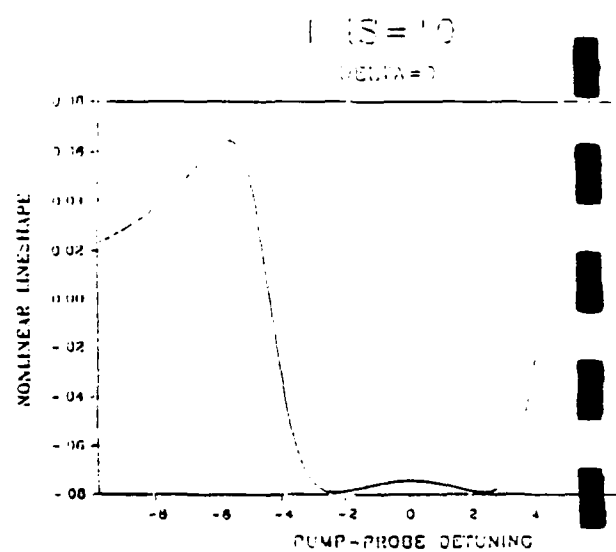
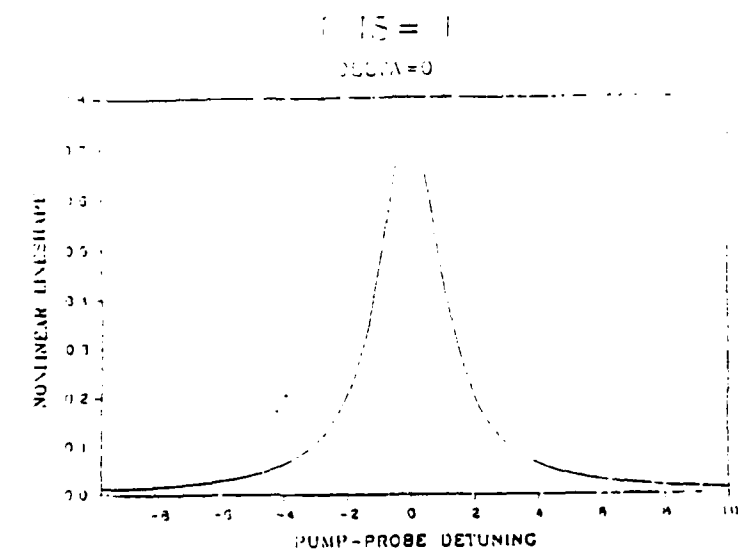


Figure G-2



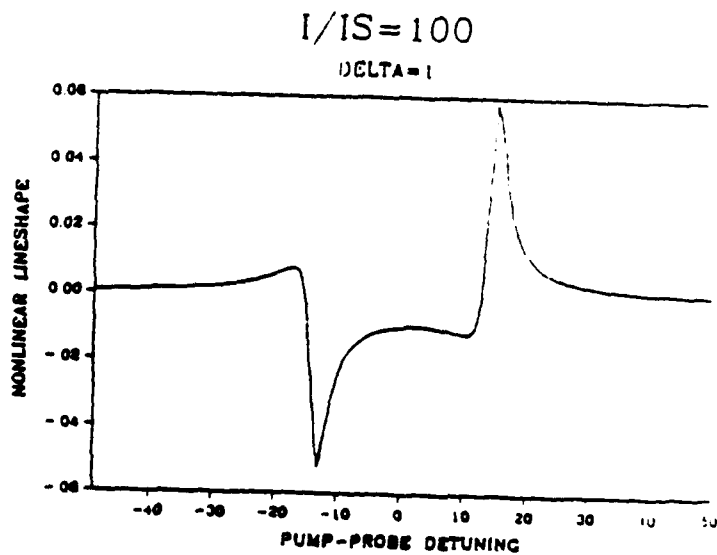
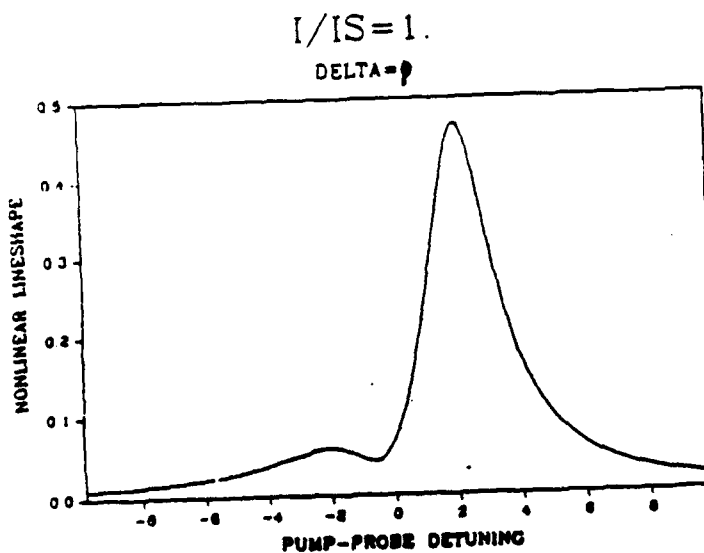
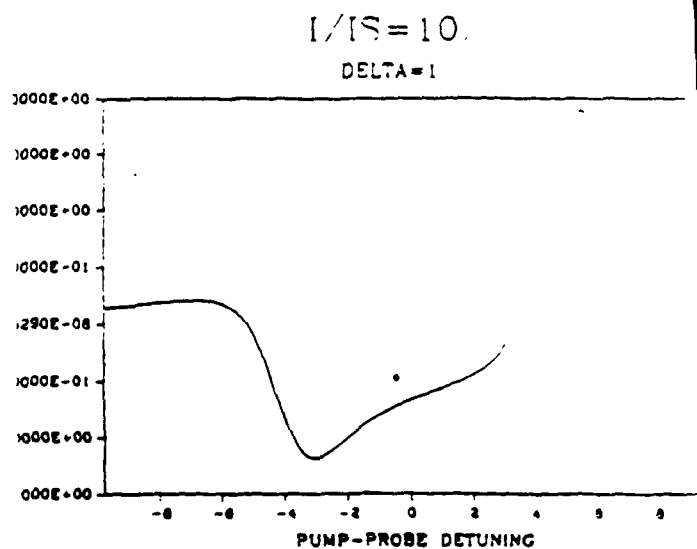
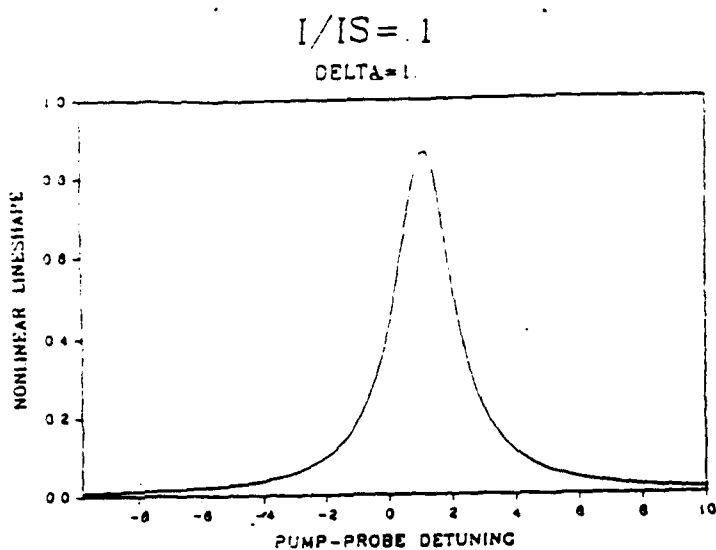


Figure G-3

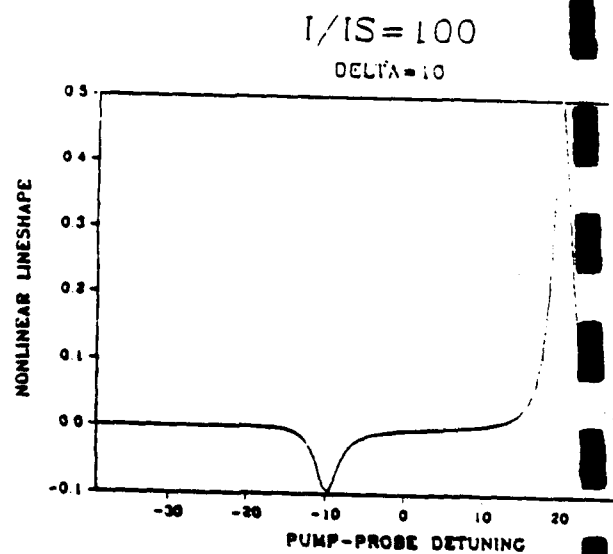
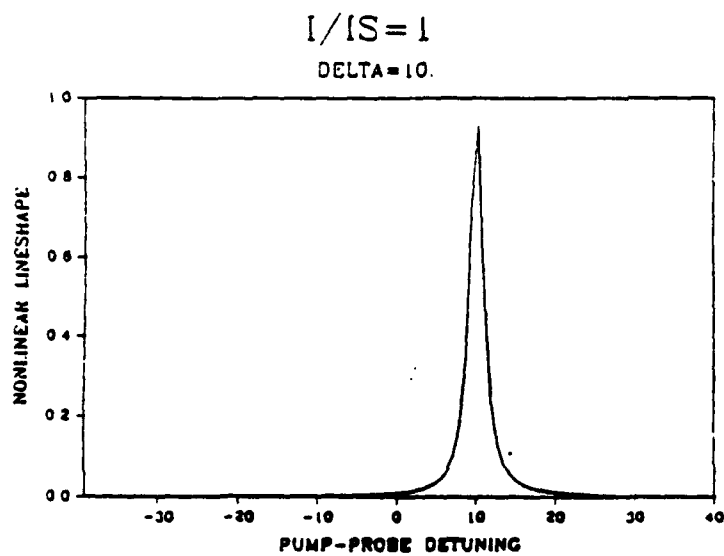
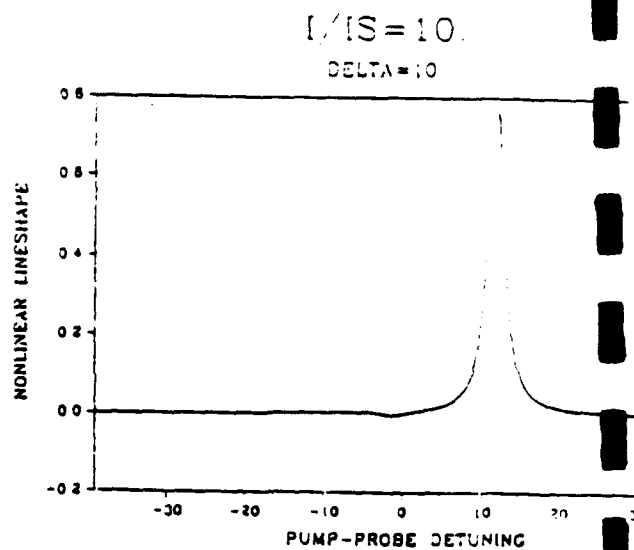
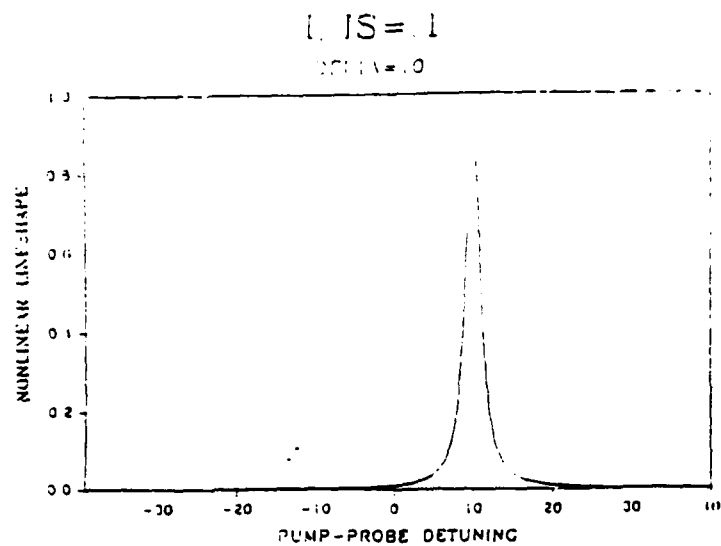


Figure G-4

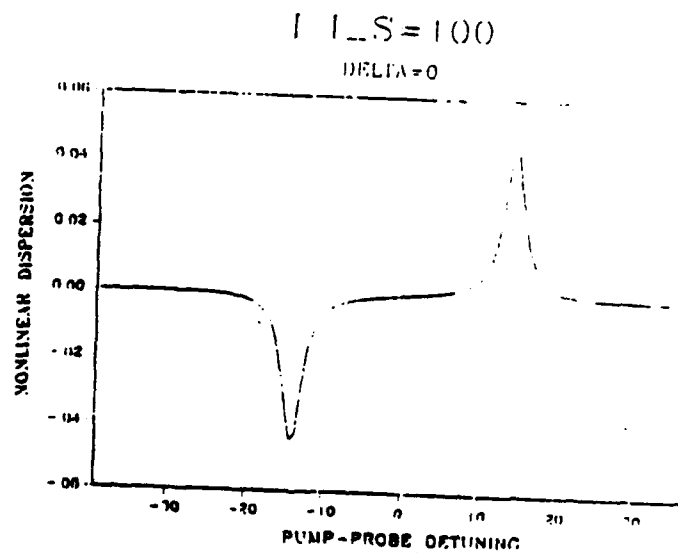
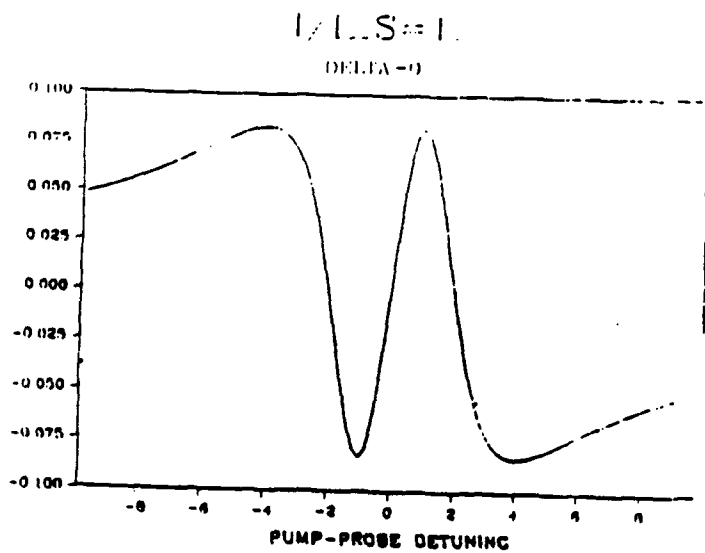
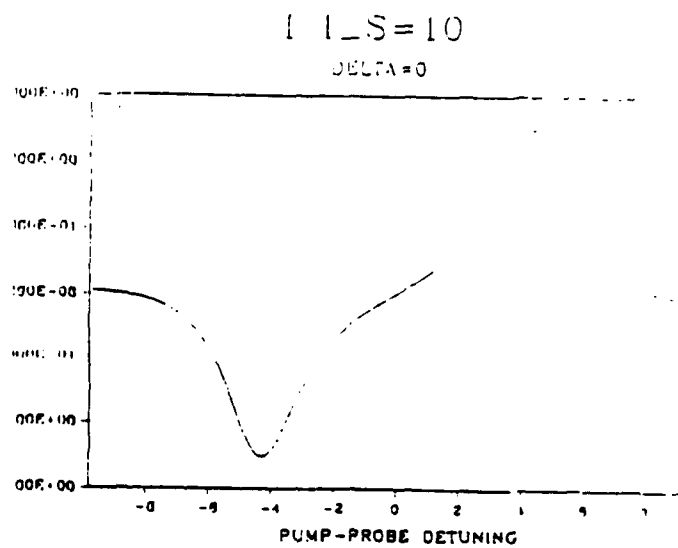
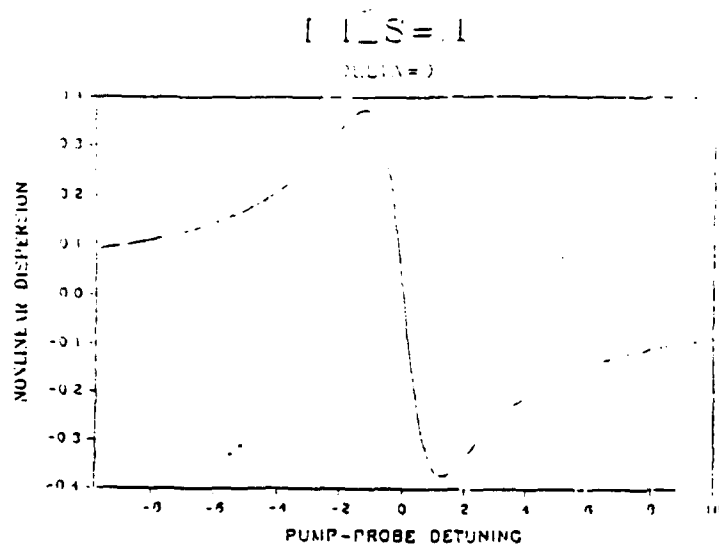


Figure G-5

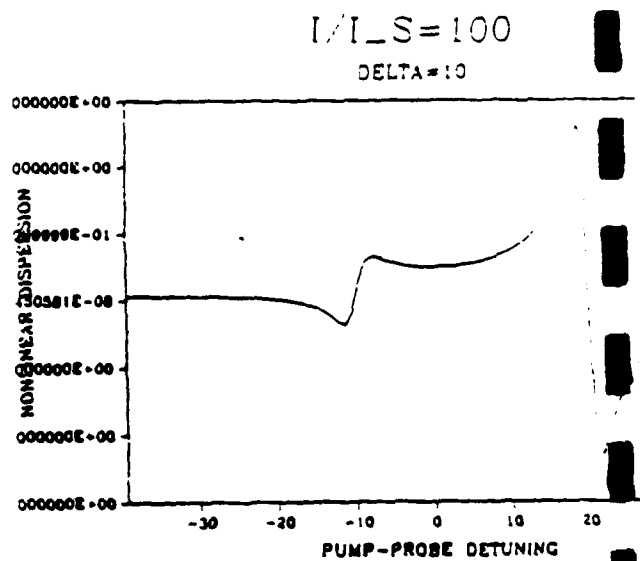
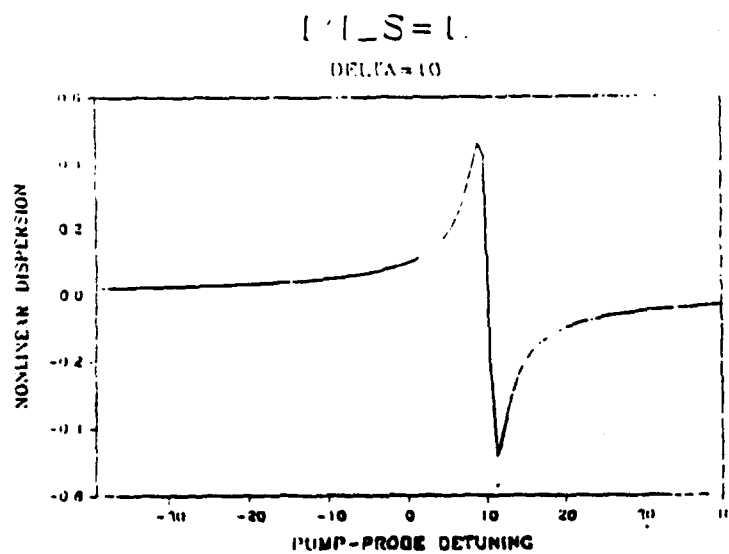
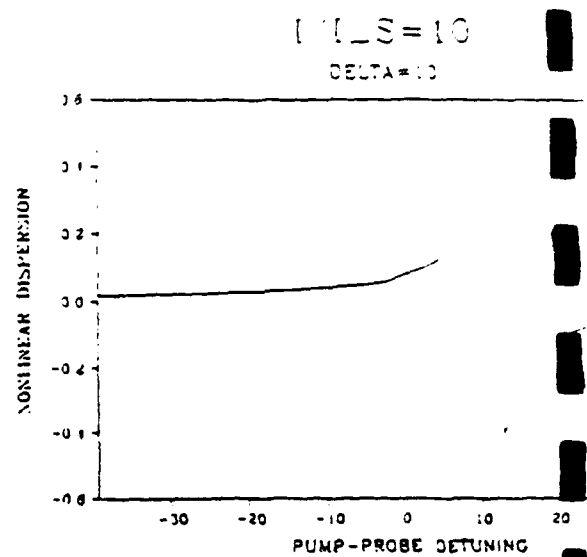
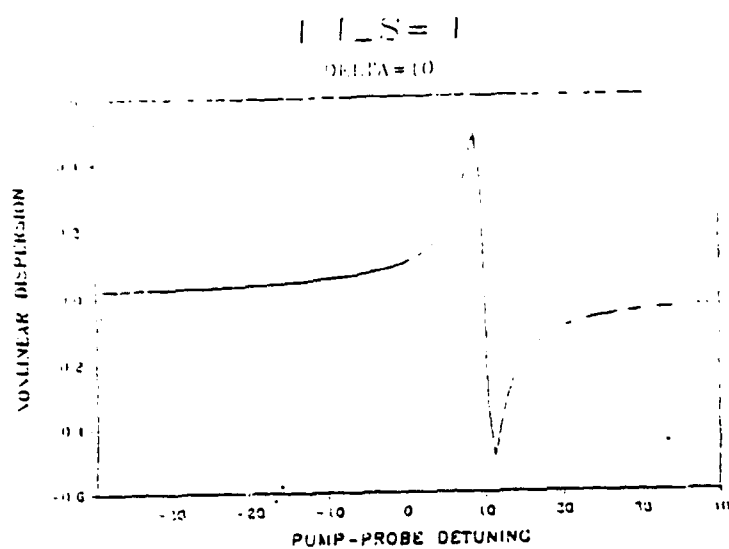


Figure G-6

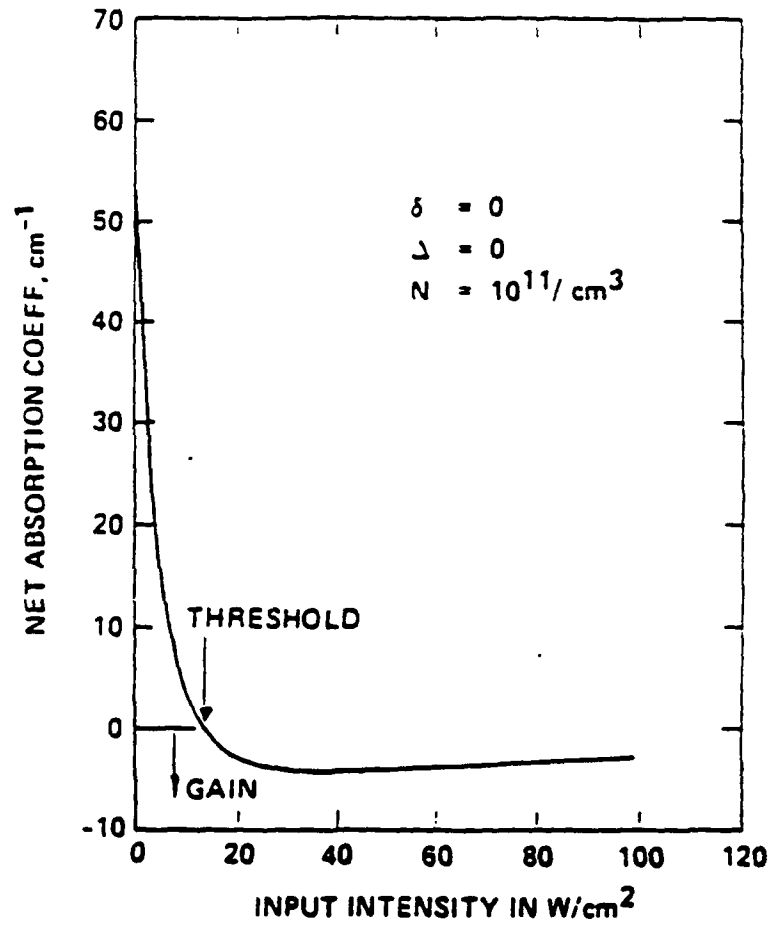


Figure G-7

# Resonant self-pumped phase conjugation in cesium vapor at .85 micron

Celestino J. Gaeta and Juan F. Lam

Hughes Research Laboratories, Malibu, California 90265

We report the first observation of resonant self-pumped phase conjugation at diode laser wavelengths. A phase conjugate reflectivity of 0.1%, and a cw threshold intensity of  $35 \text{ W/cm}^2$  were measured.

The search for an ideal self-pumped phase conjugate mirror has been an objective of active research in optics recently. This special mirror must have the following desirable properties: fast response and build-up times, a large phase conjugate reflectivity and a small frequency mismatch between the input and phase conjugate waves. Stimulated scattering processes<sup>1</sup> via acoustic and molecular vibrations have the disadvantage of high threshold intensity ( $> \text{MW/cm}^2$ ) and large frequency mismatch ( $> 1 \text{ GHz}$ ). Photorefractive materials<sup>2,3</sup> are restricted by their slow build-up time ( $> \text{minutes}$ ) and an intensity dependent response time ( $> \text{seconds}$  for typical cw laser input power). However both share the unique advantage of possessing large phase conjugate reflectivity. For example, reflectivity as large as 60% in barium titanate and  $> 90\%$  for stimulated Brillouin scattering have been measured.

Recently, we reported the demonstration of self-pumped phase conjugation in sodium vapor at visible wavelengths.<sup>4</sup> A measured reflectivity of 2%, response times of tens of nsecs, small frequency mismatch (within 500 kHz which is on the same order as the frequency jitter of the laser) and a threshold intensity of  $10 \text{ W/cm}^2$  indicated the potential of alkali vapors as a reasonable self-pumped phase conjugate mirror. This letter reports the observation of self-pumped phase conjugation in cesium vapor,<sup>5</sup> whose  $6S_{1/2} \rightarrow 6P_{3/2}$  electric dipole allowed transition is accessible by 852 nm sources. This demonstration opens the door for

the potential role of resonant materials in self-generated nonlinear optical applications that employ compact semiconductor laser diodes.

The physical mechanism responsible for self-pumped phase conjugation in resonant materials is self-generated intracavity four-wave mixing through two-wave mixing gain.<sup>4,6</sup> In a nutshell, the input optical beam induces resonance fluorescence radiation, a small portion of which propagates along the optical axis of the cavity. Energy transfer from the input beam to the nearly co-propagating fluorescence radiation takes place by means of coherent scattering of the input beam from the traveling wave grating produced by the interference of the input and nearly co-propagating fluorescence radiations. Hence it leads to an enhancement of the intracavity radiation. Phase conjugation occurs via a four-wave mixing process,<sup>7</sup> where the counterpropagating pumps are the standing waves in the cavity and the probe is the input beam. The intracavity four-wave mixing process can take place provided that the fluorescence radiation is coherent with the input beam. This is the case for resonant medium whose linewidth is larger than the laser linewidth. Such a condition is satisfied in our experiments.

A 3 cm long glass cell fitted with Brewster-angled windows placed at the center of an linear optical cavity comprised the self-pumped conjugator. Curved high reflector mirrors ( $r = 30$  cm) placed 56 cm apart produced a beam waist at the center of the resonator with a radius of approximately 120  $\mu\text{m}$ . The incoming laser beam was directed into the cesium cell at an angle on the order of half a degree with respect to the resonator axis so that its 115  $\mu\text{m}$  radius waist was spatially coincident with that of the resonator mode.<sup>4</sup>

Experiments were conducted with the cw laser source set near the  $D_2$  line in cesium ( $\lambda = 852$  nm) at detunings on the order of 1 GHz on the low frequency side of the resonance. A typical scan of the reflectivity as a function of laser frequency is shown in Fig. 1 for a pump intensity of 290 W/cm<sup>2</sup> in the cell and a cesium temperature of 109 °C. The phase conjugate return signal is obtained over a frequency span just under 1 GHz, although a relatively small amount of return energy is obtained at larger detunings. At the larger detunings the cesium

resonator was still oscillating at a power level that was about the same at that obtained for the range of detunings that produced a strong return signal. This behavior is similar to results obtained previously in sodium vapor.<sup>4</sup> It is attributed to the different gain mechanisms associated with the two-wave mixing process. In general, the resonator will oscillate due to both a nearly-degenerate (Raleigh) gain process and a three photon gain process that provides gain over a range of frequency that is shifted from that of the original laser beam by approximately the generalized Rabi frequency.<sup>6</sup> However, the return signal is obtained at frequencies close to that of the pump beam that experience net gain in the resonator due to the Raleigh feature. At the larger detunings mentioned previously the net gain is due mainly to the three photon process and thus does not yield a strong return signal.

The effects of varying the pump beam intensity within the cesium vapor are shown in Fig. 2. A threshold intensity of about  $35 \text{ W/cm}^2$  was measured for the phase conjugation process. This measurement was performed at a detuning of about  $-0.8 \text{ GHz}$  from line center which maximized the reflectivity at the highest pumping level shown in the figure. This threshold is not, in general, the same as that for oscillation in the resonator since the three photon process will typically yield a different oscillation threshold. However, the oscillation threshold for frequencies at which gain is provided by the Raleigh feature does appear to be the same as that for the phase conjugation process, as expected.

Varying the temperature of the cesium reservoir (number density) showed that phase conjugation is obtained for a finite range of temperature with a maximum reflectivity obtained at about  $110^\circ \text{C}$  for the conditions of our experiment. This effect (shown in Fig. 3) is consistent with the variation of the Raleigh gain with temperature that we have determined from two-wave mixing experiments in sodium vapor.

We have demonstrated and characterized a self-pumped optical phase conjugation process in cesium vapor at typical laser diode wavelengths. This work has shown that the threshold for this process is low enough that it is feasible to attempt to employ this type of conjugator in applications which utilize laser diode sources.



The authors wish to thank Dr. Monica Minden for stimulating technical discussion concerning the spectroscopy of cesium. The work is supported by DARPA/ONR (contract #N00014-87-C-0090), Army Research Office (contract #DAAL03-87-C-0001), and Air Force Office of Scientific Research (contract #F49620-88-C-0042).

## REFERENCES

1. B. Ya. Zel'dovich, V.I. Popovichev, V.V. Ragul'skii and F.S. Faizullov, J.E.T.P. Lett. **15**, 109 (1972).
2. J. Feinberg, Opt. Lett. **7**, 486 (1982).
3. J.O. White, M. Cronin-Golomb, B. Fischer and A. Yariv, Appl. Phys. Lett. **40**, 450 (1982); M. Cronin-Golomb, B. Fischer, J.O. White and A. Yariv, Appl. Phys. Lett. **41**, 689 (1982).
4. C.J. Gaeta, J.F. Lam and R.C. Lind, Opt. Lett. **14**, 245 (1989).
5. C.J. Gaeta and J.F. Lam, "Self-pumped optical phase conjugation in cesium vapor," I.E.E.E. NLO Talk #THP22 (Kauai, Hawaii, 1990).
6. S. Haroche and F. Hartmann, Phys. Rev. A **6**, 1280 (1972); M.T. Gruneisen, K.R. MacDonald and R.W. Boyd, JOSA B **5**, 123 (1988); G. Khitrova, P.R. Berman and M. Sargent III, JOSA B **5**, 160 (1988); C. Cohen-Tannoudji and S. Reynaud, J. Phys. B: Atom. Molec. Phys. **10**, 345 (1977); B.R. Mollow, Phys. Rev. A **5**, 2217 (1972).
7. D.M. Bloom and G.C. Bjorklund, Appl. Phys. Lett. **31**, 592 (1977); R.L. Abrams and R.C. Lind, Opt. Lett. **2**, 94 (1978); D.M. Bloom, P.F. Liao and N.P. Economou, Opt. Lett. **2**, 58 (1978).

## LIST OF FIGURES

Figure 1 Phase conjugate reflectivity as a function of laser frequency.

Figure 2 Variation of reflectivity with pump beam intensity within the cesium vapor.

Figure 3 Dependence of the phase conjugate reflectivity upon the temperature of the cesium reservoir (number density).

9027-04-06

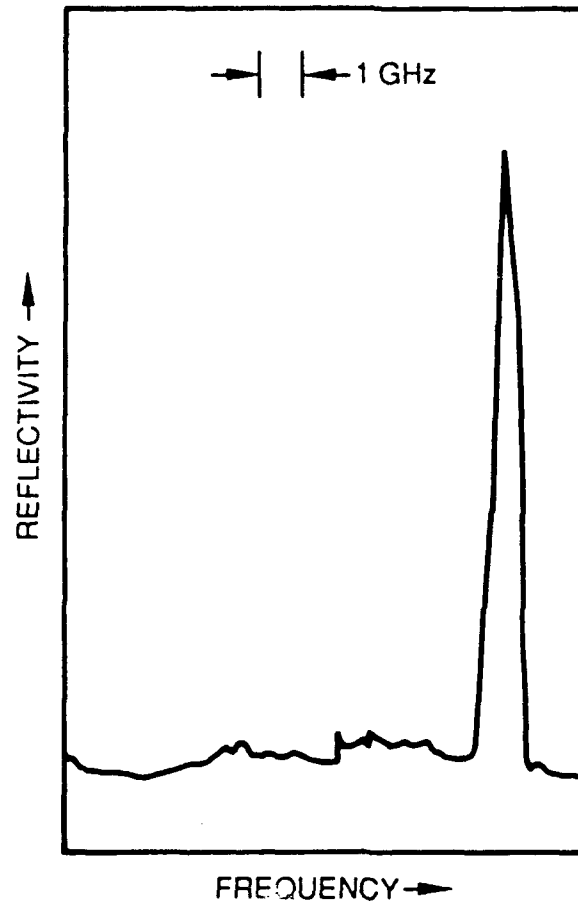


Figure H-1

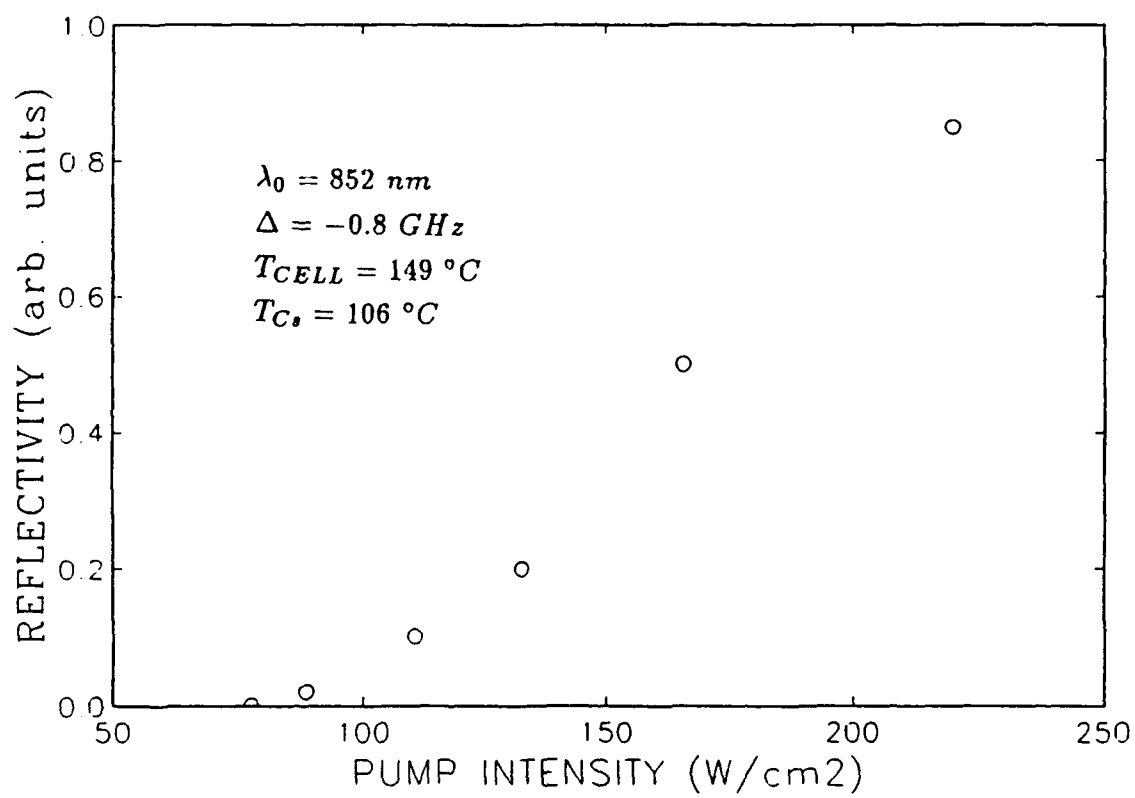


Figure H-2

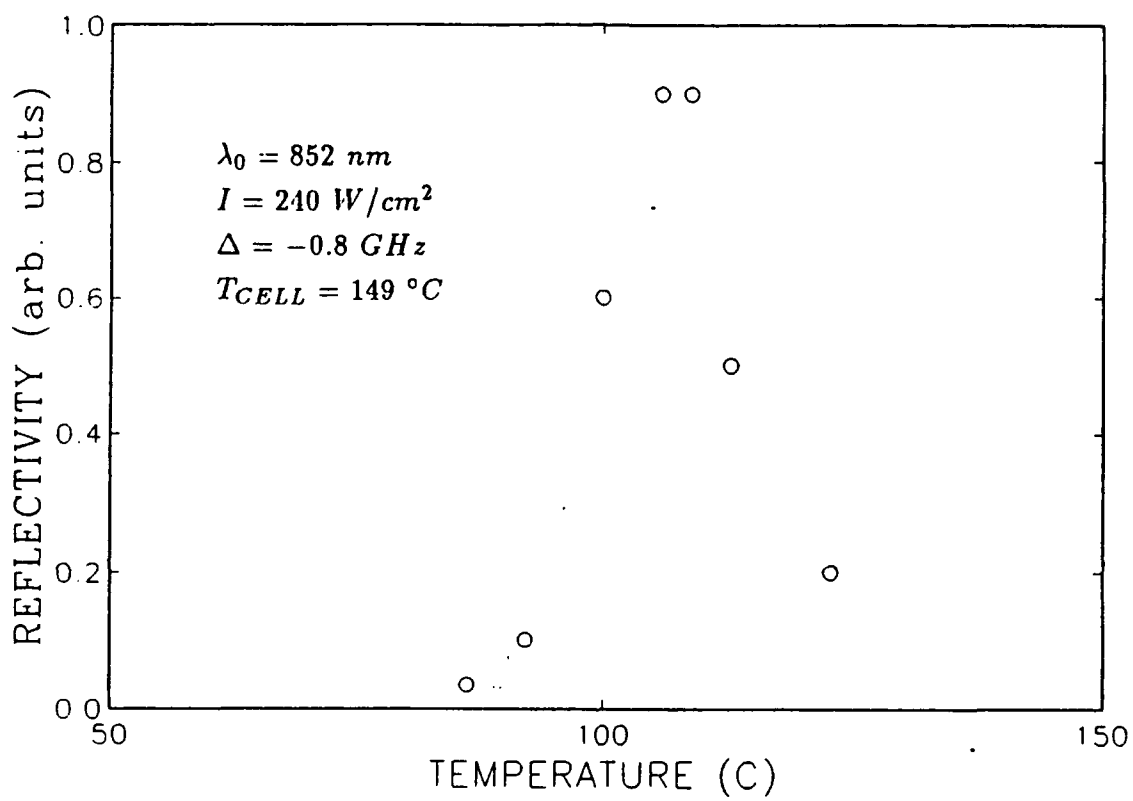


Figure H-3

# Pressure-induced coherent energy transfer and temporal oscillations of two-wave mixing in sodium vapor

Celestino J. Gaeta and Juan F. Lam

Hughes Research Laboratories, Malibu, California 90265

An experimental investigation of collision-assisted energy transfer from a strong pump beam to a weak probe in pressure-broadened sodium vapor is discussed. A peak gain coefficient of  $0.7 \text{ cm}^{-1}$  was measured for a cw pump intensity of  $25 \text{ W/cm}^2$ . At higher intensities temporal oscillations of both two-wave mixing gain and the transmission of an isolated cw laser beam were observed and characterized. An explanation for this latter effect in terms of light-induced drift and diffusion is also presented.

The study of collision-aided processes in atom-laser interactions has led to the understanding of novel nonlinear optical phenomena. Pressure-induced extra resonances<sup>1</sup>, collisional narrowing of the population<sup>2</sup> and Zeeman<sup>3</sup>-mediated spectral lineshapes and pressure-induced cavity oscillation<sup>4</sup> are just recent examples in the context of four-wave mixing. A physical interpretation of the changes in the four-wave mixing signal is the non-cancellation of the quantum mechanical amplitudes due to the presence of a state-selective collisional process.

We report the observation of collision-aided energy transfer between two optical beams oscillating at different frequencies. The theory of such a process was put forward by Berman, Khitrova and Lam<sup>5</sup>. Using a density matrix approach, the two-beam coupling coefficient exhibits a pressure dependent term that provides an intensity gain for the weak optical beam at the expense of the strong optical beam. Collisions play a significant role. It induces a phase shift ( $> 0^\circ$ ) between the interference pattern of the two beams and the population

difference. This phase shift allows a transfer of energy from the strong optical beam to the weak optical beam. At higher intensities we observed and characterized temporal oscillations in both the pump beam transmission through sodium vapor and the associated two-wave mixing gain in the presence of a buffer gas.

Nonlinear wave mixing processes involving the interaction of two optical fields in a resonant medium which allow the transfer of energy from one beam to the other have been used to demonstrate low-power techniques for producing phase conjugate waves that do not require separate pump beams.<sup>6</sup> Such a self-pumped phase conjugator is in the form of a laser resonator which uses two-wave mixing as the gain mechanism. The counterpropagating fields within this resonator would then interact with the pump laser beam to produce a fourth optical field (phase conjugate to the pump beam) via an internal four-wave mixing process.

Two-wave mixing gain due to both the ac-Stark effect<sup>7</sup> and stimulated Raman scattering<sup>8</sup> has been observed in sodium vapor. These gain processes typically require cw pump intensities in the range of hundreds of watts per square centimeter. We report here the observation of gain using a collision-assisted process which may be implemented using a pump intensity that is an order of magnitude lower. In this type of interaction a strong pump beam and a relatively weak probe beam are overlapped with each other at a small angle ( $< 0.5^\circ$ ) inside of a nonlinear resonant medium. The two beams produce an interference pattern which results in an index of refraction grating through the nonlinear response of the medium. Energy transfer from the pump to the probe beam can occur when the population grating is temporally delayed with respect to the interference pattern. Normally the interference pattern and the grating are in phase. However, in the presence of collisions and when the pump and probe laser frequencies do not coincide, the population grating can be delayed. The pump beam can then reflect from this grating into the probe path (in phase with the probe beam) resulting in gain for the optical field of the probe laser.

A diagram of the experimental arrangement is presented in Figure 1. The mixing process



occurred in a 1 cm long metal cell with sodium densities on the order of  $10^{11} \text{ cm}^{-3}$ . Since the theory of the two wave optical process to be studied here assumes a pressure-broadened transition in the sodium vapor, argon gas was introduced into the cell at pressures up to 100 Torr. A Coherent model 590 passively stabilized single frequency dye laser served as the pump beam. This laser is capable of providing power densities in the range of tens of watts per square centimeter in a single longitudinal mode, which is close to the theoretically determined levels needed to drive the nonlinear susceptibility. Part of the output from the 590 was directed into a reference sodium cell equipped with an orthogonal viewport to allow the fluorescence to be monitored. Observation of both the fluorescence level and the 590 spectrum on a scanning Fabry Perot was used to set the 590 laser frequency to the desired detuning from the center of the sodium resonance.

A relatively weak probe beam from a Coherent 699 autoscan single frequency ring dye laser was introduced into the metal cell so that it overlapped with the pump beam at a small angle ( $\leq 0.5^\circ$ ). The probe beam was amplitude modulated using a chopper at a rate of approximately 1 kHz allowing lock-in amplifiers to be used in the detection system to provide a better signal/noise ratio. Part of the probe beam was diverted into a detector so that probe beam power could also be monitored. Both the reference and transmitted probe beam power levels were recorded as the probe frequency was scanned through the sodium  $D_2$  resonance. The 699 autoscan laser system is computer controlled and includes an integral wavemeter and interface electronics which record data as a function of laser frequency.

Gain was observed for the forward probe beam within the resonance with the pump laser frequency detuned by about 1.5 GHz on either side of the center of the sodium transition. The transmission of the probe beam through the sodium cell as a function of probe laser frequency is shown in Figure 2 for three cases. These curves actually represent the ratio of transmitted probe beam power to a reference probe power level, measured before the cell (see Figure 1), so that the effects of output power variations in the probe laser could be reduced. One scan (Figure 2a) is a reference in which the pump laser was blocked and no

buffer gas was present. Under these conditions the probe beam is strongly absorbed within the resonance. When argon buffer gas was introduced into the sodium system at pressures in the range of 10–80 Torr the transmission characteristic for the probe beam was modified in the presence of the pump beam and exhibited gain, as shown in Figures 2b and 2c. A peak gain coefficient of  $0.7 \text{ cm}^{-1}$  was obtained for an argon buffer gas pressure of 60 Torr (Figure 2c). Higher buffer gas pressures appeared to have a quenching effect on the gain. We believe that this is due to collisional depopulation of the upper level of the sodium transition. This is a competing process which reduces the gain at sufficiently high pressure. Pump beam intensity is estimated to have been approximately  $25 \text{ W/cm}^2$  while the probe intensity was about a factor of 50 below the pump level. The dip in the center of the curve in Figure 2b is believed to be due to the fact that the absorption is strongest in the center of the resonance and may dominate over the gain under certain conditions. In the wings of the resonance the absorption is reduced so that the two-wave mixing gain dominates.

Later the experimental set-up was upgraded by replacing the pump source with a Coherent 699-21 actively stabilized ring dye laser. A 3 cm long quartz cell fitted with Brewster-angled windows was also substituted for the metal cell as a prelude to work with sodium oscillators. Laser beam waist radii in the cell were  $125 \text{ }\mu\text{m}$  and  $260 \text{ }\mu\text{m}$  for the probe and pump beams, respectively.

When the two-wave mixing experiments were resumed much higher pump powers were employed in order to evaluate two-wave mixing gain resulting from the ac-Stark effect. Under the appropriate conditions, and only in the presence of a buffer gas (argon), oscillations were observed in the transmission of both the cw pump and probe optical fields. The probe field was still amplitude modulated at  $1 \text{ kHz}$  prior to injection into the cell to allow for phase-sensitive detection. However, the oscillations were observed to have much longer periods (on the order of seconds to tens of seconds) and were present on the pump beam even with the probe beam blocked. Such oscillations have previously been observed in sodium vapor for a cw laser beam but the phenomenon was not fully characterized as a function of experimental

parameters. We have extended the previous work to include such a characterization, as well as the effects upon two-wave mixing gain.

A typical temporal sequence is shown in Fig. 3 for the case of both the pump and probe beams present. The plots represent the transmission of the laser beams through the sodium cell as a function of time. At the start of the sequence both laser beams are blocked before the cell in order to mark the zero transmission levels. After a time, the probe beam is unblocked to indicate its transmission level without a two-wave mixing assist. Next, the pump beam is unblocked causing the probe beam transmission to approximately double. After a few seconds argon buffer gas is added to the cell at a pressure of 1 Torr. At this time the transmission of the pump beam through the cell decreases rapidly to zero while the probe beam transmission increases by about 50% (a factor of 2.5 increase due to two-wave mixing overall). The pump and probe beam power levels at the output of the cell then begin to oscillate with a period of about 10 seconds and a phase difference of approximately  $270^\circ$  (transmitted probe oscillation delayed about 7.5 seconds with respect to that of the pump. During the oscillations the transmitted pump beam power alternated between zero and a level about 30% lower than the level obtained prior to the introduction of the buffer gas. It is interesting to note that during the on state for the pump its transmitted power level decreases approximately linearly until it is reduced by a factor of about two and then switches very quickly to zero. During this decrease the transmitted probe beam power level is increasing relatively slowly as shown in Fig. 3 until the pump beam transmission switches to the off state resulting in the probe transmission suddenly switching to its maximum level. In contrast, the transition from off state to on state for the pump, or the converse for the probe, is very rapid. When the buffer gas is removed the pump and probe beam power levels at the output of the cell are once again constant in time.

These results were obtained for temperatures of  $261^\circ\text{C}$  and  $227^\circ\text{C}$  for the cell body and reservoir regions, respectively, and a pump beam intensity of  $280\text{ W/cm}^2$  in the cell region. The pump beam frequency was about  $0.5\text{ GHz}$  below the center of the sodium  $D_2$  resonance

while that of the probe beam was about 5.7 GHz below linecenter.

The oscillations were also observed at other values of probe detuning with that of the pump beam set at approximately the same value as in the previous case. For example, when the probe detuning was set at  $\Delta = 2.9$  GHz (above linecenter) and the pump beam was unblocked the probe transmission was reduced to 1/3 of its original level. In the presence of argon buffer gas (1 Torr) the pump and probe power levels at the output of the cell dropped to zero and after an interval of about 25 seconds began to oscillate with a period of about 6 seconds. The oscillation of the probe transmission was delayed from that of the pump by approximately 5 seconds ( $300^\circ$ ). When the buffer gas was removed the pump and probe power levels after the cell returned to their respective values before the buffer gas was added after a buildup on the order of 50 seconds. The pump beam was then blocked and the probe transmission returned to its initial level. The experiment was repeated for a probe detuning equal to that of the pump. In this case the same oscillations were present for the pump beam transmission but that of the probe was essentially zero at all times. This is because the probe frequency was set closer to linecenter and the probe was highly absorbed. Since its frequency was nearly identical to that of the pump beam the population and interference gratings were not properly delayed with respect to each other and two-wave mixing gain did not occur for the probe beam.

Oscillations were observed for the pump beam even with the probe beam absent. A plot of the variation of the oscillation period with buffer gas pressure is presented in Fig. 4a for a pump beam intensity of  $280$  W/cm<sup>2</sup> and pump beam detuning of  $-0.5$  GHz from linecenter. The period increases from just under 10 seconds at a pressure of 1 Torr to almost 200 seconds at 40 Torr. The functional relationship appears to be nonlinear. Fig. 4b shows the effect of varying the pump beam intensity for a buffer gas pressure of 1 Torr. The oscillation period appears to vary nonlinearly with intensity. A threshold for the oscillations was also observed and measured to be about  $165$  W/cm<sup>2</sup>. Below this threshold the pump beam transmission went to zero when the buffer gas was added and did not recover. It is

interesting to note that although the period increases as the intensity is increased the buildup time for the oscillations to occur after the introduction of the buffer gas was observed to decrease dramatically from ten's of seconds for intensities close to the threshold level to a few seconds at higher intensities. The period obtained for an intensity of  $280 \text{ W/cm}^2$  is slightly higher in Fig. 4b than that discussed earlier in the temporal sequences and is probably due to the fact that the data in Fig. 4b was taken on a different day and the detuning may have been slightly different.

A plausible explanation of the temporal oscillation can be given in terms of the phenomenon of light induced drift. In a nutshell, the different collisional cross sections for the excited and ground states of the  $D_2$  line of sodium atoms produce a net macroscopic velocity of the atoms along the axis of the optical beam. This atomic drift produces a cluster of atoms towards the end of the cell, leading to a light-assisted temporal increase of the sodium vapor density in that location. The higher density gives rise to a decrease of optical transmission because of increase absorption. However, the effects of diffusion eventually lead to a decrease of the density of the cluster, leading to increase optical transmission. This process repeats itself provided that the buffer gas pressure is maintained in the cell.

We carried a detailed calculation of the effect of light-induced drift on the temporal behavior of two-wave mixing processes. Starting from the density matrix equations, we derived the microscopic equations for the population difference and the optical coherence, and the macroscopic equations for the average density and velocity of the atoms. A nonlinear diffusion equation for the atomic density was derived, and whose qualitative solution exhibits oscillatory behavior as a function of time. Furthermore, the theoretical model predicts that the rise time of the oscillation is inversely proportional to the laser intensity and the buffer gas density, in qualitative agreement with experiments.

The measurements described above show that a relatively low power cw-pumped two-wave mixing process is possible in resonant systems. In fact, this type of gain has been used to demonstrate a unidirectional ring laser. This process may also be useful in reducing the

operating intensity levels of self-pumped phase conjugate mirrors in resonant media such as sodium and cesium vapors from hundreds to tens of watts per square centimeter. The oscillations observed in the presence of buffer gas have a definite impact upon devices based upon two-wave mixing gain and our characterization is an important step in understanding and possibly controlling this phenomenon and its implications.

The authors would like to thank Rick Harold for his assistance in performing the experiments, as well as Tony Pepitone for his help with the vacuum system used to evacuate the sodium cell. This work was supported by DARPA/ONR under contract #N00014-87-C-0090, Army Research Office under contract #DAAL03-87-C-0001, and Air Force Office of Scientific Research under contract #F49620-88-C-0042. The results of this work were first presented at CLEO'88 and IQEC'90.

## REFERENCES

1. J. Ducuing, **Nonlinear Optics**, Academic Press 1977. N. Bloembergen, **Laser Spectroscopy IV**, Springer-Verlag, 1979
2. J.F. Lam, D.G. Steel and R.A. McFarlane, *Phys. Rev. Lett.* **49**, 1628 (1982)
3. J.F. Lam, D.G. Steel and R.A. McFarlane, *Phys. Rev. Lett.* **50**, 1679 (1986)
4. D. Grandclement, G. Grynberg and M. Pinard, *Phys. Rev. Lett.* **59**, 44 (1987)
5. P.R. Berman, G. Khitrova and J.F. Lam, in **Spectral Line Shapes**, edited by F. Rostas, W. de Gruyter, Berlin 1985
6. C.J. Gaeta, J.F. Lam and R.C. Lind, *Opt. Lett.* **14**, 245 (1989)
7. G. Grynberg, E. Le Bihan and M. Pinard, *J. Physique* **47**, 1321 (1986)
8. M.T. Gruneisen, K.R. McDonald and R.W. Boyd, *JOSA B* **5**, 123 (1988)

## LIST OF FIGURES

- 1 Basic two-wave mixing geometry.
- 2 Plots of the transmission of the probe beam through a pressure-broadened sodium vapor for (a) no pump beam or buffer gas present. Two-wave mixing gain lineshapes for a pump intensity of  $25 \text{ W/cm}^2$  and argon buffer present at pressures of (b) 40 Torr and (c) 60 Torr.
- 3 Temporal oscillations of the transmission of pump and probe beams through sodium vapor in the presence of argon buffer gas.
- 4 Variation of the oscillation period with (a) buffer gas pressure for a pump beam intensity of  $25 \text{ W/cm}^2$  and (b) pump beam intensity for a buffer gas pressure of 1 Torr.



**PROBE**

**PUMP**

**SODIUM CELL  
+  
BUFFER GAS**

**Figure I-1**

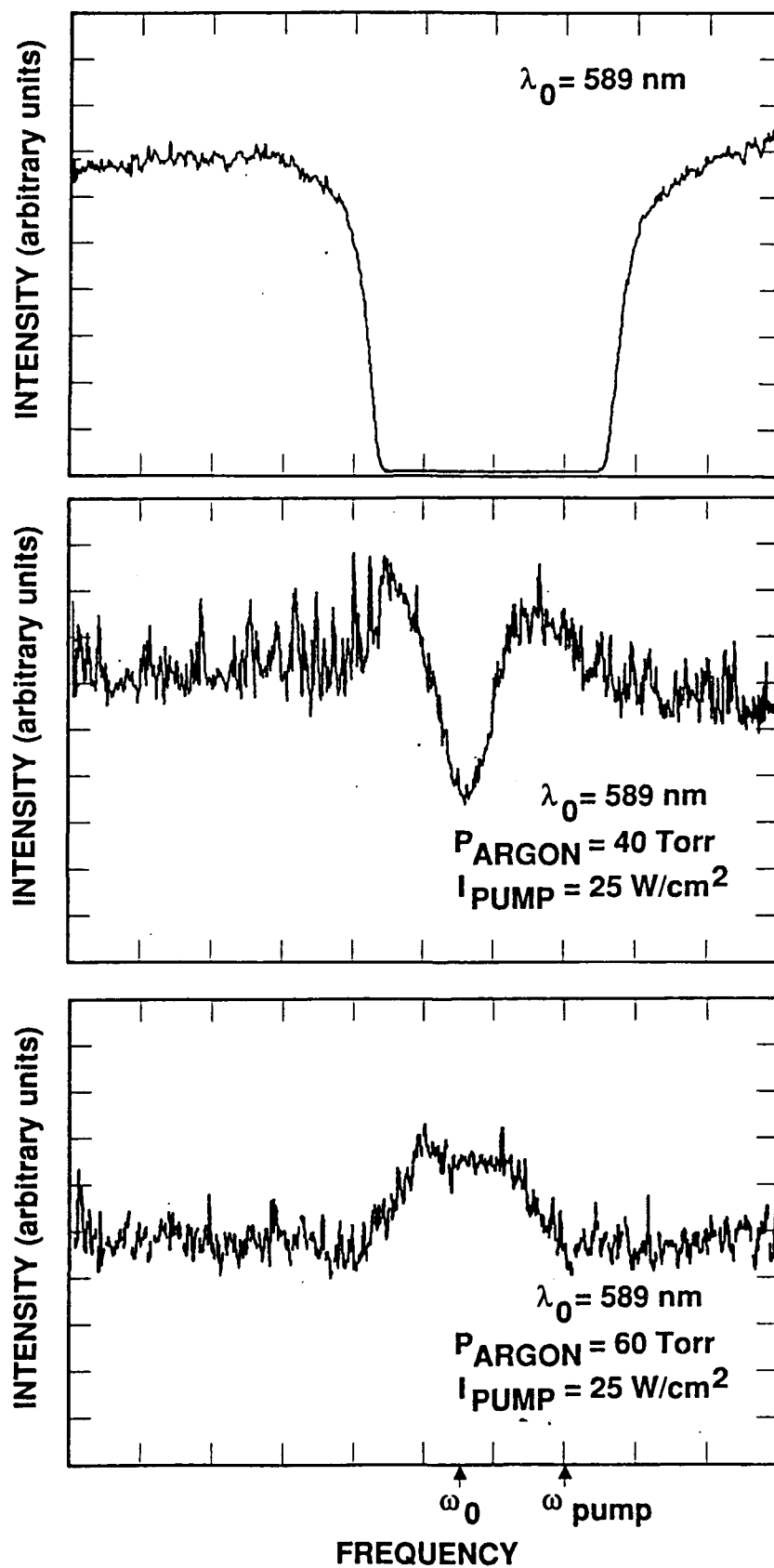


Figure I-2

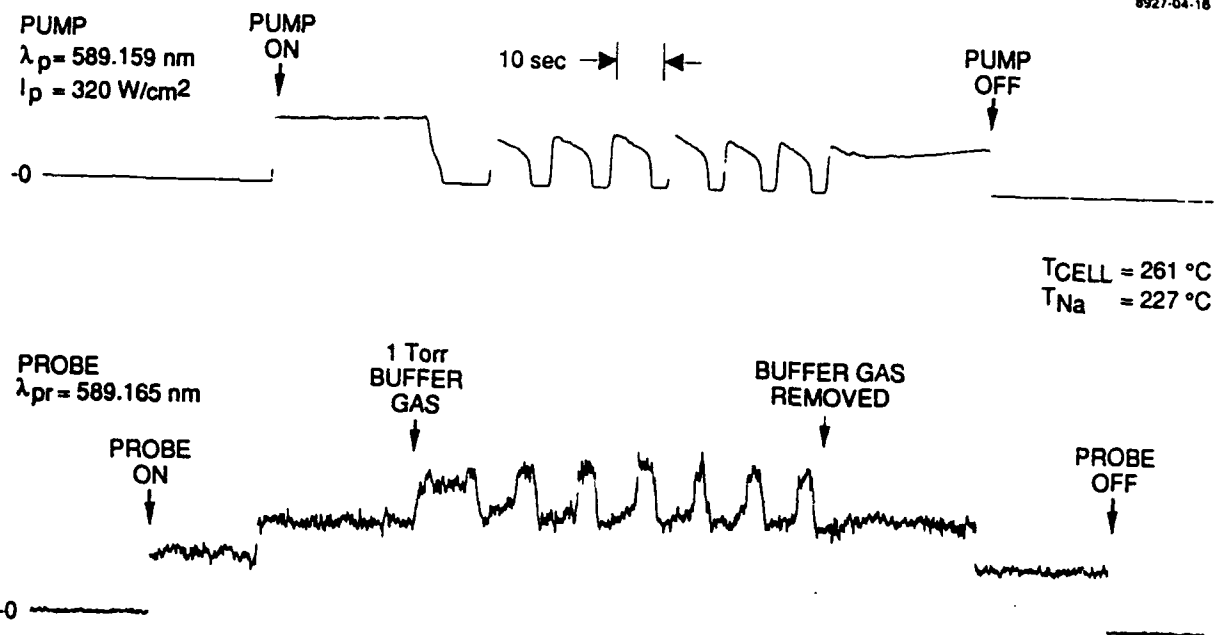
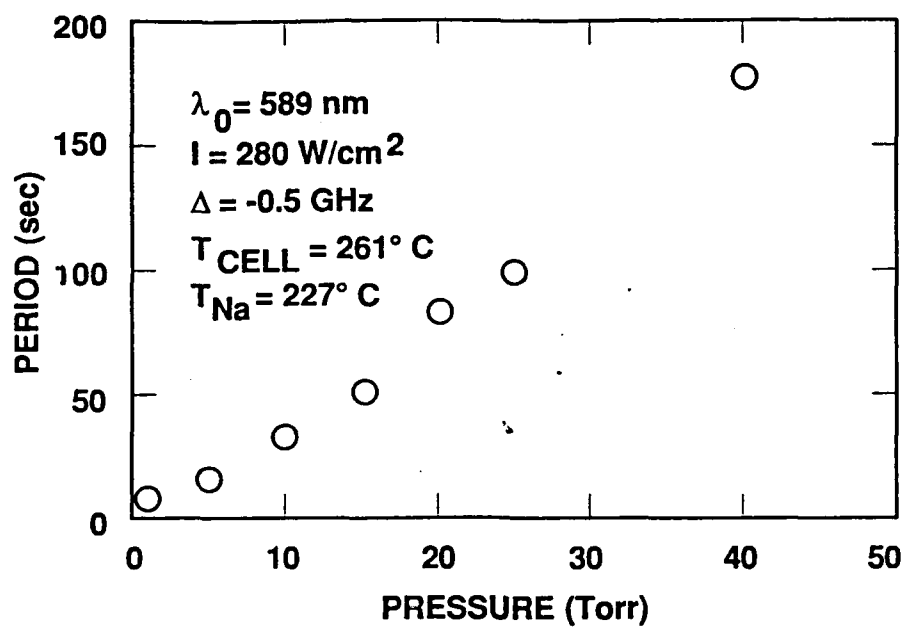


Figure I-3



9027-04-11

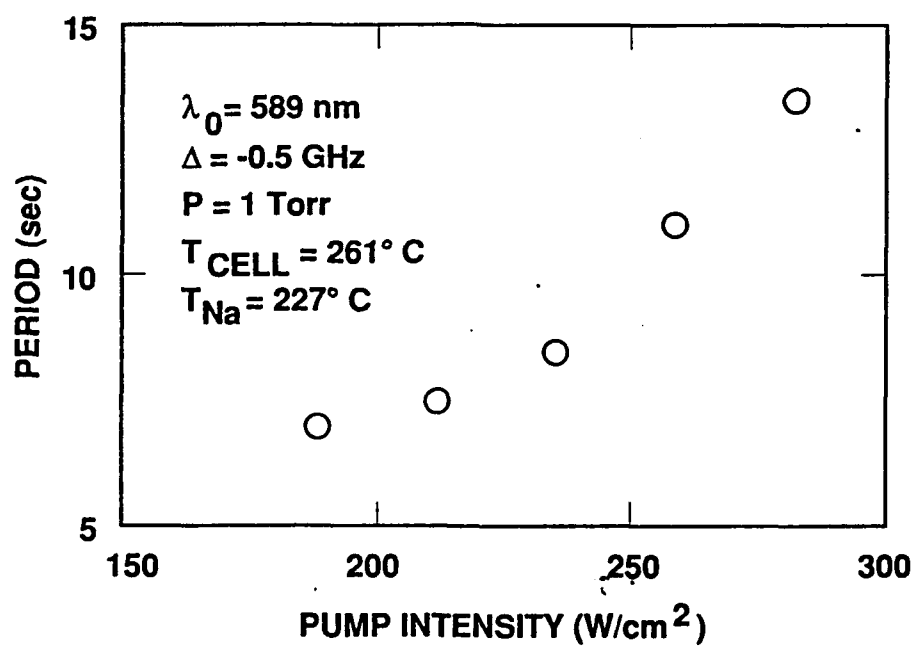


Figure I-4

# Two-Wave Mixing Processes In Resonant Systems

Celestino J. Gaeta, Juan F. Lam and David M. Pepper

Hughes Research Laboratories, Malibu, California 90265

A review of near-resonant two-wave mixing processes in atomic systems is presented. The physical mechanisms giving rise to energy transfer between two optical beams are discussed and competing effects from light-induced drift in the presence of buffer gases are quantified. Applications to ring resonators, self-pumped phase conjugate mirrors, retro-modulators and beam clean-up and combining are described.

## 1. INTRODUCTION

The study of coherent nonlinear optical processes has led to the discovery of energy transfer phenomena among spatially overlapping optical beams. The best known examples are the processes of stimulated Brillouin<sup>1</sup> and Raman scattering.<sup>2</sup> These phenomena are characterized by the optical excitation of spontaneous noise arising from the random fluctuation in the material properties, followed by a coherent amplification of the noise at the expense of the energy of the input optical beam. The key energy transfer mechanism is the 90° phase difference that exists between the material excitation (acoustic phonons in stimulated Brillouin scattering) and travelling wave excitation (optical intensity interference pattern), as set up by the input optical beam and its associated noise.

An important property of stimulated Brillouin scattering was discovered by Zeldovich et al.<sup>3</sup> and Nosach et al.<sup>4</sup> If an input optical beam is passed through a distorting medium and its output is focused into the Brillouin cell, the stimulated Brillouin backscattered beam has

an optical phase which is the conjugate of that at the entrance of the cell. Hence, it allows the backscattered beam to trace back through the aberrating medium, producing an output optical beam which is as clean as the input optical beam. This simple experimental finding gave birth to the field of nonlinear optical phase conjugation.

Recently, much excitement<sup>5</sup> has been generated in the field of photorefractive materials which possess the energy transfer behavior when two optical beams are set up inside the crystal with the appropriate orientation of their polarization states. However, the mechanism responsible for the origin of this phenomena traces back to the 90° phase shift. In the case of photorefractive materials the internal space charge field plays the role of acoustic phonons, while an optical intensity interference pattern is always present. Phase conjugation was also discovered to be naturally occurring if stimulated backscattering of radiation is made possible.

The concept of energy transfer can be extended to the case of resonant systems. Indeed, early experiments<sup>6</sup> using an atomic beam of sodium and two tunable dye lasers demonstrated the optical gain experienced by one laser at the expense of the other laser. Since then, several experiments<sup>7-10</sup> have also shown that the addition of buffer gases to the atomic cell can provide an enhanced energy transfer between two optical beams. The subject of this article is to provide a comprehensive review of our present understanding of energy transfer in resonant atomic systems as well as to describe novel applications that employ this concept.

Section 2 is devoted to the detailed physics of resonant two-wave mixing. The effects of high optical intensity and buffer gases on the behavior of the gain coefficient are examined. Dynamical phenomena such as light-induced drift are reviewed in order to guide the reader to the subject of temporal oscillations of optical beams. Section 3 represents a state-of-the-art review of four different applications in optical signal processing that result from the physical behavior of the resonant systems in the presence of two or more optical beams. Applications such as optical resonators, self-pumped optical phase conjugators, retro-modulators and laser beam clean-up and combining will be discussed. We conclude in Section 4 by pointing

out several outstanding problems that deserve further study.

## 2. PHYSICS OF RESONANT TWO-WAVE MIXING

In the following sections we will discuss the basic physics of two-wave interactions in two-level atomic systems, including important collisional effects.

### 2.1 Dynamic Stark Effect

Coherent energy transfer between two optical beams was predicted by both Haroche and Hartmann,<sup>11</sup> and Mollow<sup>12</sup> in their analyses of strongly driven two-level atoms. Wu et al<sup>6</sup> observed the effect of energy transfer between two optical beams when they overlap inside an atomic beam of sodium. They found that the optical beam with an oscillating frequency which is downshifted by the Rabi flopping frequency experiences gain. Their explanation of the phenomena is based on the existence of the dynamic Stark effect.

The dynamic Stark effect was first discussed by Autler and Townes<sup>13</sup> and is just a manifestation of the saturation behavior of an atomic system when acted upon by a coherent radiation field. In the jargon of laser physics, it gives rise to power broadening.<sup>14</sup> In the jargon of atomic spectroscopy, it originates the dressed atom picture.<sup>15</sup>

Coherent energy transfer is quite easily understood within the dressed atom picture, as described by Cohen-Tannoudji and Reynaud<sup>16</sup> in their classic description of driven stationary two-level atoms exhibiting homogenous broadening. In this picture, the effect of a radiation field  $\vec{E}$  on an atomic transition is treated in equal footing with the atomic and radiation Hamiltonian. That is,

$$H = H_{atom} + H_{field} - \vec{\mu} \cdot \vec{E}(\vec{r}, t) \quad (1)$$

where  $H_{atom}$  is the atomic Hamiltonian with eigenstates  $|\alpha\rangle$ ,  $H_{field}$  is the radiation field Hamiltonian with eigenstates  $|n\rangle$ ,  $\vec{\mu}$  is the electric dipole moment operator and  $\vec{E}(\vec{r}, t)$  is the radiation field at position  $\vec{r}$  and time  $t$ . The unperturbed state of the system of atoms

and the radiation field is given by the set  $\{|\alpha\rangle \otimes |n\rangle\}$ . The effect of the electric dipole coupling to the radiation field is to induce a coherent mixing of the unperturbed states. In the quantum mechanical regime, the Schrödinger equation can be solved for the Hamiltonian (Equation (1)) using the rotating wave approximation. Consider the case where an incident strong pump and a weak probe beam interact with a set of two-level atoms. A perturbative approach is used in order to study the behavior of the weak probe beam as the strong pump beam modifies the atomic states. Hence, a solution is found first for the case of the strong pump beam and subsequently used to study the evolution of the weak probe beam.

In the presence of the strong pump beam, the eigenstates of  $H$  are given as a linear superposition of the unperturbed states in the following form

$$|+, n\rangle = \sin\theta |g, n\rangle + \cos\theta |e, n-1\rangle \quad (2a)$$

$$|-, n\rangle = \cos\theta |g, n\rangle - \sin\theta |e, n-1\rangle \quad (2b)$$

where  $\tan\theta = 4\Omega/\Delta$ . Here,  $\Delta$  and  $\Omega = \vec{\mu} \cdot \vec{E}/\hbar$  are the light detuning from resonance and the Rabi flopping frequency, respectively. The physical description of the new eigenstates is illustrated in Figure 1. In the absence of electric dipole coupling to the radiation field, the system consists of a series of pairs of ground state with  $n$  photons present,  $|g, n\rangle$ , and an excited state with  $n-1$  photons present,  $|e, n-1\rangle$ . The frequency separation between two adjacent pairs is given by the laser frequency,  $\omega$ . The separation between components of the same pair is determined by  $\Delta$ , as illustrated in Figure 1a. In the presence of an electric dipole coupling to the radiation field, each atomic eigenstate is split into a pair of dressed states, as shown in Figure 1b. The separation between pairs of eigenstates is given by the laser frequency, while the separation within a given pair is determined by the generalized Rabi flopping frequency,  $\sqrt{\Delta^2 + \Omega^2}$ .

The population of each dressed state obeys a rate equation in the limit that the radia-



tion field is classical (photon number  $n$  is large compared to unity). Cohen-Tannoudji and Reynaud derived an expression for the population,  $P_i$ , of the components of each pair of dressed states. They are given by

$$P_+ = \frac{\sin^4 \theta}{\sin^4 \theta + \cos^4 \theta} \quad (3a)$$

$$P_- = \frac{\cos^4 \theta}{\sin^4 \theta + \cos^4 \theta} \quad (3b)$$

These equations have a simple physical interpretation in the limit of small pump intensity. Expanding the trigonometric expansion for small values of  $\theta$ , one finds that  $P_- > P_+$ . This fact represents the absorption of the pump beam. Equations (3a) and (3b) are valid, however, for all values of pump intensity and show that there is no population inversion as seen by the pump optical field.

However, if a probe beam has an oscillating frequency which is distinct from that of the pump beam, it is possible for the probe beam to acquire gain at the expense of the pump beam. The energy transfer process in the presence of a dressed atom is illustrated in Figure 2. It depicts the dressed states induced by the strong pump beam. Taking into account that the  $P_- > P_+$ , the probe beam experiences amplification if its frequency is tuned between dressed states  $| -, n >$  and  $| +, n - 1 >$  at a frequency  $\omega_L - \sqrt{\Delta^2 + \Omega^2}$ .

An important result obtained by Cohen-Tannoudji and Reynaud is the condition at which the amplification of the probe beam is optimized. They found that the maximum gain was obtained for  $\Delta = 0.334\Omega$  which yielded a value of approximately 4.6% for the conditions of their analysis.

The analysis of energy transfer processes in inhomogeneously broadened systems has been carried out in great detail by Khitrova, Berman and Sargent,<sup>17</sup> and Gruneisen, MacDonald and Boyd.<sup>10</sup> The latter set of researchers performed experimental, as well as theoretical, studies of this type of two-wave interaction. Their results confirm the dressed atom picture.

We also conducted two-wave mixing experiments in sodium vapor using a pair of Coherent 699 actively stabilized single frequency ring dye lasers. One of the lasers is an autoscanner laser system which is computer controlled and includes an integral wavemeter and interface electronics which record data as a function of laser frequency. This laser served as the probe laser while the other functioned as the pump in the nonlinear mixing process. The nonlinear interaction occurred in a 3 cm long quartz cell with windows cut at Brewster's angle in order to minimize Fresnel reflections. The outputs from both sources were directed into this cell. Pump beam power was maintained at a constant cw level while the probe beam was amplitude modulated using a chopper at a rate of approximately 1 kHz allowing a lock-in amplifier to be used in the detection system to provide a better signal/noise ratio. Part of the incident probe beam was diverted into a detector so that probe beam power could also be monitored. Both the reference and transmitted probe beam power levels were recorded as the probe frequency was scanned through the sodium  $D_2$  resonance.

Plots of the probe beam transmission through the sodium vapor are presented in Figure 3. All three sets of data were taken with the cell body temperature set at 250 °C. A reference scan is shown in Figure 3a with the pump beam blocked at the cell entrance. This data simply illustrates the strong absorption of the probe beam by the atomic system at the sodium reservoir temperature (which drives the number density) of 200 °C. When the pump beam was unblocked the probe laser beam was amplified as it propagated through the cell for certain detunings from the center of the resonance and from the pump laser frequency (see Figure 3b). The frequency of the pump laser was tuned to approximately 1.8 GHz below the center of the resonance and its intensity was adjusted to be about 500 W/cm<sup>2</sup> in the sodium cell. Two gain features are readily discernable in the figure. One, due to a three photon (Raman gain) process, is relatively broad (about 2 GHz) and shifted in frequency from the pump by approximately the generalized Rabi frequency. The other is due to Rayleigh gain and is very close to the pump in frequency (on the order of a few hundred kilohertz to a few megahertz which is similar to the laser frequency jitter). The

Rayleigh peak is about 300 MHz wide. Although the two features have roughly the same magnitude in this plot, one feature can be emphasized over the other as shown in Figure 3c which considers the effect of a lower sodium number density (reservoir temperature  $\sim 180^\circ\text{C}$ ). In this case the Rayleigh gain is higher than that due to the three photon process by over a factor of two. Other values for the sodium and cell temperatures provide a much larger three photon peak compared to the nearly-degenerate feature, as shown in Figure 4. One can, therefore, somewhat control the strength of each process and determine the dominant gain feature by adjustment of the experimental parameters. This procedure is illustrated in Figure 5 which plots the gain coefficients of the Rayleigh (nearly-degenerate) and three photon processes as a function of the temperature of the sodium reservoir (number density). Other experimental parameters were held constant at the same values used for the data in Figures 3b and 3c. It is evident that at the lower temperature ranges the Rayleigh feature dominates while the opposite is true at high temperatures. The gain coefficient for the Rayleigh feature increases to a maximum with increasing temperature and then drops back to zero while the analogous quantity for the other process continues to climb until it begins to level off. Higher temperatures were not attempted due to problems with sodium deposition onto the cell windows.

## 2.2 Pressure-Induced Effects

The first analysis of the effects of buffer gas pressure on two-wave mixing processes in homogeneously broadened atomic systems was discussed by Berman, Khitrova and Lam.<sup>18</sup> It predicted the existence of pressure-induced coherent energy transfer between two optical beams, even in the absence of the dynamic Stark effect. Recently, experimental studies performed in sodium vapor<sup>7-9</sup> have confirmed all of the features predicted by the theory.

The origin of the energy transfer process is the additional phase shift imposed on the atoms by the phase interrupting collisions. These collisional processes affect the optical coherence of the atoms, leading to a net energy exchange.

We shall consider the physical model of a two-level atom with ground state  $|1\rangle$  and an excited state  $|2\rangle$ , separated by frequency  $\omega_0$ . The excited state spontaneously decays back to the ground state at a rate  $\gamma$ . It interacts with radiation fields  $E_p$  and  $E_s$  oscillating at frequencies  $\omega$  and  $\omega + \delta$ , respectively. We shall assume that  $\omega$  and  $\omega + \delta$  are near  $\omega_0$  so that the rotating wave approximation can be invoked.

The analysis involves the perturbative solution of the density matrix equations

$$i\hbar\left(\frac{\partial\rho}{\partial t} + \vec{v} \cdot \nabla\rho\right) = [H_0, \rho] + [V, \rho] + i\hbar\frac{\partial\rho}{\partial t}|_{relax} \quad (4)$$

for an ensemble of two-level atoms where  $V = -\vec{\mu} \cdot \vec{E}$  and  $H_0$  is the atomic Hamiltonian. The effect of buffer gas is included in the relaxation term of the density matrix equation. We shall consider only phase interrupting collisions. In this case,

$$\frac{\partial\rho_{21}}{\partial t}|_{relax} \approx -\left(\frac{\gamma}{2} + \Gamma\right)\rho_{21} \quad (5)$$

where  $\Gamma = \alpha P$ ,  $\alpha$  is the phase-interrupting collision coefficient and  $P$  is the pressure of the buffer gas.

The third order perturbative solution for the optical coherence gives.

$$\rho_{21} = (-2i\mu^3/\hbar^3) N \{A |E_p|^2 E_s + B |E_s|^2 E_p\} e^{i\vec{k}_s \cdot \vec{r} - i\omega t} \quad (6)$$

where

$$A = L^*(\Delta + \delta) \left(\frac{1}{\gamma}\right) (L(\Delta) + L^*(\Delta)) + \left(\frac{1}{\gamma - i\delta}\right) (L^*(\Delta + \delta) + L(\Delta)) \quad (7)$$

$$B = L^*(\Delta + \delta) \left(\frac{1}{\gamma}\right) (L^*(\Delta + \delta) + L(\Delta + \delta)) \quad (8)$$

with  $L(\Delta) = 1/(\gamma_{21} + i\Delta)$  is the Lorentzian lineshape function,  $\Delta = \omega - \omega_0$  is the detuning of  $E_p$  from atomic resonance,  $\gamma_{21} = \gamma/2 + \alpha P$  is the optical dephasing rate,  $N$  is the density

of atoms and  $\mu$  is the magnitude of the electric dipole moment between excited and ground states.

Equation (6) has simple physical interpretation. The first term on the right hand side is the two-wave mixing contribution. It gives rise to energy exchange between two optical beams, as well as an additional optical phase shift due to the presence of  $E_p$ . The second term is just the self-induced change in the index of refraction and nonlinear absorption coefficient. The third order optical coherence is used in the definition of the polarization density  $P(\vec{r}, t) = \text{Trace}(\rho\mu)$ , which is the source term in the Maxwell's equations.

The evolution of the slowly varying envelope quantity  $E_s$  is described by

$$\frac{dE_s}{dz} = -\Lambda \left( A |E_p|^2 + B |E_s|^2 \right) E_s \quad (9)$$

where  $\Lambda$  is a constant. Hence, the real part of  $A$  describes the effects of energy exchange, while the imaginary part of  $A$  is the pump-induced index of refraction. A simple expression can be obtained for the real part of  $A$  in the regime where  $\Delta \gg \gamma_{21}$ , i.e. the case of far detuned from resonance. An expansion of the real part of  $A$  as a function of the ratio of  $\gamma_{21}/\Delta$  gives

$$\text{Re}(A) = \frac{1}{(\Delta + \delta)^2} \left\{ \frac{\gamma_{21}}{\Delta^2} \left( 1 + \frac{2\alpha P}{\gamma} \right) - \frac{\delta}{\Delta} 2\alpha P \frac{1}{\gamma^2 + \delta^2} \right\} \quad (10)$$

The first term is just the linear absorption coefficient while the second term is the nonlinear contribution. There are three important conclusions from this analysis. First, the nonlinear contribution to the absorption coefficient depends on the sign of  $\delta/\Delta$ . It gives rise to gain if it is positive. Second, the nonlinear contribution is proportional to the pressure of buffer gas for low enough pressure and saturates at higher pressures. Finally, the spectra of the weak optical beam will exhibit a dispersion profile as a function of  $\delta$ . The effect of inhomogeneous broadening on the gain of the weak beam has been carried out in detail by Khitrova et al.<sup>17</sup>

We have observed two-wave mixing gain using such a collision-assisted process.<sup>7,8</sup> In this type of interaction a strong pump beam and a relatively weak probe beam are overlapped with each other at a small angle ( $< 0.5^\circ$ ) inside of a nonlinear resonant medium. The two beams produce an interference pattern which results in an index of refraction grating through the nonlinear response of the medium. Energy transfer from the pump to the probe beam can occur when the population grating is temporally delayed with respect to the interference pattern. Normally the interference pattern and the grating are in phase. However in the presence of collisions and when the pump and probe laser frequencies do not coincide, the population grating can be delayed. The pump beam can then reflect from this grating into the probe path (in phase with the probe beam) resulting in gain for the optical field of the probe laser.

The mixing process occurred in a 1 cm long metal cell with sodium densities on the order of  $10^{11} \text{ cm}^{-3}$ . Since the theory of the two wave optical process to be studied here assumes a pressure-broadened transition in the sodium vapor, argon gas was introduced into the cell at pressures up to 100 Torr. A Coherent model 590 passively stabilized single frequency dye laser served as the pump beam. This laser is capable of providing power densities in the range of tens of watts per square centimeter in a single longitudinal mode, which is close to the theoretically determined levels needed to drive the nonlinear susceptibility. Part of the output from the 590 was directed into a reference sodium cell equipped with an orthogonal viewport to allow the fluorescence to be monitored. Observation of both the fluorescence level and the 590 spectrum on a scanning Fabry Perot was used to set the 590 laser frequency to the desired detuning from the center of the sodium resonance.

A relatively weak probe beam from a Coherent 699 autoscan single frequency ring dye laser was introduced into the metal cell so that it overlapped with the pump beam at a small angle ( $\leq 0.5^\circ$ ). The probe beam was amplitude modulated ( $f = 1 \text{ kHz}$ ) and phase-sensitive detection techniques were employed in the same manner as was done for the ac-Stark gain measurements.

Gain was observed for the forward probe beam within the resonance with the pump laser frequency detuned by about 1.5 GHz on either side of the center of the sodium transition. The transmission of the probe beam through the sodium cell as a function of probe laser frequency is shown in Figure 6 for three cases. These curves actually represent the ratio of transmitted probe beam power to a reference probe power level, measured before the cell, so that the effects of output power variations in the probe laser could be reduced. One scan (Figure 6a) is a reference in which the pump laser was blocked and no buffer gas was present. Under these conditions the probe beam is strongly absorbed within the resonance. When argon buffer gas was introduced into the sodium system collisional narrowing of the resonance was observed (in the absence of the pump beam). At buffer gas pressures in the range of 10–80 Torr the transmission characteristic for the probe beam was modified in the presence of the pump beam and exhibited gain, as shown in Figures 6b and 6c. A peak gain coefficient of  $0.7 \text{ cm}^{-1}$  was obtained for an argon buffer gas pressure of 60 Torr (Figure 6c). Higher buffer gas pressures appeared to have a quenching effect on the gain. We believe that this is due to collisional depopulation of the upper level of the sodium transition. This is a competing process which reduces the gain at sufficiently high pressure. Pump beam intensity is estimated to have been approximately  $25 \text{ W/cm}^2$  while the probe intensity was about a factor of 50 below the pump level. The dip in the center of the curve in Figure 6b is believed to be due to the fact that the absorption is strongest in the center of the resonance and may dominate over the gain under certain conditions. In the wings of the resonance the absorption is reduced so that the two-wave mixing gain dominates.

### 2.3 Light-Induced Drift and Oscillations

A new phenomenon, called light-induced drift, was discovered by Bjorkholm, Ashkin and Pearson<sup>19</sup> who observed the macroscopic motion of the sodium vapor along the optical beam axis. The first explanation of the phenomenon was advanced by Gel'mukhanov and Shalagin.<sup>20</sup> Since then, many experimental and theoretical studies<sup>21–26</sup> confirmed the basic physical picture of Gel'mukhanov and Shalagin.

The fundamental physics can be described in the following manner. Consider the collision of a buffer gas on a two-level atom. In general, the collision cross sections for the ground and excited states are different.<sup>27</sup> Next, we consider the presence of a radiation field which is detuned from atomic resonance. Due to the existence of the Doppler effect, a specific velocity group of the atoms is resonant with the radiation field. The motion of this group of atoms is disturbed by the buffer gas through a frictional force due to the collisional effect. The net atomic current is given by

$$\vec{J} = M \langle \vec{v} S_1(\vec{v}) \rangle + M \langle \vec{v} S_2(\vec{v}) \rangle \quad (11)$$

where  $M$  is the mass of the atom,  $\vec{v}$  is the atomic velocity and  $S_\alpha(\vec{v})$  is the collisional integral for state  $|\alpha\rangle$ . In the absence of a buffer gas, there exists no net atomic current. However, with the introduction of a buffer gas whose interaction with the resonant atoms is state-dependent, a net macroscopic current is possible. The directional motion of this atomic current depends strongly on the sign of the laser detuning from resonance as well as the difference between the collision cross section of the ground and excited states.

The analysis of light-induced drift has been extensively worked out by Gel'mukhanov and Shalagin,<sup>28</sup> Nienhaus,<sup>29</sup> and Gel'mukhanov et al.<sup>30</sup> For the sake of completeness we point out the steps of the calculations and the analytical result for the atomic current. The starting point in the analysis is the density matrix Equations (4), with the addition of collisional integral for the ground and excited states,

$$\frac{\partial \rho_{\alpha\alpha}}{\partial t} |_{\text{collision}} = S_\alpha = -\gamma_\alpha \rho_{\alpha\alpha}(\vec{r}, \vec{v}, t) + \int d\vec{v}_1 K_\alpha(\vec{v}_1 \rightarrow \vec{v}) \rho_{\alpha\alpha}(\vec{r}, \vec{v}_1, t) \quad (12)$$

where  $K_\alpha(\vec{v}_1 \rightarrow \vec{v})$  is the collisional kernel for state  $|\alpha\rangle$  and it represents the changes in the velocity for that state upon a collision with a buffer gas.  $\gamma_\alpha$  is the collisional decay rate of state  $|\alpha\rangle$ . The equations are solveable in the case of strong collisions. In this regime, memory is lost after a single collision event, and the collision kernel becomes Maxwellian in



velocity, i.e.

$$K_{\alpha}(\vec{v}_1 \rightarrow \vec{v}) = \gamma_{\alpha} \left( \frac{1}{\pi u_o^2} \right)^{3/2} e^{-(v/u_o)^2} \quad (13)$$

where  $m\mu_o^2/2 = 3k_B T/2$ ,  $k_B$  is Boltzman's constant,  $T$  is the temperature and  $m$  is the atomic mass. The equations for the density matrix are then decomposed into two time scales. The fast (atomic) time regime is just the microscopic density matrix equation whose solutions are the population difference and the optical coherence as a function of velocities. The slow (hydrodynamic) time regime describes the continuity equation for the space-time behavior of the macroscopic density  $N(\vec{r}, t)$ ; i.e.

$$\frac{\partial N}{\partial t} + \nabla \cdot \int d\vec{v} \vec{v} (\rho_{11}(\vec{r}, \vec{v}, t) + \rho_{22}(\vec{r}, \vec{v}, t)) \quad (14)$$

where  $\rho_{\alpha\alpha}$  is the population of state  $\alpha$ .

The homogenously broadened solution for the atomic current density is given by

$$J = ku_o^2 \frac{2\gamma}{\gamma_1} \left( \frac{\gamma_{21}}{\gamma_{21}^2 + \Delta^2} \right) \frac{AN}{1 - 2\gamma A(1 + \kappa)/\gamma_1} \quad (15)$$

with the following definitions,

$$A = \frac{1}{2} \frac{\gamma_1 - \gamma_2}{\gamma_2 + 2\gamma(1 + \kappa)} \frac{\kappa}{1 + \kappa} \quad (16)$$

where  $\kappa = I/I_s(\Delta)$ ,  $I$  and  $I_s$  are the optical intensity and detuning-dependent saturation intensity, respectively, and  $k$  is the propagation constant.

The physics now becomes clear from the functional dependence of Equation (15). The atomic current is zero if either there are no collisions or the collisional effect is state independent. The atomic current is directed along the axis of the optical beam. The sense of the flow depends upon the difference on the collisional decay rates,  $\gamma_1 - \gamma_2$ .

The analytical solutions obtained have reflected the condition in which there is a steady-state flow of atoms along the optical axis. They did not consider the temporal behavior of the macroscopic density when diffusion becomes important. This is a very interesting case since, as the density increases there exists a regime where atomic diffusion balances out the increase in density, and eventually leads to a strong diffusive flow. This last event yields a decrease in atomic density. The test of this simple phenomenon was the observation of temporal oscillation of the transmission of a cw optical beam propagating inside of a sodium vapor cell by Verkerk and Grynberg.<sup>31</sup> However, the conditions of their experiments were not ideal for the understanding of the phenomenon.

The physics of temporal oscillation can be tentatively described as follows assuming that light-induced drift is playing a role. An input cw optical beam will experience linear absorption as it propagates inside the vapor cell. In the absence of a buffer gas, the optical beam will not exhibit any temporal behavior. However, as a buffer gas is allowed to mix in with the vapor, light-induced drift of the atoms will take place, leading to a concentration of atomic density at one end of the cell. Since the number of atoms is fixed, the density of atoms increases in that location, leading to a bleaching of the optical transmission. That is, the input optical beam will cease to be transmitted in an optically thick medium. At this stage, diffusion of the atoms starts to act as to lead to a decrease of the density of atoms at the end of the cell. The optical beam now begins to transmit since it sees an optically thin medium. The process is repeated again, and one observes effectively a turn-on/turn-off event as a function of time. This process appears to be correct in view of recent related experiments, where the oscillatory migration of the fluorescent spot has been documented in sapphire capillaries.<sup>26</sup> Those authors concluded that light-induced drift was probably not the cause due to the fact that they observed the oscillations over detunings as large as 25 GHz, which was an order of magnitude larger than the Doppler width of the resonance. This reasoning is incorrect, however, since it neglects pressure broadening, which can easily increase the linewidth by an order of magnitude.

The analysis that leads to the explanation of this physical process proceeds in the same manner as discussed above, with only one exception. The temporal dependence of the density is retained. In the homogeneously broadened regime, the macroscopic density of the atoms obeys the following equation.

$$\frac{\partial N}{\partial t} + \langle v_z \rangle \frac{\partial N}{\partial z} - D \frac{\partial^2 N}{\partial z^2} - C \left( \frac{I}{I_s} \right) N^2 = 0 \quad (17)$$

where the second term is the convective derivative describing the flow of atoms with velocities  $v_z$  along the  $z$  direction ( $z$  is chosen to be the direction of optical propagation), the third term is the diffusion of atoms and the fourth term describes the effect of light-induced drift. The coefficients  $C$  and  $D$  depend upon the properties of the material. This equation is coupled with the Beers' law

$$\frac{dI}{dz} = -GNI \quad (18)$$

where  $G$  depends upon the material characteristics. Equations (17) and (18) have the simple physical interpretation that is consistent with the above physical picture.

We have performed experimental studies<sup>8,32</sup> of the oscillatory phenomenon which extend previous work<sup>26,31</sup> in this area to include a characterization as a function of experimental parameters such as laser intensity and buffer gas pressure, as well as the effects upon two-wave mixing gain.

Under the appropriate conditions (described below), and only in the presence of a buffer gas (argon), we observed oscillations in the transmission of both the cw pump and probe optical fields during two-wave mixing experiments using gain mediated by the ac-Stark effect. The probe field was still amplitude modulated at 1 kHz prior to injection into the cell to allow for phase-sensitive detection. However, the oscillations were observed to have much longer periods (on the order of seconds to tens of seconds) and were present on the pump beam even with the probe beam blocked.

A typical temporal sequence is shown in Fig. 7 for the case of both the pump and probe beams present. The plots represent the transmission of the laser beams through the sodium cell as a function of time. At the start of the sequence both laser beams are blocked before the cell in order to mark the zero transmission levels. After a time, the probe beam is unblocked to indicate its transmission level without a two-wave mixing assist. Next, the pump beam is unblocked causing the probe beam transmission to approximately double. After a few seconds argon buffer gas is added to the cell at a pressure of 1 Torr. At this time the transmission of the pump beam through the cell decreases rapidly to zero while the probe beam transmission increases by about 50% (a factor of 2.5 increase due to two-wave mixing overall). The pump and probe beam power levels at the output of the cell then begin to oscillate with a period of about 10 seconds and a phase difference of approximately  $270^\circ$  (transmitted probe oscillation delayed about 7.5 seconds with respect to that of the pump). During the oscillations the transmitted pump beam power alternated between zero and a level about 30% lower than the level obtained prior to the introduction of the buffer gas. It is interesting to note that during the on state for the pump its transmitted power level decreases approximately linearly until it is reduced by a factor of about two and then switches very quickly to zero. During this decrease the transmitted probe beam power level is increasing relatively slowly as shown in Fig. 7 until the pump beam transmission switches to the off state resulting in the probe transmission suddenly switching to its maximum level. In contrast, the transition from off state to on state for the pump, or the converse for the probe, is very rapid. When the buffer gas is removed the pump and probe beam power levels at the output of the cell are once again constant in time.

These results were obtained for temperatures of 261 °C and 227 °C for the cell body and reservoir regions, respectively, and a pump beam intensity of 280 W/cm<sup>2</sup> in the cell region. The pump beam frequency was about 0.5 GHz below the center of the sodium  $D_2$  resonance while that of the probe beam was about 5.7 GHz below linecenter.

The oscillations were also observed at other values of probe detuning with that of the

pump beam set at approximately the same value as in the previous case. For example, when the probe detuning was set at  $\Delta = 2.9$  GHz (above linecenter) and the pump beam was unblocked the probe transmission was reduced to 1/3 of its original level. In the presence of argon buffer gas (1 Torr) the pump and probe power levels at the output of the cell dropped to zero and after an interval of about 25 seconds began to oscillate with a period of about 6 seconds. The oscillation of the probe transmission was delayed from that of the pump by approximately 5 seconds ( $300^\circ$ ). When the buffer gas was removed the pump and probe power levels after the cell returned to their respective values before the buffer gas was added after a buildup on the order of 50 seconds. The pump beam was then blocked and the probe transmission returned to its initial level. The experiment was repeated for a probe detuning equal to that of the pump. In this case the same oscillations were present for the pump beam transmission but that of the probe was essentially zero at all times. This is because the probe frequency was set closer to linecenter and the probe was highly absorbed. Since its frequency was nearly identical to that of the pump beam the population and interference gratings were not properly delayed with respect to each other and two-wave mixing gain did not occur for the probe beam.

Oscillations were observed for the pump beam even with the probe beam absent. A plot of the variation of the oscillation period with buffer gas pressure is presented in Fig. 8a for a pump beam intensity of  $280 \text{ W/cm}^2$  and pump beam detuning of  $-0.5$  GHz from linecenter. The period increases from just under 10 seconds at a pressure of 1 Torr to almost 200 seconds at 40 Torr. The functional relationship appears to be nonlinear. Fig. 8b shows the effect of varying the pump beam intensity for a buffer gas pressure of 1 Torr. The oscillation period appears to vary nonlinearly with intensity. A threshold for the oscillations was also observed and measured to be about  $165 \text{ W/cm}^2$ . Below this threshold the pump beam transmission went to zero when the buffer gas was added and did not recover. It is interesting to note that although the period increases as the intensity is increased the buildup time for the oscillations to occur after the introduction of the buffer gas was observed to

decrease dramatically from ten's of seconds for intensities close to the threshold level to a few seconds at higher intensities. The period obtained for an intensity of  $280 \text{ W/cm}^2$  is slightly higher in Fig. 8b than that discussed earlier in the temporal sequences and is probably due to the fact that the data in Fig. 8b was taken on a different day and the detuning may have been slightly different.

### 3. APPLICATIONS

Now we turn our attention to some devices and systems which can be realized using the two-wave interactions we have discussed in Section 2. Optical resonators and self-pumped phase conjugate mirrors will be discussed in the following two sections. Then potential systems applications will be described in which such phase conjugate mirrors with a modulation capability may be utilized. Finally, we will discuss the use of two-wave mixing gain in beam clean-up and combining.

#### 3.1 Resonators

An obvious application of gain resulting from a two-wave interaction is the construction of optical resonators based upon this process. Since the gain occurs only in the forward (relative to the pump laser beam) direction it is natural to consider only ring resonators. Several groups have indeed experimentally demonstrated such devices,<sup>9,34</sup> based upon a two-wave interaction, which may be useful in laser gyroscopes, for example.

Grandclément, Grynberg and Pinard<sup>9</sup> have achieved oscillation in a sodium-based ring oscillator using gain due to collisional effects. Their results are in agreement with Equation (10) and our own pump/probe gain measurements (see Section 2.2). Ring lasing in sodium vapor using the ac-Stark effect was accomplished by Khitrova, Valley and Gibbs<sup>34</sup> who also (briefly) considered optical instabilities.

Another application of two-wave mixing that is not quite so apparent is its use as the gain mechanism in linear (standing wave) resonators. Since the gain is unidirectional the optical field inside of the resonator that is propagating in a direction almost opposite to

that of the pump beam will, in general, experience absorption resulting in extra loss for the resonator mode on a round-trip basis. However, the gain can be obtained with the pump laser frequency detuned far enough from resonance so that net gain is possible on a round-trip basis. This format, which allows for counterpropagating fields within the oscillator, makes self-pumped phase conjugate mirrors possible in resonant media such as sodium vapor. This is the subject of the next two sections.

### 3.2 Self-Pumped PCM

Optical fields traveling through aberrating media like the earth's atmosphere often encounter lateral variations in the refractive index of the media. These variations result in a random transverse spatial modulation of the optical wavefront. When the fields are so distorted, any spatial information carried by them will be more difficult for imaging (or other) processing systems to extract. Furthermore, temporally or spectrally encoded information may also be rendered useless since wavefront aberrations can adversely affect the ability of a detection system to gather and focus the light onto a detector. Compensation for such distortions is thus highly desirable. One method that has the potential for correcting the distortions of optical wavefronts is optical phase conjugation.<sup>3,4,35-42</sup>

Recently, we have demonstrated a self-pumped phase conjugation process in resonant atomic systems.<sup>43-45,48,49</sup> This approach offers a fast response time (tens of nanoseconds) and may be implemented using relatively low power optical fields, typically tens to hundreds of watts per square centimeter.

This method requires only a single laser beam and employs a two-wave interaction as the gain mechanism to form a linear standing-wave sodium vapor oscillator. Similar geometries have previously been used for barium titanate<sup>42</sup> and carbon disulfide.<sup>36</sup> Some earlier work with sodium oscillators<sup>9,34</sup> employed a unidirectional ring format which lacked the internal counterpropagating fields which are necessary to obtain a phase conjugate optical field. Four-wave mixing<sup>39</sup> in sodium has also been employed as the gain mechanism in both linear

cavities<sup>46</sup> and ring cavities.<sup>47</sup>

Initial experiments were performed in sodium vapor.<sup>43-45</sup> The oscillator construction that we utilized consists of 60 cm radius of curvature high reflector mirrors placed on both sides of a sodium cell equipped with Brewster angle windows in order to minimize Fresnel reflection losses for the cavity mode. A mirror spacing of 56 cm supports resonator modes with a waist radius of about 240  $\mu\text{m}$  at a wavelength near the sodium  $D_2$  resonance ( $\lambda = 589$  nm). The nominally 3 cm long sodium cell is positioned in the center of the cavity lengthwise so that its midpoint is coincident with the waist of the resonator mode. A pump beam from a single frequency ring dye laser was directed into the sodium cell at a small angle ( $\sim 0.5^\circ$ ) to the longitudinal axis of the resonator, as shown in Fig. 9. The pump beam was focussed to a 125  $\mu\text{m}$  radius waist at the location of the waist of the resonator mode. This arrangement ensured that the mode of the pump beam fit well within that of the resonator. A two-wave mixing interaction mediated by the ac-Stark effect then produced net gain for the oscillator at cw pump intensities on the order of a few hundred watts per square centimeter.

While the sodium resonator was oscillating a return signal was detected using a beam-splitter placed in the path of the input pump beam. Far-field intensity profiles of the return signal with a static aberrator placed in the incident beam path are shown in Fig. 10. When a flat mirror was used in place of the sodium cell the pattern shown in Fig. 10a was obtained. The data in this figure indicate an order of magnitude increase in the far-field spot size from the diffraction-limited case. Using the sodium cell resulted in most of the return energy residing in a spot that is close to diffraction limited, as shown in Fig. 10b. The expected diffraction-limited spot size was estimated by calculation as well as by measurement of the return from the flat mirror with no aberrator present in the system (see Fig. 10c).

A typical scan of the variation of the return signal with the frequency of the pump laser is shown in Fig. 11a for a pump intensity of about 1140  $\text{W}/\text{cm}^2$  in the sodium cell and a sodium temperature of 240  $^\circ\text{C}$  (the cell temperature is 260  $^\circ\text{C}$ ). Two peaks are evident in the figure. One peak has a maximum reflectivity slightly greater than 2% and is centered



about -3.5 GHz from the center of the sodium resonance with a span of approximately 0.75 GHz while the other feature has a peak reflectivity of about 0.2% located at 2.2 GHz on the low frequency wing of the sodium transition and spanning roughly 2 GHz. The higher reflectivity feature shown in Fig. 11a has only been observed at sufficiently high sodium temperature ( $\geq 220$  °C) and optical intensity ( $\geq 1000$  W/cm<sup>2</sup>) for the input laser beam. Threshold intensity for the phase conjugation process has been measured to be about 100 W/cm<sup>2</sup> at the sodium temperature mentioned above.

The output power of the resonator is plotted in Fig. 11b as a function of pump laser frequency. These scans show that oscillation occurred over a slightly wider pump frequency range than was observed for the conjugate signal but with peak locations that coincide for the two cases. At the maximum oscillator output (or maximum return signal) the intra-cavity intensity for the oscillating field was approximately 165 W/cm<sup>2</sup>. In some scans (not shown here) the oscillation had also been observed over a similar frequency span and detuning on the high frequency side of the resonance but with about 1/3 the intensity of the low frequency feature. When oscillation was obtained for positive detunings there was also a return signal present but at a relatively low power level.

An examination of the frequency content of the output of the oscillator, shown in Fig. 12a, reveals two distinct features separated by the generalized Rabi flopping frequency. One is a single longitudinal mode due to a nearly-degenerate (with respect to the pump frequency) gain process and the other is an ensemble of longitudinal modes due to a much broader three-photon gain process. In contrast, the phase conjugate return from the sodium cell (Fig. 12b) is composed of essentially one longitudinal mode which is close in frequency to the nearly-degenerate oscillating mode in the resonator, as determined by a beat frequency measurement using a frequency-shifted sample of the pump beam as a reference. Although frequency shifts are expected between the input laser, oscillator and return optical fields, no frequency shift has yet been observed between the oscillator and return fields. This is believed to be due to the frequency jitter in both the oscillator output and the return signal

due to optical path length instabilities in the resonator which is on the order of the expected frequency shifts. The single longitudinal mode of the input laser field is shown in Fig. 12c for reference.

Self-initiated nearly-degenerate four-wave mixing is believed to be the physical mechanism that produces phase conjugate waves in this experimental geometry. Specifically, the input pump beam coherently excites the sodium atoms and generates resonance fluorescence radiation, modified by the ac-Stark effect. Part of the fluorescence radiation is directed along the resonator axis and forms a standing-wave radiation field. The subsequent interference between the input beam and the intra-cavity radiation field leads to a buildup of the cavity radiation field by means of two-wave mixing gain. Oscillation is established under the condition that the intra-cavity radiation fields and the incident pump field serve as the input radiation fields in a standard four-wave mixing configuration. A phase conjugate field is produced by coherent scattering of one of the intra-cavity fields from the interference pattern generated by the other two radiation fields. The spectral lineshape of the two-wave mixing process employed here has two resonances that exhibit net gain behavior (see Section 2.1). The first resonance (Rayleigh) occurs near the input pump frequency and has a dispersive character while the second one (Raman) is shifted away from the pump frequency by the Rabi flopping rate in agreement with the experimental results.

We also conducted experiments with the cw laser source set near the  $D_2$  line in cesium<sup>48,49</sup> ( $\lambda = 852$  nm) at detunings on the order of 1 GHz on the low frequency side of the resonance. A typical scan of the reflectivity as a function of laser frequency is shown in Fig. 13 for a pump intensity of  $290 \text{ W/cm}^2$  in the cell and a cesium temperature of  $109^\circ\text{C}$ . The phase conjugate return signal was obtained over a frequency span just under 1 GHz, although a relatively small amount of return energy was obtained at larger detunings. At the larger detunings the cesium resonator was still oscillating at a power level that was about the same at that obtained for the range of detunings that produced a strong return signal. This behavior is similar to the results obtained in sodium vapor and is attributed to the different

gain mechanisms associated with the two-wave mixing process.

The effects of varying the pump beam intensity within the cesium vapor are shown in Fig. 14. A threshold intensity of about  $35 \text{ W/cm}^2$  was measured for the phase conjugation process. This measurement was performed at a detuning of about  $-0.8 \text{ GHz}$  from line center which maximized the reflectivity at the highest pumping level shown in the figure. This threshold is not, in general, the same as that for oscillation in the resonator since the three photon process will typically yield a different oscillation threshold. However, the oscillation threshold for frequencies at which gain is provided by the Rayleigh feature does appear to be the same as that for the phase conjugation process, as expected.

Varying the temperature of the cesium reservoir (number density) showed that phase conjugation is obtained for a finite range of temperature with a maximum reflectivity obtained at about  $110^\circ \text{C}$  for the conditions of our experiment. This effect (shown in Fig. 15) is consistent with the variation of the Rayleigh gain with temperature (see Section 2.1).

It should be noted that the reflectivities mentioned here do not represent fundamental limits. In fact, Grynberg<sup>50</sup> has demonstrated about 20% phase conjugate reflectivity in sodium vapor using a variation of the oscillator discussed in this section.

### 3.3 Retro-Modulators

In this section, we describe a set of experiments that demonstrate the ability of a self-pumped atomic vapor-based phase conjugate mirror to function as a retro-modulator/phase-conjugate mirror (RM-PCM). We first motivate the topic by illustrating two potential laser communication systems (over free-space and through an optical fiber) that employ such a generic device as a remote sensor, followed by a brief overview of previously performed experiments using photorefractive materials as the nonlinear element for a self-pumped RM-PCM. We then discuss results of our experimental investigation using atomic sodium as the nonlinear optical medium, as well as fundamental issues.

One basic goal of a system employing a RM-PCM is to relay temporally encoded infor-

mation, such as amplitude or pulse position encoded messages, from one point to another. This data link can be over a turbulent atmospheric path or through an optical fiber. In either of these scenarios, dynamic phase errors can result in deleterious amplitude-modulated noise over long-distance data links, which can obscure the desired encoded information. Through the use of a PCM, however, this noise can be significantly reduced by virtue of the wavefront reversal process. This enables a high signal-to-noise communications link to be established, since only the desired information will persist, encoded onto an essentially noiseless, wavefront-reversed optical carrier.

The heart of this class of communication link is the retromodulator/phase-conjugate mirror. This device is passive and performs the following operations: (1) receives an incident optical beam; (2) encodes temporal information onto the beam; and (3) returns the encoded information back to the point of origin in a wavefront-reversed manner. We sketch below two potential application scenarios using this device: a free space communications link and a remote optical fiber sensor system.

A free space communications link involving such a device is sketched in Figure 16, where the goal is to relay information from Station #2 to Station #1. Note that Station #1 in this case possesses an optical source, whereas Station #2 has a RM-PCM and no optical source. In this scenario, the RM-PCM is passive in that no active optical source is needed to activate the device, other than the incident beam; that is, the RM-PCM is basically a self-pumped conjugator.

The communications link is established by the following sequence of events: (1) Station #1 illuminates the general vicinity of Station #2 with a broad field-of-view beacon beam; (2) upon illumination by the beacon, the RM-PCM located at Station #2 generates a backward-going beam which retraces its path back to Station #1, thereby establishing the link; (3) the information to be communicated back to Station #1 is encoded onto the RM-PCM by modulating the phase conjugate reflectivity of the device; (4) the encoded retro beam signal propagates back to Station #1, where the desired information is detected. By virtue

of the conjugation process, not only are the intervening path distortions corrected, but the conjugated beam also provides a means for an automatic pointing-and-tracking function by returning the beam back to its point of origin. As we discuss below, the temporal encoding of the RM-PCM can be realized by myriad techniques which depend on the physics behind the specific class of interaction.

An optical fiber remote sensor using a RM-PCM is sketched in Figure 17, and involves placing the device at one end of an optical fiber. The interrogation beam is launched into the other end of the fiber. The RM-PCM serves a dual function: (1) it conjugates the beam which emanates from the fiber, thereby efficiently coupling the beam back into the fiber for its return transit; and (2) encodes the desired temporal information onto the return beam, which is then detected back at the source end of the fiber link. Note that the system is auto-aligned by virtue of the conjugation operation, so that the now-modulated return beam will efficiently couple back into the fiber, even in the face of mechanical and/or thermal perturbations. Note also, that a multimode fiber can be employed (obviating the power handling limit of single-mode fibers) since the conjugation process compensates for waveguide modal dispersion upon reverse transit. Use of the multimode approach may also compensate for optical missalignments at the fiber input. Again, since the RM-PCM is a passive element, no optical sources are required at the remote location; all that is required is a modulation source for temporal encoding of the return beam.

The initial experiments using the retromodulator/conjugator concept involved the use of photorefractive crystals of barium titanate as the RM-PCM.<sup>51-53</sup> Using the system, we have demonstrated high conjugate fidelity ( $\sim 73\%$ ), good signal-to-noise performance, and high bandwidth data handling capability (757 MHz), the latter limited not by the phase conjugate mirror, but by our electronics; the ultimate bandwidth of this class of nonlinear medium will be limited by conventional electro-optic engineering constraints, and is expected to approach tens of gigahertz. Proof-of-principle experiments have been performed using different classes and configurations of self-pumped phase conjugate mirrors, such as internally pumped "cat"

conjugators<sup>51,52</sup> and seeded stimulated photorefractive backscattering conjugators,<sup>53</sup> employing various modulation formats (AM, FM, PM), and using several demodulation techniques (direct and heterodyne detection). By applying a low-voltage modulation signal across the crystal, a temporally modulated, or encoded, wavefront reversed replica was realized; an argon ion laser at 514.5 nm was used as the source. In our scheme, the crystal performs two functions essentially simultaneously: (1) wavefront-reversal is obtained by virtue of the refractive-index gratings formed in the crystal volume via the photorefractive effect; and (2) temporal encoding of the diffracted output beam is achieved via bulk electro-optic modulation of the crystal. It turns out that photorefractive crystals typically possess relatively large electro-optic coefficients, so that modest modulation voltages (as low as 2 V peak-to-peak have been demonstrated) can yield detectable returns. Although the photorefractive-based interaction is simple, has broadband spectral response (throughout the visible and into the near-infrared), and possesses a large field-of-view, a potential drawback lies in the finite photorefractive response time of the crystal to dynamic input (spatial) wavefront errors.

We now discuss the results of an experimental investigation where a retro-modulator was demonstrated using a resonantly enhanced, atomic sodium phase conjugate mirror.<sup>54,55</sup> As opposed to the electro-optic phase modulation mechanism exploited in the above photorefractive crystal-based devices, retro-modulation in the present system is realized by amplitude modulating the threshold characteristic of the conjugator. The sodium-based device should be capable of tracking input wavefront dynamic errors that change on a time scale of 10's of nanoseconds, enabling this device to easily track atmospheric distortions.<sup>38</sup>

It also has several desirable features including high spatial bandwidth, the ability to respond to rapid (on the order of ten's of megahertz) changes in the optical wavefronts and low threshold power (a few ten's of milliwatts). High temporal data rates should also be possible (projected 100's of megahertz to a few gigahertz bandwidth, depending upon the modulation scheme). These features indicate that such classes of retro-modulators may be useful in low power level free-space and guided-wave communication links, as well as in

novel optical resonators and gyroscopes.

The basic geometry for this device consists of the same self-pumped configuration described in Section 3.2 above, with an added intracavity acousto-optic beam deflector to convert the phase conjugate mirror into a retro-modulator. Figure 18 shows a sketch of the experimental apparatus. The acousto-optic modulator is placed in the sodium resonator on the output side of the sodium cell with respect to the incident laser beam. When no drive signal is applied to the modulator, the intracavity fields pass through the acousto-optic crystal unperturbed, resulting in a steady-state conjugate return. However, when a voltage is applied to the modulator, some of the energy of the cavity mode is deflected away from the resonator axis, thus effectively misaligning the resonator and terminating the oscillation, as well as the phase conjugate return beam. Therefore, the acousto-optic modulator encodes temporal information onto the return beam by amplitude modulating the phase conjugate reflectivity. For the purposes of modulation the time required for the population gratings to decay is not as significant as the time necessary to form them. This is because the return (phase conjugate) signal is turned off as soon as the backward travelling resonator mode is blocked by the modulator since it is this optical field that forms the return when it diffracts from the grating formed by the incident field and the forward travelling resonator mode. Therefore, the ultimate limitation in the turn-off time lies with the modulator. In contrast, the population grating buildup rate in the nonlinear medium must be much faster than the modulation rate. Since the response time of sodium vapor is on the order of 10 nsec, this means that the ultimate modulation rate that could, in principle, be achieved using amplitude modulation is on the order of 100 MHz. However, in practice this limit may be reduced depending on the buildup time for oscillation in the cavity.

Experiment parameters were a sodium temperature of 240 °C and a detuning of -3.5 GHz from line-center of the sodium  $D_2$  resonance ( $\lambda = 589$  nm) for the incident laser beam. The intensity of the optical field in the cell was about 1140 W/cm<sup>2</sup> (this is an estimate for the case of no thermal lensing).

Using a square wave modulation drive signal (applied to the acousto-optic modulator) the conjugate beam was observed to be amplitude modulated as shown in Figure 19. Two different modulation frequencies are shown in this figure. One at 10 kHz with a modulation depth of about 90% and the other at 1 MHz with a 70% modulation depth. The highest modulation frequency obtained was 4 MHz, limited by the intracavity modulator, and not due to fundamental constraints. The acousto-optic deflector was also characterized separately to determine the degree to which the deflector performance was limiting that of the sodium retro-modulator. This comparison showed that the decrease of modulation depth of the retro-modulator with increasing frequency of the drive voltage was due to the acousto-optic modulator itself. In fact, the modulation depths were better when this modulator was used inside the sodium resonator due to the threshold condition for oscillation. Depths of modulation for the isolated deflector were only 60% and 30% for drive voltage frequencies of 10 kHz and 1 MHz, respectively. The rise and fall times were determined to be about 300 nsec and 50 nsec, respectively, for both the phase conjugate return and the output of the deflector when it was tested outside the resonator cavity. This result again indicates that the limitation was due to the acousto-optic modulator and/or its associated drive electronics. For the length of the resonator used in these experiments the cavity round-trip time was on the order of 3 nsec. Since a few roundtrips are normally required to build up to cw oscillation the response time of the cavity is seen to be about the same as that for the sodium vapor itself and much less than the measured rise and fall times.

It is interesting at this point to contrast the physical mechanism for this type of retro-modulator/conjugator with that involving a crystal of  $\text{BaTiO}_3$ . In the case of the device geometry employed for our retro-modulator using a photorefractive material, the modulation is obtained through the electro-optic effect for the bulk crystal. The modulation rate can therefore be greater than the rate at which the photorefractively induced gratings can be changed within the crystal, completely the opposite from the sodium-based device.

We have demonstrated a retro-modulator/conjugator in sodium vapor with the ability



to simultaneously compensate for dynamic propagation phase errors (such as atmospheric turbulence) and to remotely relay information back to an optical beacon source, essentially free of intervening noise and with an inherent pointing and tracking capability. Modulation rates up to 100 MHz are projected for amplitude modulation. Higher modulation rates may also be possible using phase or frequency modulation. In this method the cavity mode is steered through the two-wave mixing gain envelope in order to frequency modulate the intracavity pump beams and, in turn, the phase conjugate return signal. The limitation upon the modulation rate in this case will depend upon the modulator which could, for example, be of the electro-optic variety.

### 3.4 Beam Clean-Up and Combining

In the earlier discussion on self-pumped optical phase conjugators in atomic systems we have indicated how two-wave mixing can be used to correct for distortions of the wavefronts of optical fields. Actually, in those applications it was really internal *four-wave* mixing that produced a phase conjugate beam that would then be free of wavefront aberrations after it had retraversed its path through any phase-distorting material encountered on the way to the phase conjugate mirror. However, it should also be possible to effectively clean up laser beams by transferring energy from an aberrated beam to a (second) high quality laser beam using two-wave mixing alone. Although beam clean-up using two-wave mixing has been demonstrated in photorefractive media<sup>5</sup> it has not yet been accomplished in a resonant atomic system to our knowledge.

Alternatively, one could combine the power of two laser beams in a two-wave mixing process for power scaling. This has been demonstrated in both sodium<sup>7,8,10</sup> and potassium<sup>56</sup> vapors. The experiments in sodium involved the transfer of energy from a strong laser beam to a weak probe beam while the potassium vapor experiments were used to transfer over 85% of the energy from one laser beam to another of approximately equal intensity. The latter set of experiments were conducted under conditions of pulsed excitation. Two-wave mixing

may also affect the ability to frequency-lock lasers using internal four-wave mixing.<sup>57-59</sup>

#### 4. CONCLUSIONS

This chapter has reviewed some of the physics of nonlinear two-wave interactions in resonant atomic systems. In particular, the physical mechanisms behind the processes of energy exchange between two optical fields were explored theoretically and experimentally. Collisional effects resulting from the inclusion of buffer gases into the mixing process were also considered. An interesting phenomena of temporal oscillations in the transmission of a cw laser beam through pressure-broadened sodium vapor and the associated effect upon two-wave mixing was discussed. This oscillatory behavior could have an important impact upon the performance of devices and basic energy transfer processes based upon multi-wave interactions.

Some of these devices have been covered here including optical resonators, self-pumped phase conjugators and retro-modulators. Atomic systems that were investigated experimentally are sodium, cesium and potassium vapors. However, the results are general and should apply to other media that may be modeled as two-level systems.

In spite of this extensive work, there are important questions that remain to be answered. From the point of view of coherent energy transfer processes, the physics of beam-induced cross saturation of the transitions is yet to be determined. An interesting topic of research is the existence of spatial dressed states produced by two optical beams of nearly identical intensities. The effect of such states upon the maximum allowed two-wave mixing gain should be considered. These questions have a direct bearing on the maximum reflectivity that can be achieved in the self-pumped phase conjugate mirror and related devices.

Regarding pressure-induced effects, an important area of research such as coherent coupling between two orthogonally polarized optical fields should merit further study. The answer to this question might open a new class of devices that possess the flexibility of information processing using non-parallel polarization states of the radiation fields.

## ACKNOWLEDGEMENT

The work of two of us (CJG and JFL) could not have been accomplished without the support of the DARPA/ONR (Shen Shey), Army Research Office (Bob Guenther) and Air Force Office of Scientific Research (Howie Schlossberg). CJG and DMP would like to acknowledge the support of the Hughes Research Laboratories for the retro-modulator studies. CJG and JFL would like to extend their sincere thanks to the following colleagues who have shared our quest for the understanding of the physics during the last few years: Mr. Rick Harold and Mr. Tony Pepitone for their assistance in the experiments; and Dr. R.C. Lind, Dr. Galina Khitrova, Prof. Paul Berman and Prof. G. Grynberg for their constant inspiration and technical prowess.

## REFERENCES

1. R.Y. Chiao, C.H. Townes and B.P. Stoicheff, Phys. Rev. Lett. **12**, 592 (1964).
2. G. Eckhardt, R.W. Hellwarth, F.J. McClung, S.E. Schwartz, D. Weiner and E.J. Woodbury, Phys. Rev. Lett. **9**, 455 (1962).
3. B. Ya. Zel'dovich, V.I. Popovichev, V.V. Ragul'skii and F.S. Faizullov, J.E.T.P. Lett. **15**, 109 (1972).
4. O.Y. Nosach, V.I. Popovichev, V.V. Ragul'skii and F.S. Faizullov, JETP Lett. **16**, 435 (1972).
5. *Photorefractive Materials and Their Applications I and II*, edited by P. Gunter and J.P. Huignard, Springer-Verlag (1989).
6. F.Y. Wu, S. Ezekiel, M. Ducloy and B.R. Mollow, Phys. Rev. Lett. **38**, 1077 (1977).
7. C.J. Gaeta, J.F. Lam and R.C. Lind, CLEO Talk #WG4 (Anaheim, California, 1988).
8. C.J. Gaeta and J.F. Lam, submitted to Phys. Rev. Lett. (1990).
9. G. Grynberg, E. Le Bihan and M. Pinard, J. of Physique **47**, 1321 (1986); D. Grandclément, G. Grynberg and M. Pinard, Phys. Rev. Lett. **59**, 40 (1987).
10. M.T. Gruneisen, K.R. MacDonald and R.W. Boyd, JOSA B **5**, 123 (1988).
11. S. Haroche and F. Hartmann, Phys. Rev. A **6**, 1280 (1972).
12. B.R. Mollow, Phys. Rev. A **5**, 2217 (1972).
13. S.H. Autler and C.H. Townes, Phys. Rev. **100**, 703 (1955).

14. M. Sargent, M.O. Scully and W.E. Lamb, *LASER PHYSICS*, Addison-Wesley (1974).
15. C. Cohen-Tannoudji and S. Reynaud, in *MULTIPHOTON PROCESSES*, edited by J.H. Eberly and P. Lambropoulos, page 103, John Wiley (1978).
16. C. Cohen-Tannoudji and S. Reynaud, *J Phys. B* **10**, 345 (1977).
17. G. Khitrova, P.R. Berman and M. Sargent III, *JOSA B* **5**, 160 (1988).
18. P.R. Berman, G. Khitrova and J.F. Lam, in *Spectral Line Shapes 3* edited by F. Rostas, page 337, (de Gruyter, Berlin, 1985).
19. J.E. Bjorkholm, A. Ashkin and D.B. Pearson, *Appl. Phys. Lett.* **27**, 534 (1975).
20. F.Kh. Gel'mukhanov and A.M. Shalagin, *JETP Lett.* **29**, 711 (1979).
21. M.C. de Lignie and E.R. Eliel, *Optics Comm.* **72**, 205 (1989).
22. H.G.C. Werij, et. al, *Phys. Rev. Lett.* **58**, 2660 (1987).
23. S.N. Atutov, St. Lesjak, S.P. Podjachev and A.M. Shalagin, *Optics Comm.* **60**, 41 (1986).
24. H.G.C. Werij, J.E.M. Haverkort and J.P. Woerdman, *Phys. Rev. A* **33**, 3270 (1986).
25. H.G.C. Werij, J.P. Woerdman, J.J.M. Beenakker and I. Kuščer, *Phys. Rev. Lett.* **52**, 2237 (1984).
26. H.G.C. Werij and J.P. Woerdman, *Physics Reports* **169**, 145 (1988).
27. E.L. Lewis, *Phys. Rep.* **58**, No. 1 (1980).
28. F.Kh. Gel'mukhanov and A.M. Shalagin, *Sov. Phys. JETP* **51**, 839 (1980).

29. G. Nienhuis, Phys. Rev. A **31**, 1636 (1985).
30. F.Kh. Gel'mukhanov, J.E.M. Haverkort, S.W.M. Borst and J.P. Woerdman, Phys. Rev. A **36**, 164 (1987).
31. P. Verkerk and G. Grynberg, Europhys. Lett. **6**, 31 (1988).
32. C.J. Gaeta and J.F. Lam, IQEC Talk #QFA8 (Anaheim, California, 1990).
34. G. Khitrova, J.F. Valley and H.M. Gibbs, Phys. Rev. Lett. **60**, 1126 (1988).
35. J.O. White, M. Cronin-Golomb, B. Fischer and A. Yariv, Appl. Phys. Lett. **40**, 450 (1982); M. Cronin-Golomb, B. Fischer, J.O. White and A. Yariv, Appl. Phys. Lett. **41**, 689 (1982).
36. A.M. Scott and P. Waggott, Opt. Lett. **12** No. 10, 835 (1987).
37. D.M. Pepper, p333 in Laser Handbook 4 (North-Holland Physics Publishing, Amsterdam, 1985); D.M. Pepper, Opt. Eng. **21** No. 2, 156 (1982).
38. R.C. Lind and G.J. Dunning, Talk #THC5 CLEO Tech. Digest (1983).
39. D.M. Bloom and G.C. Bjorklund, Appl. Phys. Lett. **31**, 592 (1977); R.L. Abrams and R.C. Lind, Opt. Lett. **2**, 94 (1978); D.M. Bloom, P.F. Liao and N.P. Economou, Opt. Lett. **2**, 58 (1978).
40. J. Feinberg and R.W. Hellwarth, JOSA **70**, 599 (1980); B. Fischer, M. Cronin-Golomb, J.O. White and A. Yariv, Opt. Lett. **6**, 519 (1981).
41. J. Feinberg, Opt. Lett. **7**, 486 (1982).
42. J.O. White, M. Cronin-Golomb, B. Fischer and A. Yariv, Appl. Phys. Lett. **40**, 450

- (1982); M. Cronin-Golomb, B. Fischer, J.O. White and A. Yariv, Appl. Phys. Lett. **41**, 689 (1982).
43. C.J. Gaeta, J.F. Lam and R.C. Lind, 16<sup>th</sup> IQEC Talk #PD29 (Tokyo, Japan, 1988).
  44. C.J. Gaeta, J.F. Lam and R.C. Lind, OSA Annual Meeting Talk #FL4 (Santa Clara, California, 1988).
  45. C.J. Gaeta, J.F. Lam and R.C. Lind, Opt. Lett. **14**, 245 (1989).
  46. D. Grandclément, G. Grynberg and M. Pinard, Phys. Rev. Lett. **59**, 44 (1987).
  47. P. Kumar and J.H. Shapiro, Opt. Lett. **10** 226 (1985).
  48. C.J. Gaeta and J.F. Lam, I.E.E.E. NLO Talk #THP22 (Kauai, Hawaii, 1990).
  49. C.J. Gaeta and J.F. Lam, submitted to Appl. Phys. Lett. (1990).
  50. G. Grynberg, I.E.E.E. NLO Talk #TI2 (Kauai, Hawaii, 1990).
  51. D.M. Pepper, Appl. Phys. Lett. **49**, 1001 (1986).
  52. D.M. Pepper, Proc. SPIE **739**, 71 (1987).
  53. M.L. Minden, R.A. Mullen, and D.M. Pepper, to be published.
  54. C.J. Gaeta and D.M. Pepper, CLEO Talk #TUA1 (Baltimore, Maryland, 1989).
  55. C.J. Gaeta and D.M. Pepper, submitted to Opt. Lett.
  56. M.T. Gruneisen, K.R. MacDonald, A.L. Gaeta and R.W. Boyd, Phys. Rev. A **40**, 3464 (1989).
  57. C.J. Gaeta, R.C. Lind, W.P. Brown and C.R. Giuliano, IEEE/LEOS Annual Meeting

Talk #EL3.5 (Santa Clara, California, 1988).

- 58. C.J. Gaeta, R.C. Lind, W.P. Brown and C.R. Giuliano, Opt. Lett. **13**, 1093 (1988).
- 59. W.P. Brown, C.J. Gaeta, R.C. Lind and C.R. Giuliano, IEEE/JQE **25**, 607 (1989).



## LIST OF FIGURES

1. (a) States of the atom + radiation field system. (b) Dressed states.
2. The dressed atom picture of amplification of the weak probe.
3. Transmitted probe (normalized to incident probe beam power) for the cases of (a) pump beam off, sodium temperature of 200 °C, (b) pump beam on, same temperature and (c) pump beam on, sodium reservoir at 180 °C.
4. Probe beam transmission exhibiting a dominant Raman gain feature.
5. Gain coefficients for Raleigh and Raman gain processes resulting from the ac-Stark effect as a function of sodium temperature.
6. Plots of the transmission of the probe beam through a pressure-broadened sodium vapor for (a) no pump beam or buffer gas present. Two-wave mixing gain lineshapes for a pump intensity of 25 W/cm<sup>2</sup> and argon buffer present at pressures of (b) 40 Torr and (c) 60 Torr.
7. Temporal oscillations of the transmission of pump and probe beams through sodium vapor in the presence of argon buffer gas.
8. Variation of the oscillation period with (a) buffer gas pressure for a pump beam intensity of 280 W/cm<sup>2</sup> and (b) pump beam intensity for a buffer gas pressure of 1 Torr.
9. Self-pumped phase conjugate mirror configuration.
10. Far-field patterns of the return signal using (a) a flat mirror and (b) a sodium cell with an aberrator present. The pattern using (c) a flat mirror with no aberrator in the system is included for comparison.
11. Variation of (a) the phase conjugate reflectivity and (b) the output of the sodium oscillator as a function of probe laser frequency.
12. Longitudinal mode spectra of the (a) output of the sodium oscillator, (b) return signal and (c) input laser field.

13. Phase conjugate reflectivity as a function of laser frequency.
14. Variation of reflectivity with pump beam intensity within the cesium vapor.
15. Dependence of the phase conjugate reflectivity upon the temperature of the cesium reservoir (number density).
16. Basic free-space remote data link scenario using a retromodulator/conjugator. RM-PCM, at Station #2 and an optical source at Station #1. The goal is to relay temporal information from the RM-PCM location to the optical source location.
17. An optical fiber remote sensor scenario with a retro-modulator/conjugator, RM-PCM. The device allows for remote encoding, as well as efficient coupling of the modulated return beam back into the fiber for the return propagation. The system functions in the face of fiber/RM-PCM misalignments and vibrations, and corrects for fiber distortions (modal dispersion, polarization scrambling, etc.), which may be induced due to hostile environmental conditions.
18. Retro-modulator/conjugator configuration utilizing an intracavity acousto-optic beam deflector.
19. Photographs of oscilloscope traces showing both the modulation drive voltage waveform (lower trace in all photographs) applied to the acousto-optic deflector and the corresponding amplitude modulation imposed on an isolated deflector for calibration purposes (upper photographs), and the modulated phase conjugate return optical field (lower photographs).

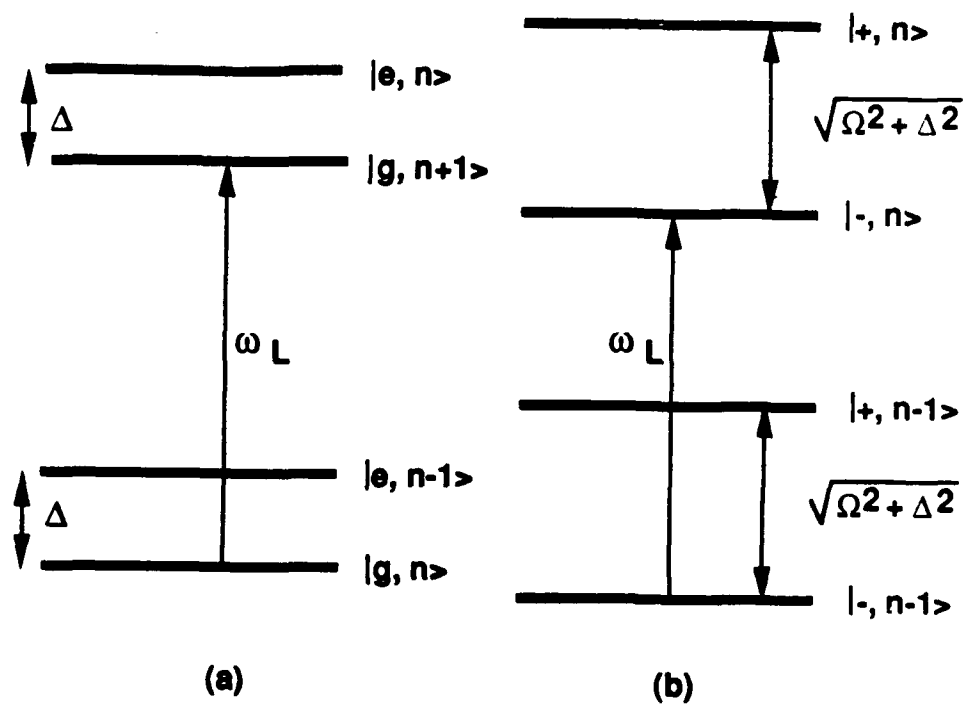


Figure 1

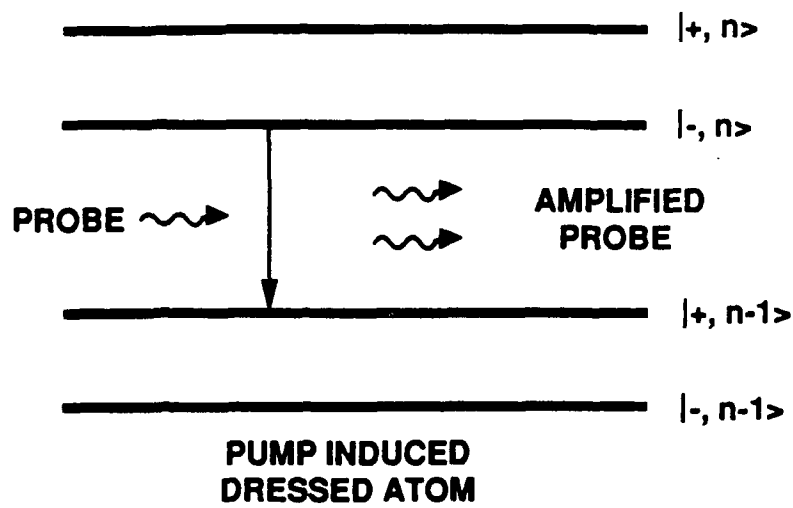


Figure 2

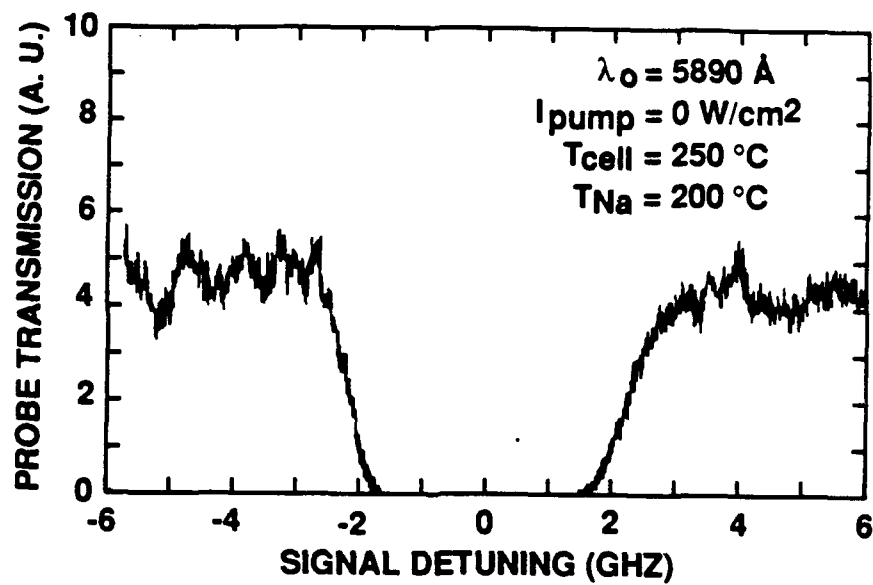


Figure 3 (a)

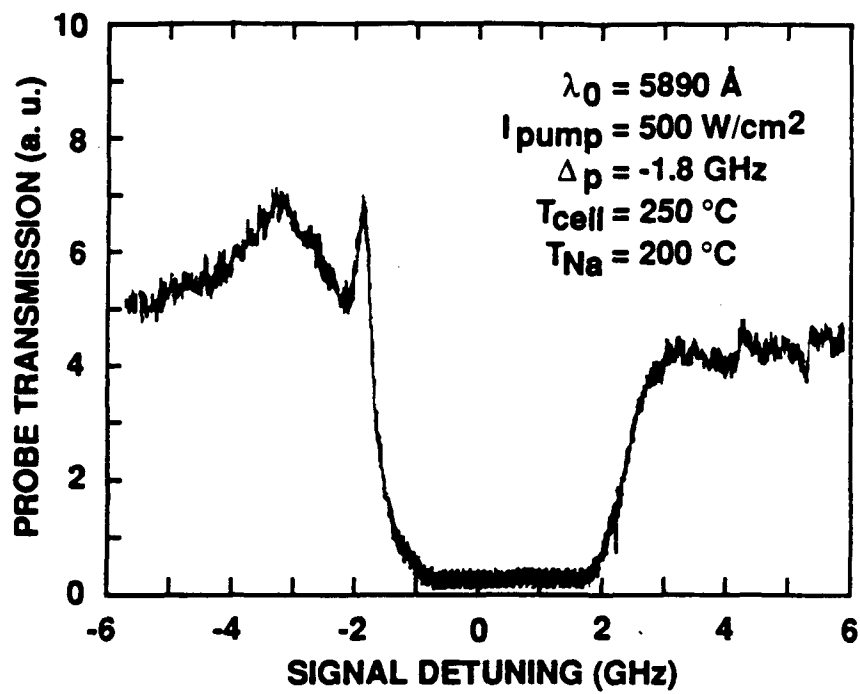


Figure 3 (b)

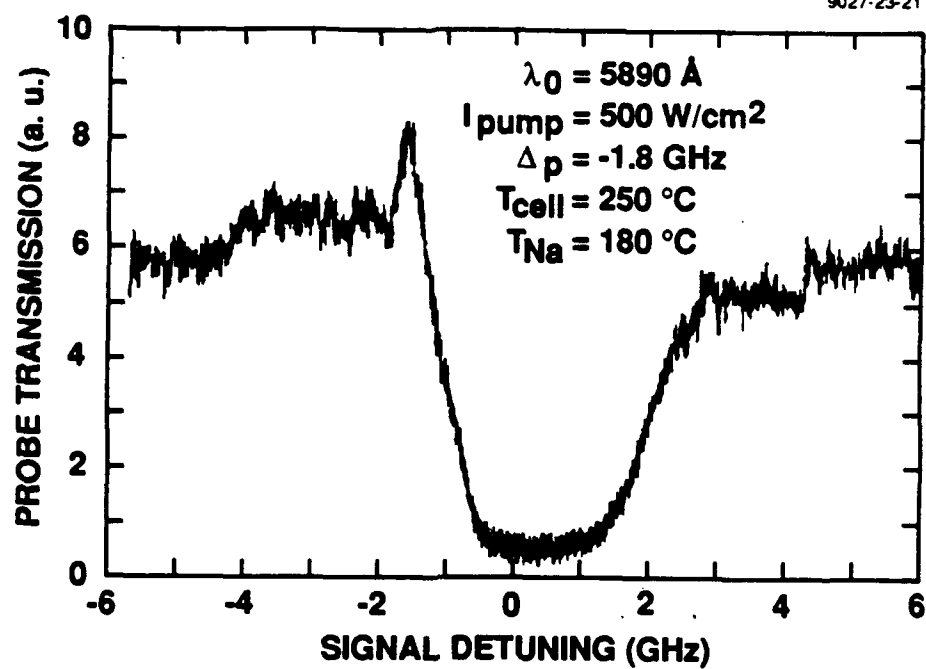


Figure 3 (c)

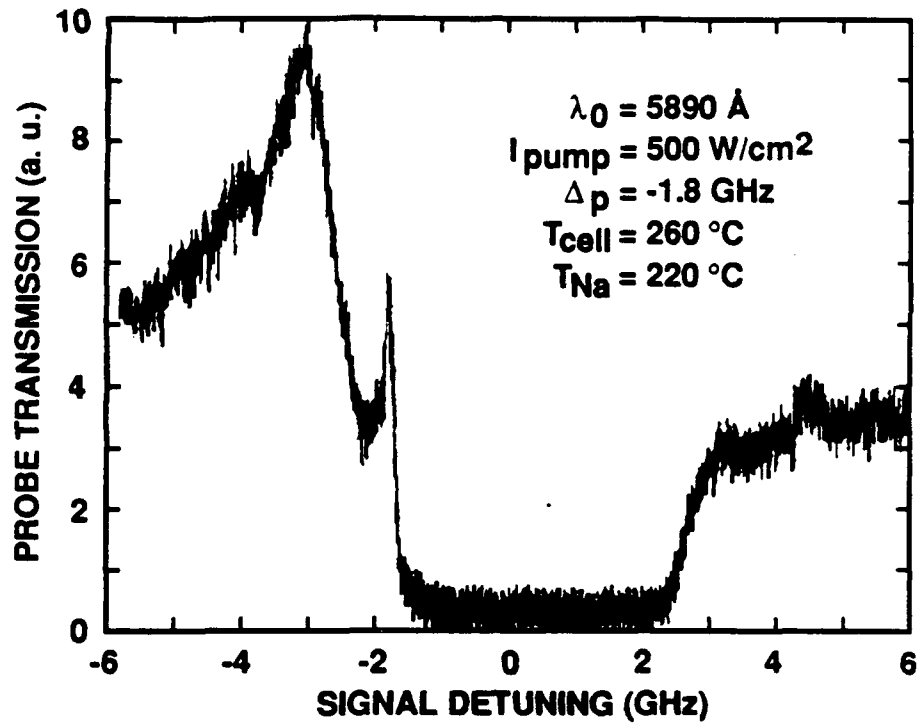


Figure 4



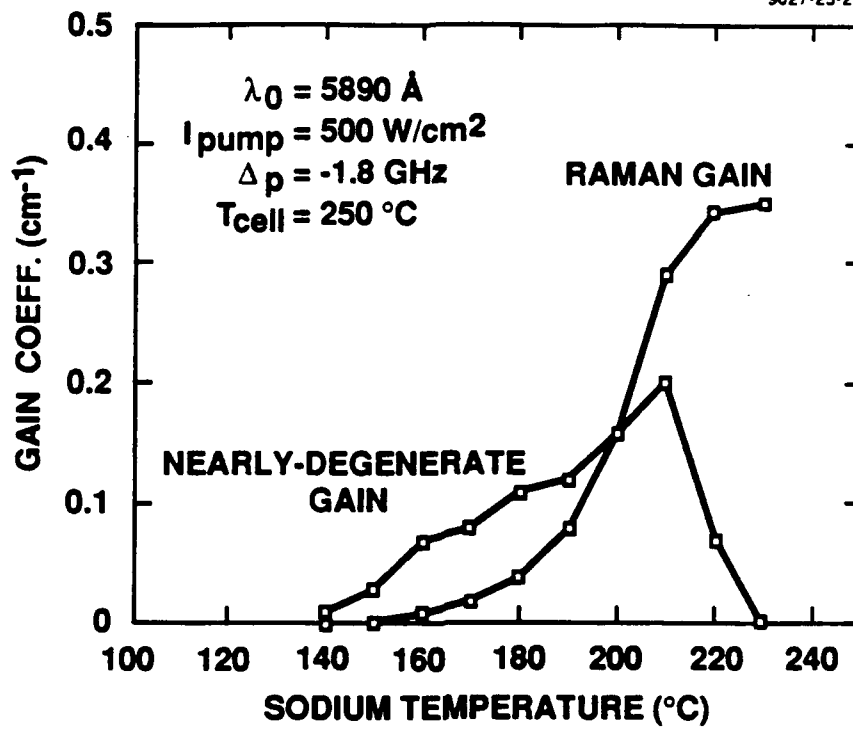


Figure 5

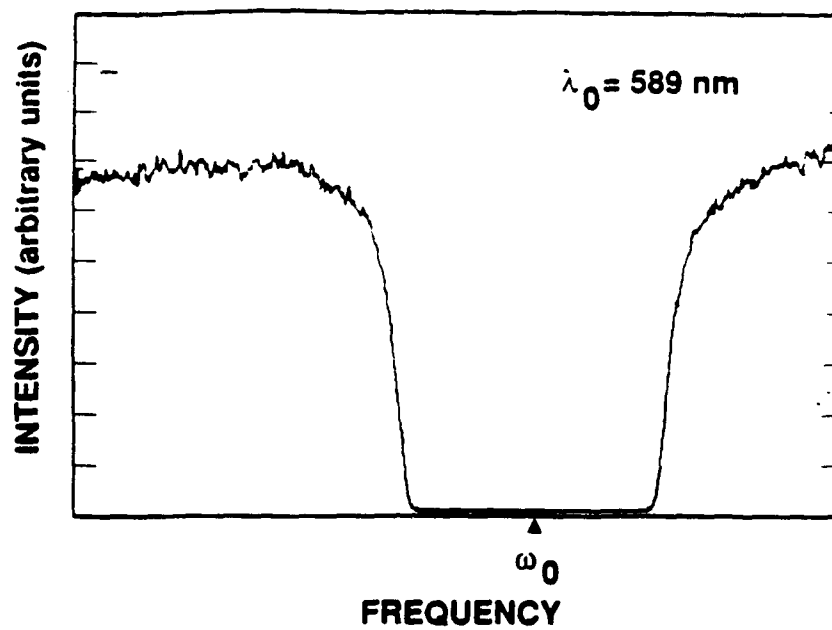


Figure 6 (a)

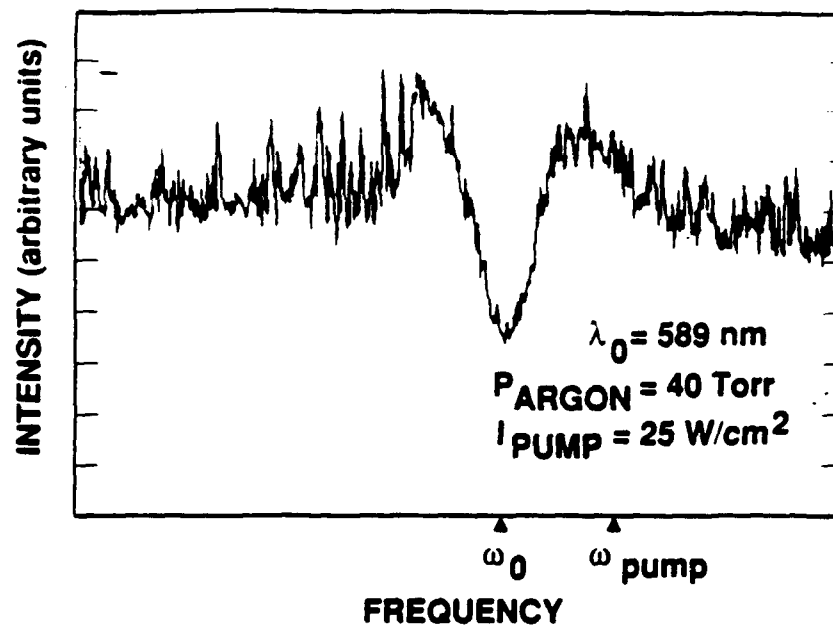


Figure 6 (b)

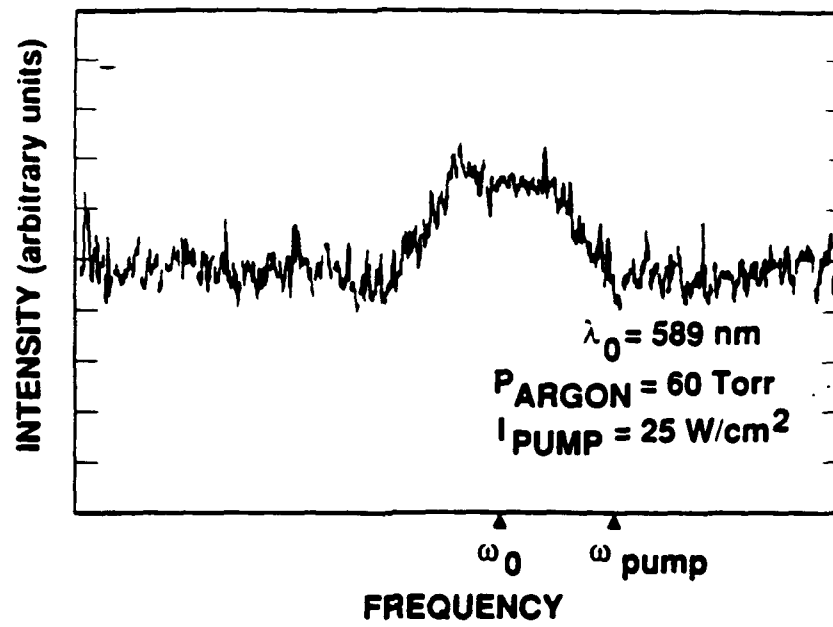
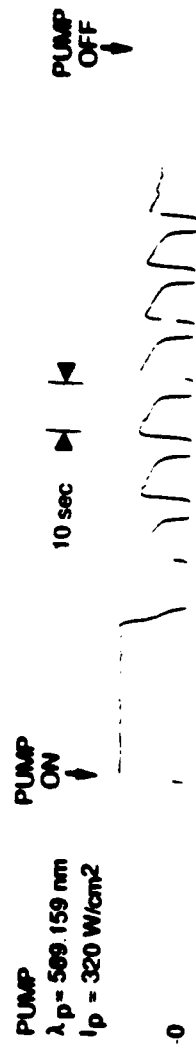


Figure 6 (c)

0027 04 10



$T_{\text{CELL}} = 201^\circ\text{C}$   
 $T_{\text{Na}} = 227^\circ\text{C}$

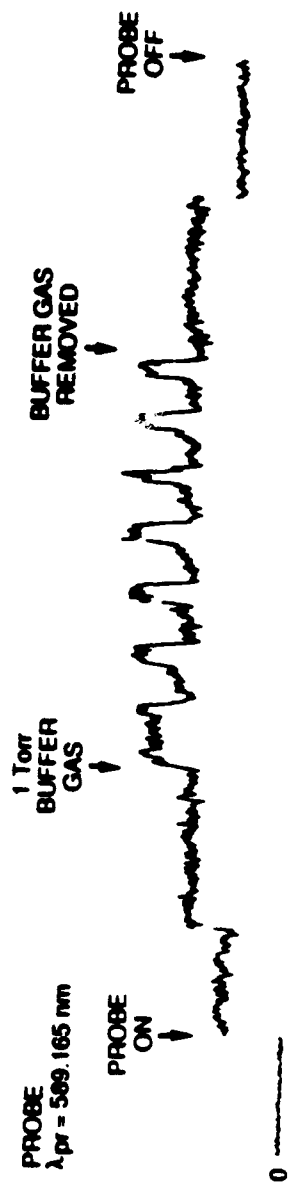


Figure 7

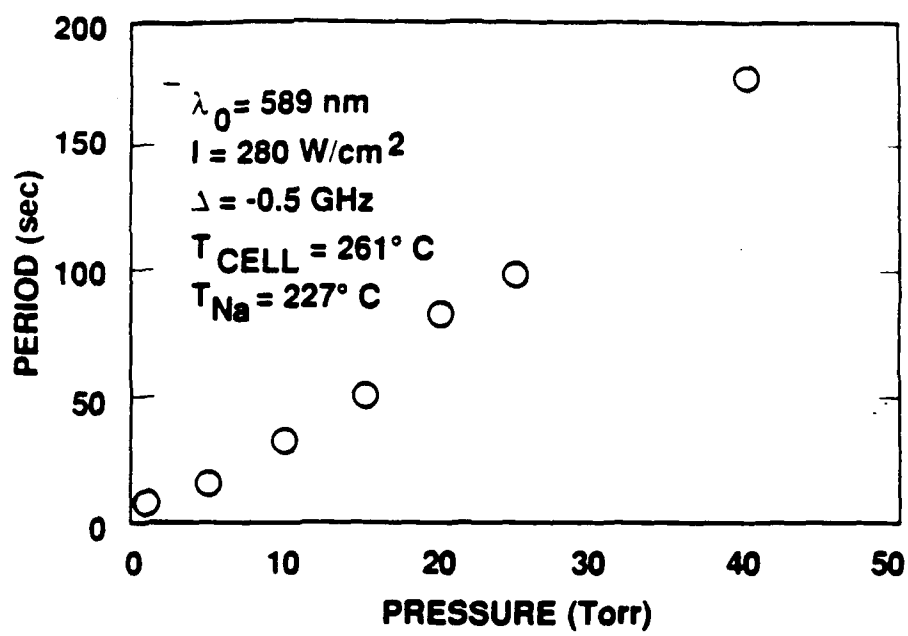


Figure 8 (a)

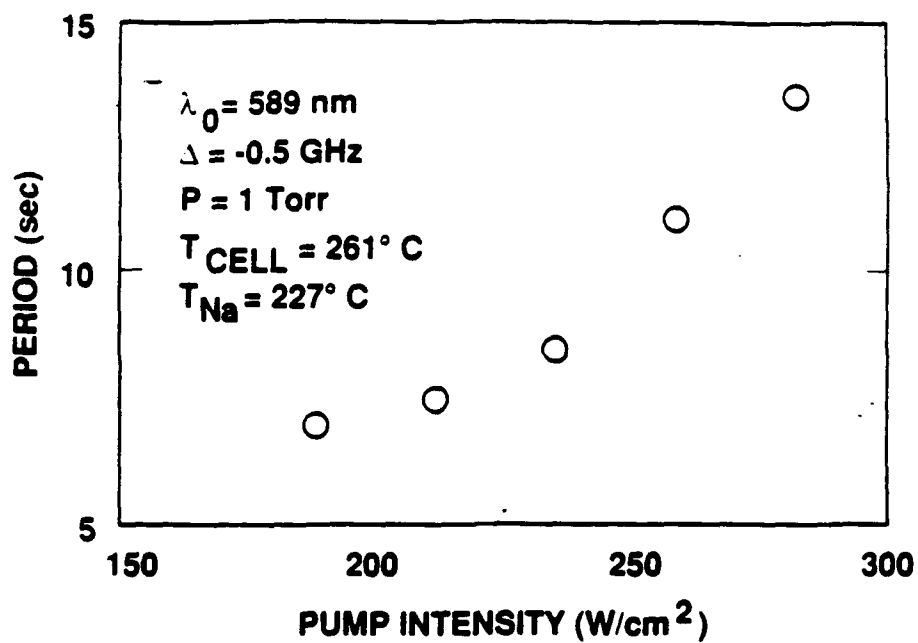
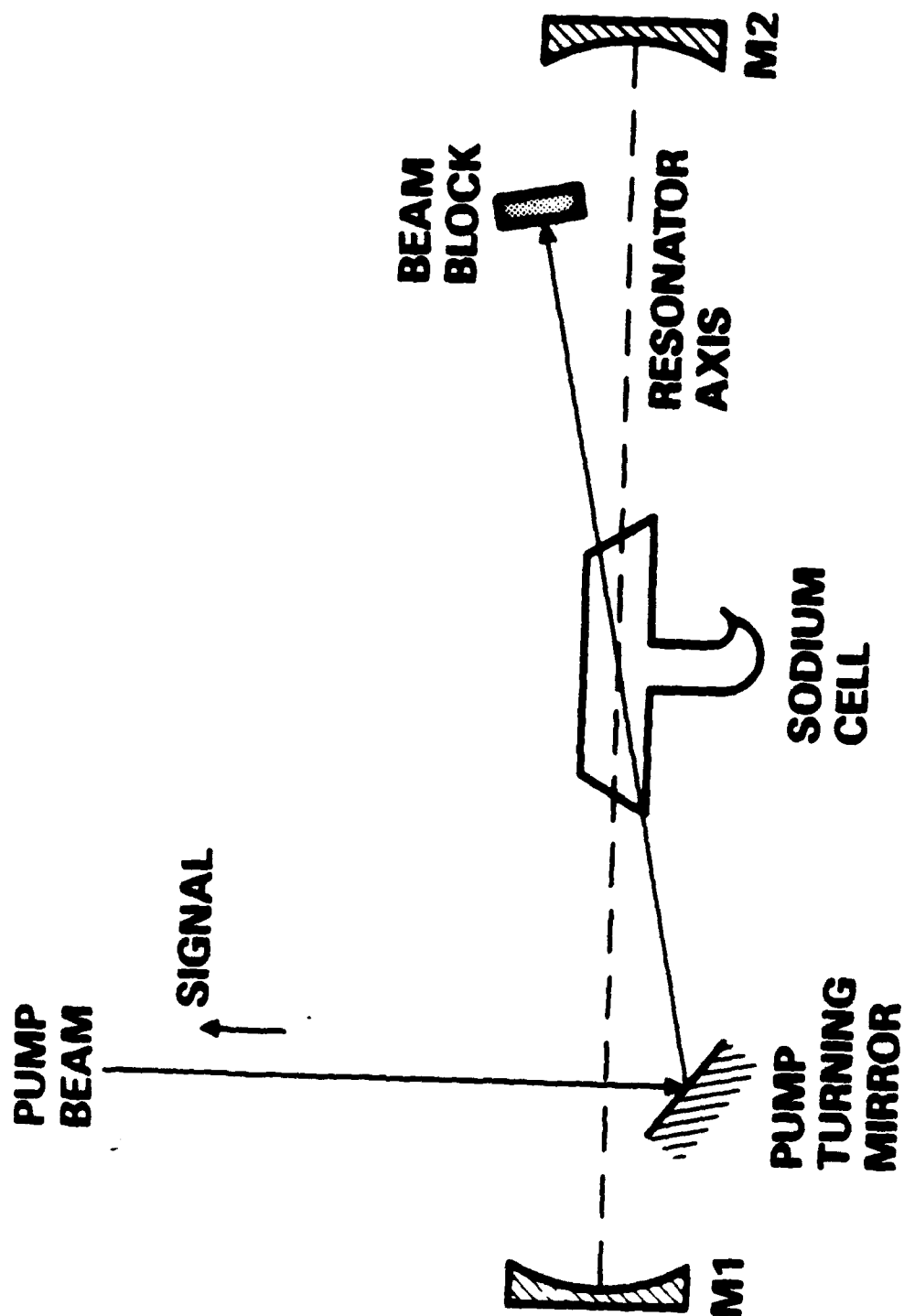


Figure 8 (b)



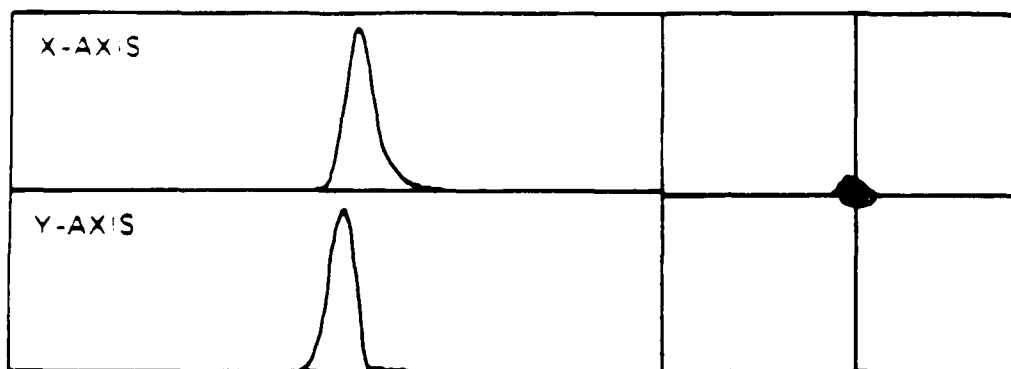
MAY 1961

Figure 9

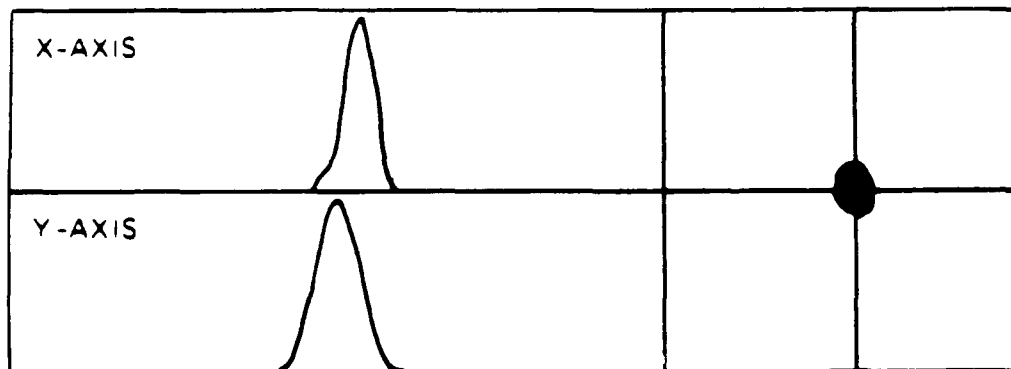




(a)

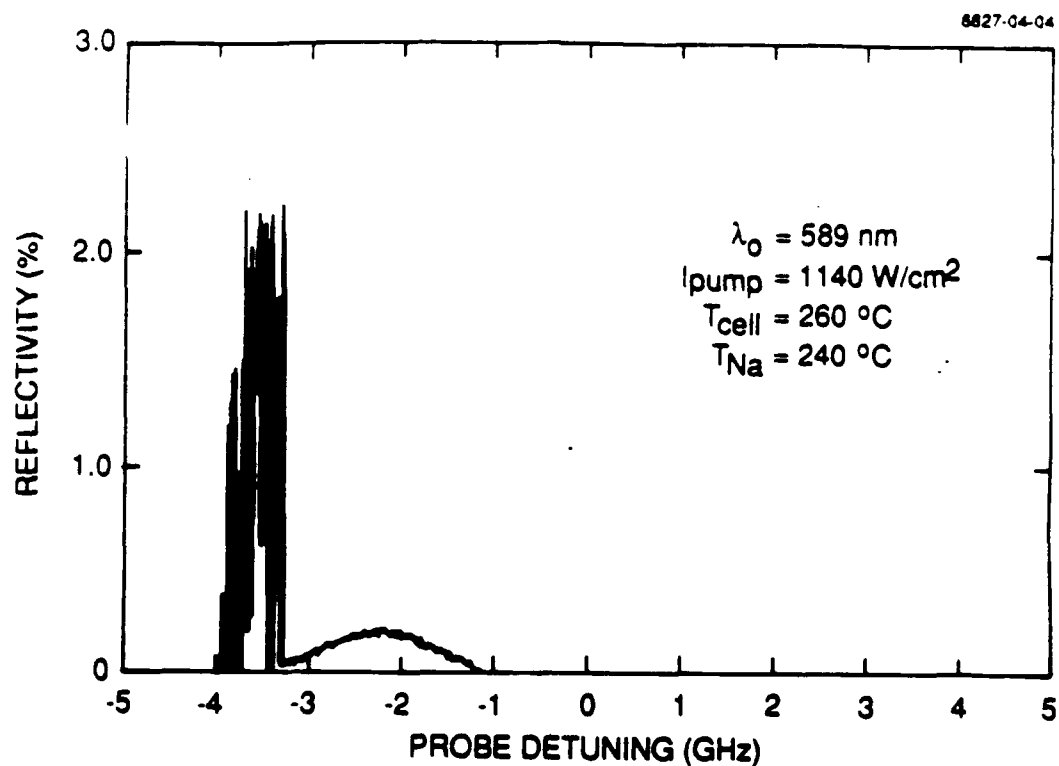


(b)

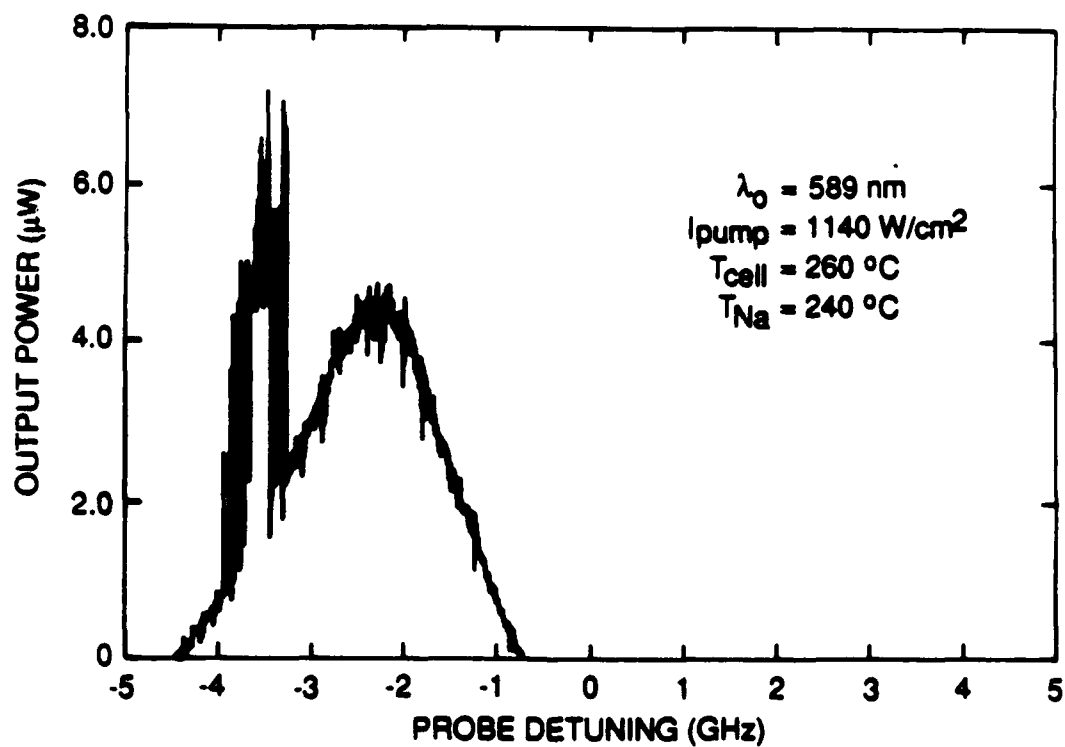


(c)

Figure 10

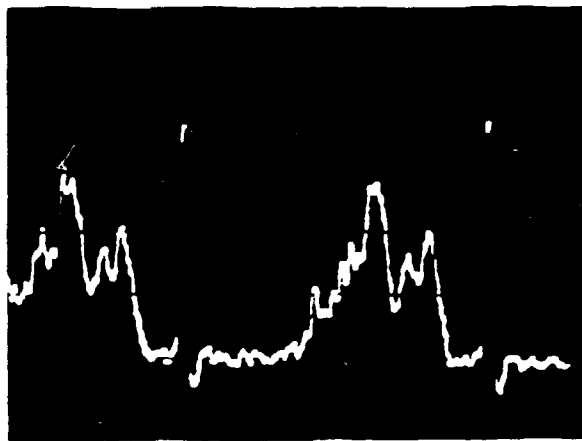


(a)

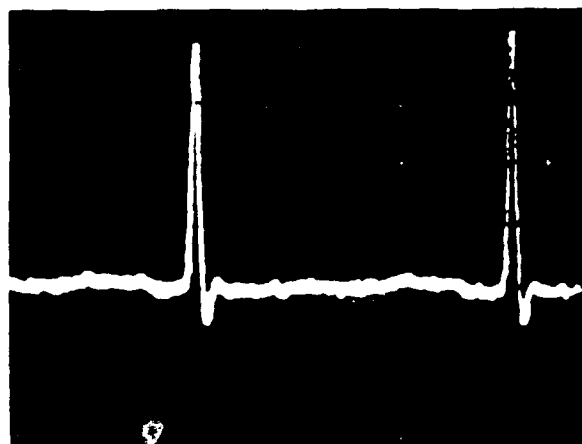


(b)

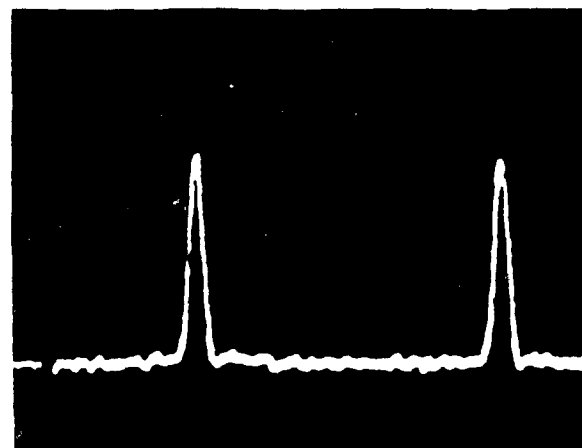
Figure 11



(a)



(b)



(c)

$$I_{\text{PUMP}} = 380 \text{ W/cm}^2$$

$$\Delta_{\text{PUMP}} = -2.2 \text{ GHz}$$

$$T_{\text{CELL}} = 260^\circ\text{C}$$

$$T_{\text{Na}} = 220^\circ\text{C}$$

Figure 12

9027-04-08

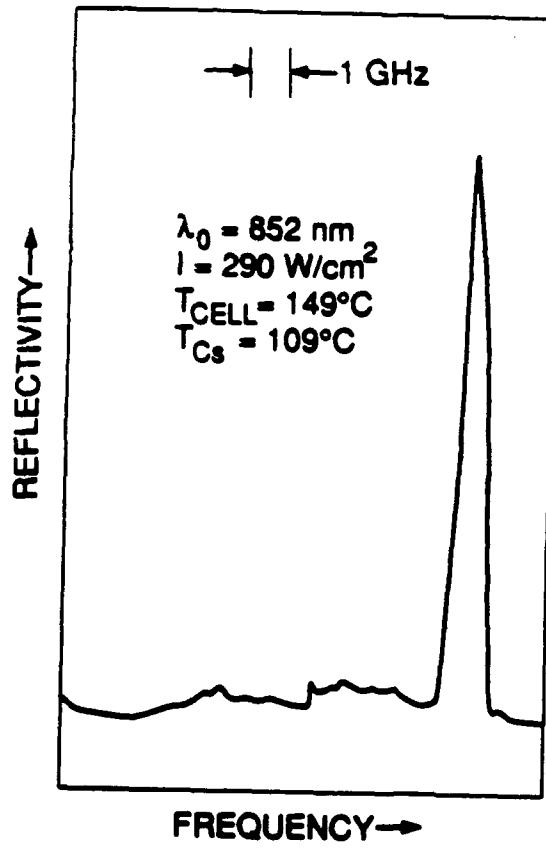


Figure 13

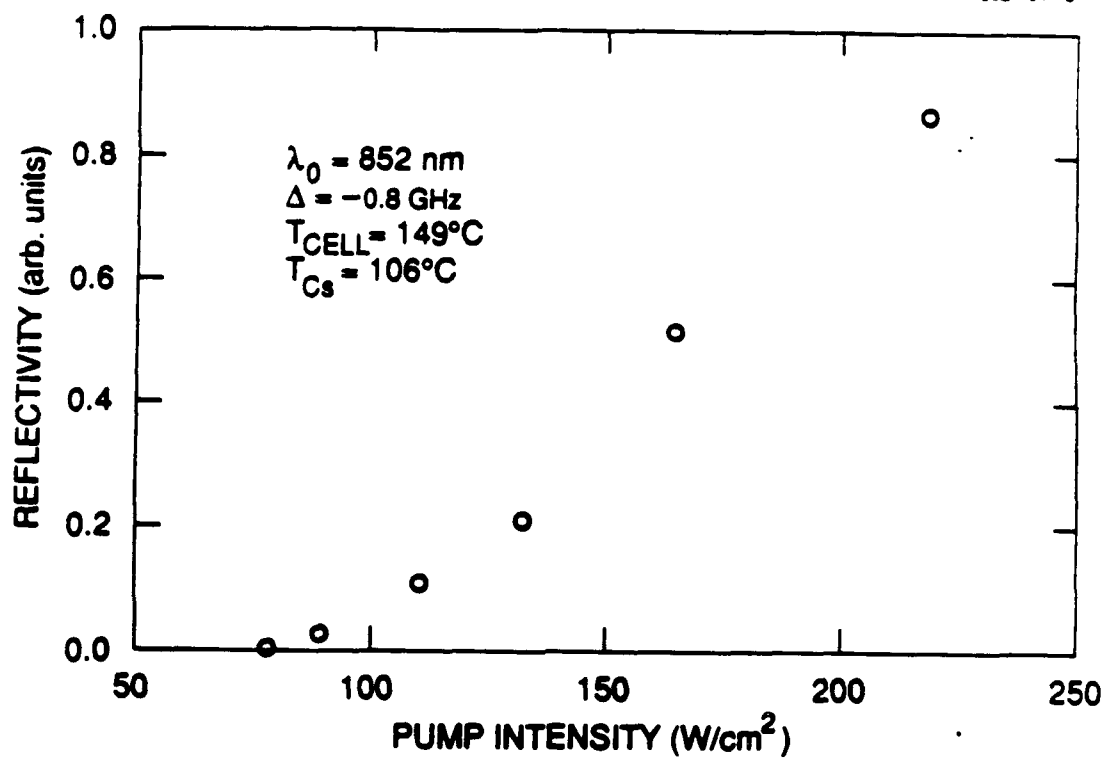


Figure 14

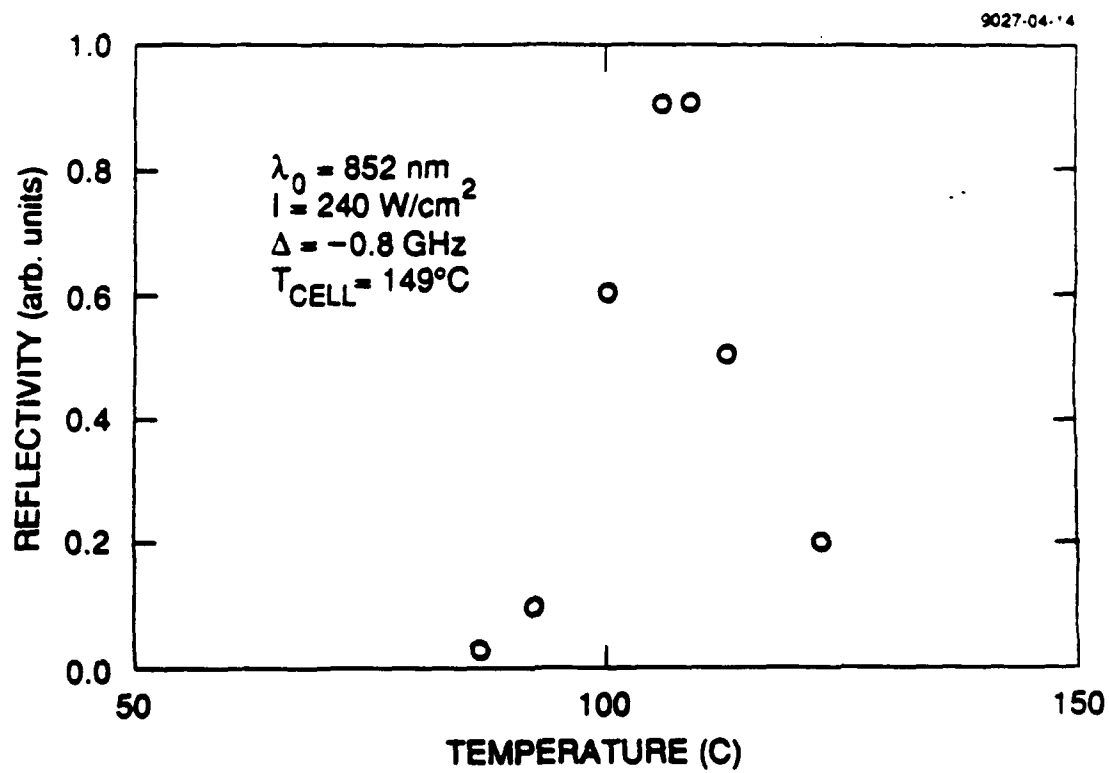
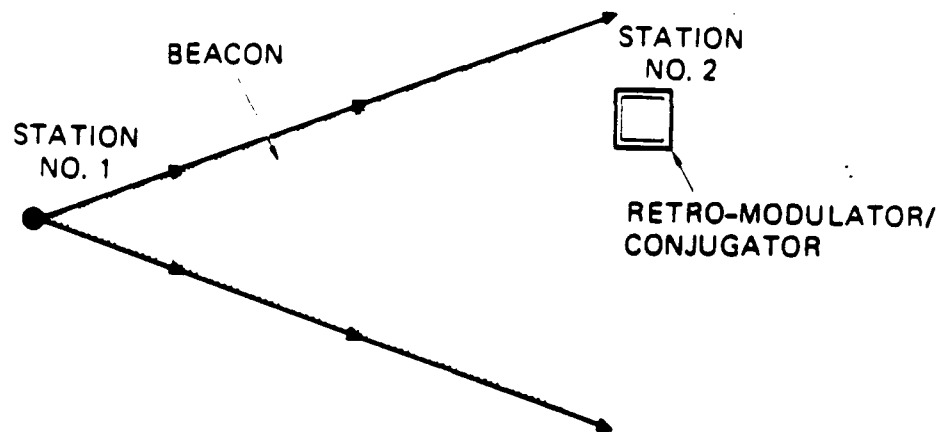
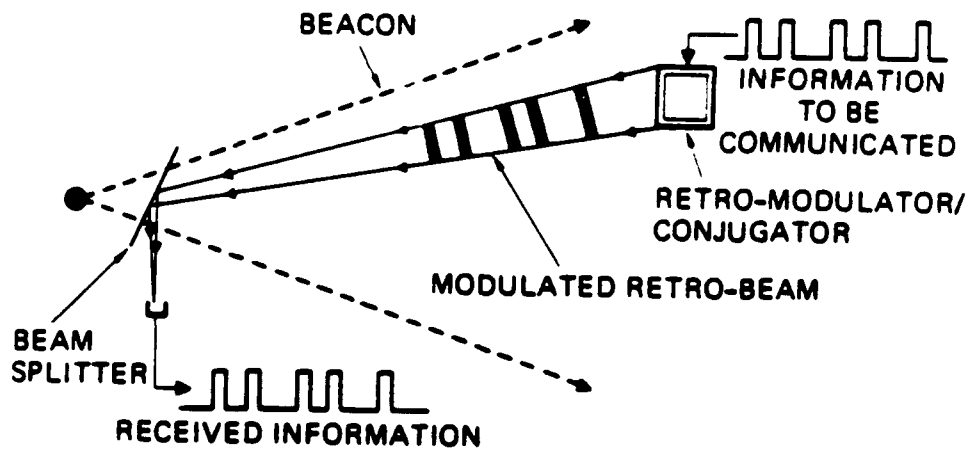


Figure 15

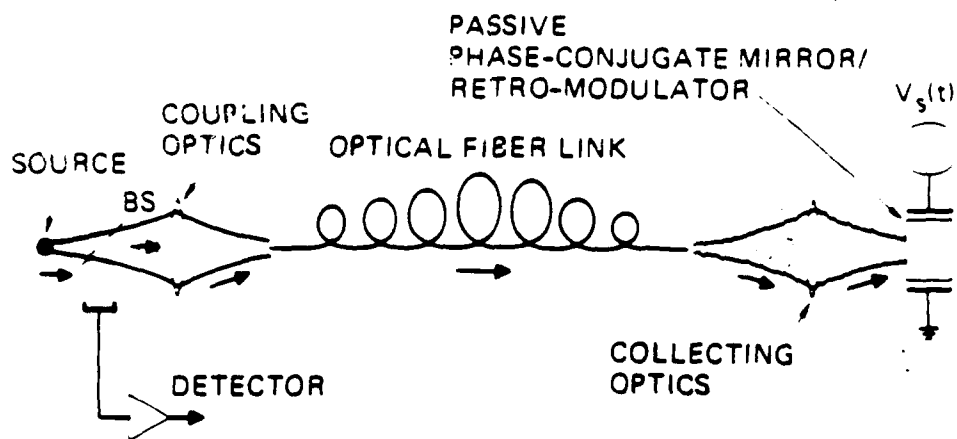


(a) STATION NO. 1 BEACON ILLUMINATES  
GENERAL VICINITY OF STATION NO. 2

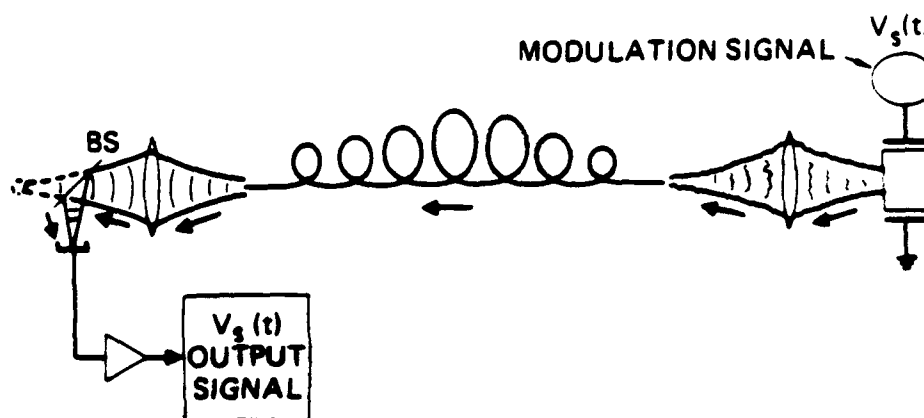


(b) RETRO-MODULATOR/CONJUGATOR AT STATION NO. 2  
ENCODS INFORMATION ON RETRO-BEAM, WHICH IS  
RECEIVED BACK AT STATION NO. 1

Figure 16



(a) INCIDENT PATH (INCIDENT PROBE BEAM, PROPAGATION DISTORTION)



(b) RETURN PATH (REMOTE ENCODING, PROPAGATION COMPENSATION, RETRO-RETURN, DETECTION)

Figure 17



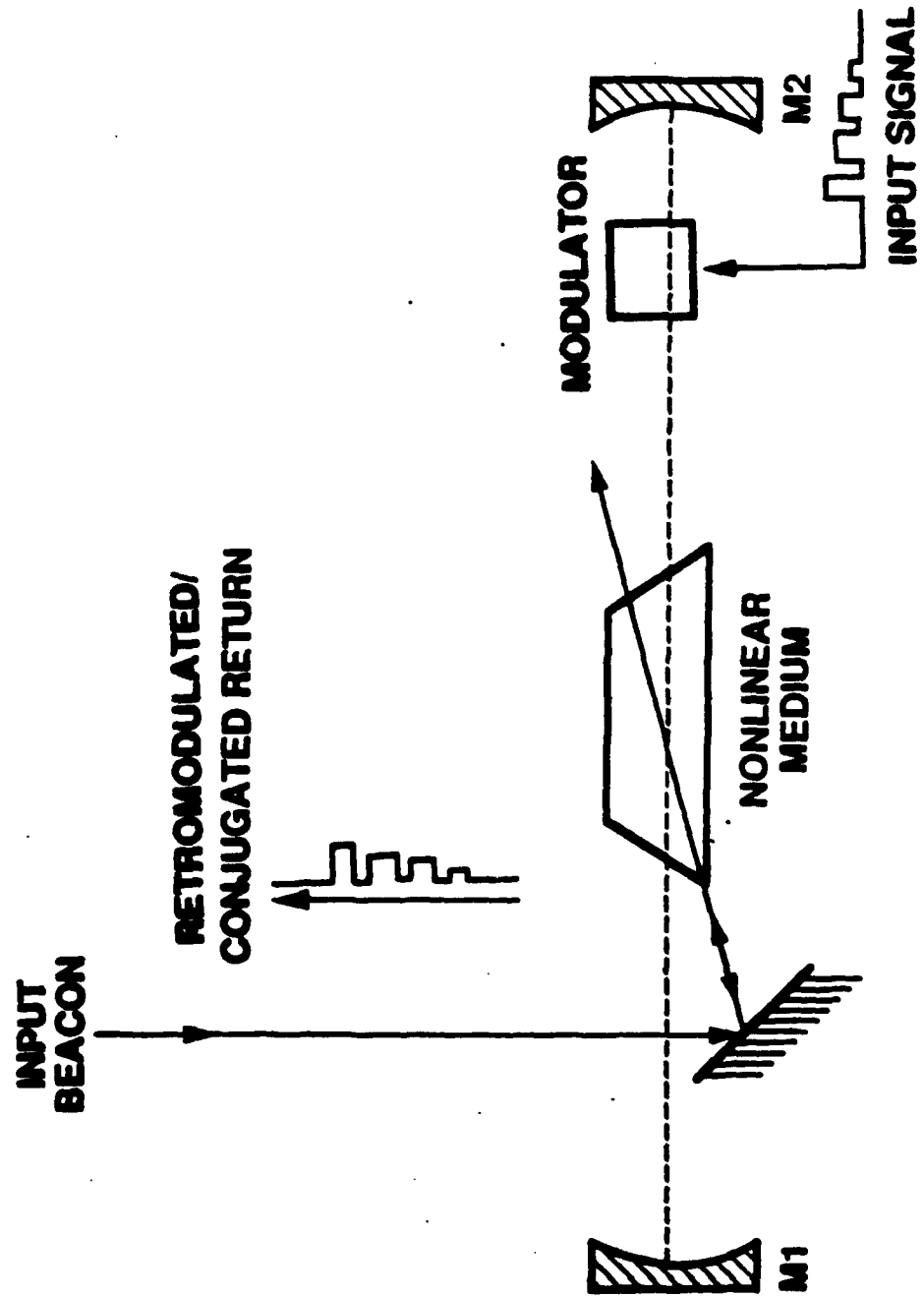
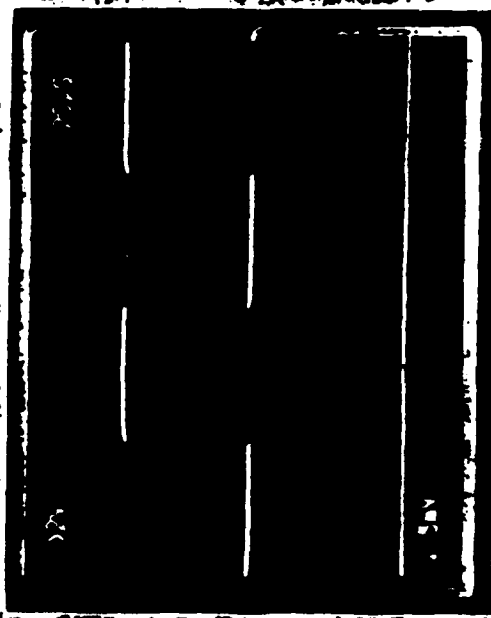


Figure 18

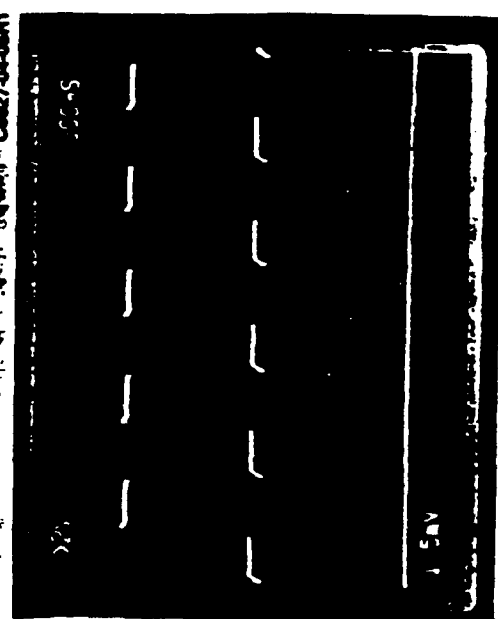
C8827-04-08A1



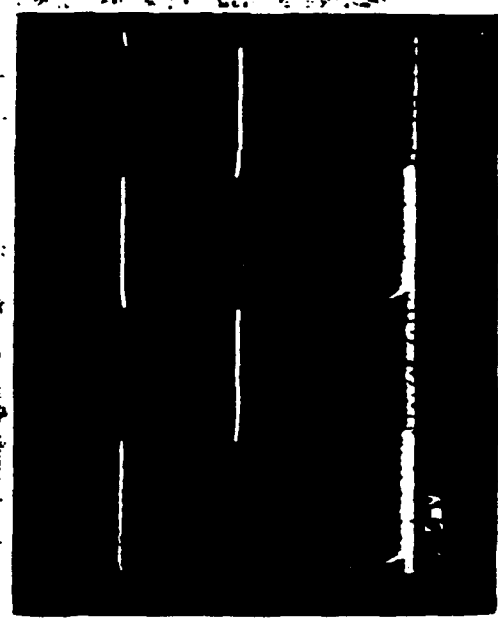
$V_M = 10 \text{ kHz}$   
(20  $\mu\text{s}/\text{DIV}$ )

A-O DRIVE VOLTAGE  
 $V_M$

MODULATED LIGHT  
(ISOLATED A-O MOD)



$V_M = 1 \text{ MHz}$   
(500 ns/DIV)



A-O DRIVE VOLTAGE  
 $V_M$

PHASE-CONJUGATE  
RETURN  
(RETRO-MODULATOR)

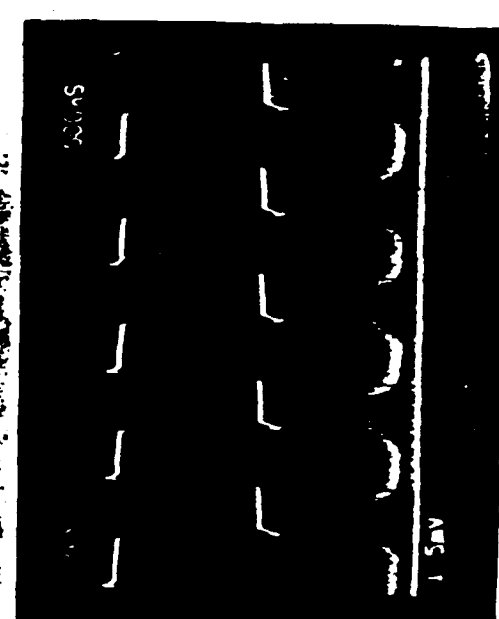


Figure 19